Genetic Control of Shoot Architecture in Barley (*Hordeum vulgare* L.)

Inaugural-Dissertation

zur Erlangung des Doktorgrades
der Mathematisch-Naturwissenschaftlichen Fakultät
der Heinrich-Heine-Universität Düsseldorf

vorgelegt von

Agatha Alexandra Walla
aus Salzkotten

Köln, Dezember 2018

aus dem Institut für Pflanzengenetik

der Heinrich-Heine-Universität Düsseldorf

und assoziiert mit dem

Department für Entwicklungsbiologie der Pflanzen

des Max-Planck-Instituts für Pflanzenzüchtungsforschung in Köln

Gedruckt mit der Genehmigung der

Mathematisch-Naturwissenschaftlichen Fakultät der

Heinrich-Heine-Universität Düsseldorf

Berichterstatter:

1. Professor Dr. Maria von Korff Schmising

2. Professor Dr. Rüdiger Simon

Tag der mündlichen Prüfung: 25.02.2019

Eidesstattliche Erklärung zur Dissertation mit dem Titel:

Genetic Control of Shoot Architecture in Barley (*Hordeum vulgare* L.)

Ich versichere an Eides Statt, dass die Dissertation von mir selbständig und ohne unzulässige fremde Hilfe unter Beachtung der „Grundsätze zur Sicherung guter wissenschaftlicher Praxis an der Heinrich-Heine-Universität Düsseldorf“ erstellt worden ist.

Außerdem versichere ich, dass ich diese Dissertation nur in diesem und keinem anderen Promotionsverfahren eingereicht habe und dass diesem Promotionsverfahren kein gescheitertes Promotionsverfahren vorausgegangen ist.

Ort, Datum	Unterschrift

Table of Contents

Summary

Shoot architecture is a major determinant of grain yield and a primary target for crop improvement. The activity of the shoot apical meristem and the axillary meristems determine branching (tillering) patterns, leaf number and inflorescence morphology. However, the genetic mechanisms underlying shoot architecture are not well characterized in the agronomically important cereal crop barley. This work reports about the identification of two important regulators of shoot architecture in barley, *SIX-ROWED SPIKE3* (*VRS3*) and *MANY NODED DWARF1* (*MND1*).

In the first part of this study, I investigated the genetic regulation of lateral spikelet development in the barley row-type mutant *six-rowed spike3* (*vrs3*). The mutant spike is characterized by fertile lateral spikelets resulting in an increased number of seeds per spike when compared to the two-rowed wild-type. I established a mapping by sequencing approach based on RNA sequencing of allelic mutants to identify the causative mutation at the *vrs3* locus. The comparison of sequence variations in two allelic backcross-derived *vrs3* mutants and the backcross recipient cultivar uncovered the size, number and position of the introgressions and revealed only one candidate gene for the *vrs3* locus in both mutant lines. The candidate gene encodes for a putative histone demethylase with a conserved zinc finger and Jumonji C and N domain. Resequencing of the candidate gene in 19 additional allelic mutant lines revealed a series of mutations in the conserved domains of the protein and thus confirmed the candidate. Analysis of differential gene expression in developing shoot apices suggested that VRS3 is a transcriptional activator of the known row-type genes *VRS1* and *INTERMEDIUM-C* (*INT-C*). Furthermore, comparative transcriptome and qPCR analyses of the row-type mutants *vrs3*, *vrs4* and *int-c* showed that the development of lateral spikelets was mediated by quantitative variation in *VRS1* expression levels. Consequently, this work advanced our understanding of the genetic network controlling lateral spikelet development and row-type in barley.

In the second part of this study, I characterized the barley high-tillering mutant *many noded dwarf1* (*mnd1*) and identified the causal gene as an acyl-CoA N-acyltransferase based on RNA sequencing and verification of the candidate gene in allelic mutant lines. Through detailed macro- and microscopic phenotyping, I could show that *MND1* acts as an important repressor of vegetative growth and is thus critical in coordinating the reproductive phase transition. The *mnd1* mutant is characterized by a prolonged phase of vegetative growth and a shortened phyllochron, resulting in an increased number of leaves and consequently tiller number. In addition, the mutant line formed aerial tillers at elongated nodes along the stem and at the inflorescence base. Scanning electron microscope images of *mnd1* mutant inflorescences showed an insufficient bract suppression at basal rachis nodes coinciding with the reversion of floral meristems to branch meristems. On a molecular level, *MND1* transcripts localized to axillary meristems in axils of young leaves and the

vasculature of the shoot apical meristem (SAM) during the phase transition from vegetative to reproductive growth. Transcriptional profiling of developing inflorescences at three early reproductive stages revealed consistent expression changes of transcripts involved in cell cycle regulation, development and defense across all stages. Known modulators of phase change, such as *LEAFY* and *TERMINAL FLOWER1* homologs, as well as floral homeotic transcription factors were deregulated in the mutant plants. Phylogenetic analysis revealed that MND1 is a close homolog of a putative rice histone H4 acetyltransferase. Future studies are required to investigate the functional conservation between MND1 and its closest rice homolog, as well as identification of direct downstream targets to reveal the underlying pathway of shoot branching control.

Taken together, I identified two putative epigenetic modifiers, VRS3 and MND1, that control transcription in the shoot apex and thereby have strong pleiotropic effects on the barley shoot and inflorescence architecture. Whereas VRS3 is modulating expression levels of known row-type regulators, MND1 is changing expression domains of genes acting in the cell-cycle machinery and modifies expression levels of transcription factors which coordinate phase transition and enhance reproductive growth. My work provides new insights into the genetic and molecular regulation of shoot and spike architecture in barley which are important traits for yield improvement in cereals.

Zusammenfassung

Die Optimierung der Pflanzenarchitektur ist ein wichtiges Ziel, um zukünftig höhere Erträge in Kulturpflanzen erwirtschaften zu können. Dennoch sind die molekularen Mechanismen, welche die Sprossarchitektur in Kulturpflanzen bestimmen, bis heute weitgehend unbekannt. Die vorliegende Arbeit befasst sich mit der Identifizierung zweier Gene der Kulturgerste, *SIX-ROWED SPIKE3* (*VRS3*) und *MANY NODED DWARF1* (*MND1*), welche für die Entwicklung der Pflanzenarchitektur maßgeblich sind.

Im ersten Teil dieser Studie beschreibe ich meine Arbeiten über die genetischen Regulationsmechanismen, welche die Entwicklung von seitlichen Blüten der Mutante *six-rowed spike3* (*vrs3)* steuern. Im Vergleich zu dem zweizeiligen Wildtypen ist die Ähre dieser Mutante durch fertile seitliche Blüten gekennzeichnet, was zu einer erhöhten Kornanzahl pro Ähre führt. Um die zugrundeliegende Mutation des *vrs3* Locus zu identifizieren, etablierte ich einen „*mapping by sequencing*"-Ansatz, welcher auf RNS-Sequenzierungsdaten basiert. Ein Vergleich der genetischen Polymorphismen zweier allelischen, mehrfach rückgekreuzten *vrs3*-Mutanten und dem Rückkreuzungselter offenbarte die Größe, Anzahl und Position der Introgressionen beider Mutantenlinien. Durch die zusätzliche RNS-Sequenzierung der Elternlinie einer *vrs3* Mutante und der anschließenden Analyse der Sequenzpolymorphismen war es möglich, ein einzelnes Kandidatengen für den *vrs3* Locus zu bestimmen. Dieses Gen kodiert für eine Histon-Demethylase, welche sowohl eine konservierte Zinkfinger-, als auch konservierte Jumonji C- und N-Domänen besitzt. Die Bestätigung des *VRS3* Kandidatengens erfolgte durch die Sequenzierung des Gens in 19 unabhängigen allelischen Mutanten, welche alle Polymorphismen in konservierten Domänen des Kandidatengens trugen. Die genomweite Transkriptionsanalyse dieser Studie zeigte, dass VRS3 als transkriptioneller Aktivator der bekannten Zeiligkeitsgene *VRS1* und *INTERMEDIUM-C* (*INT-C*) agiert. Des Weiteren zeigten vergleichende Transkriptom- und qPCR-Analysen der Zeiligkeitsmutanten *vrs3*, *vrs4* und *int-c*, dass die Entwicklung seitlicher Blüten in der Gerstenähre durch quantitative Änderungen in der Expression des *VRS1* Genes gesteuert wird. Die Ergebnisse dieser Arbeit erweitern damit das Verständnis der genetischen Regulation der Entwicklung seitlicher Blüten und der Zeiligkeit in Gerstenähren.

Im zweiten Kapitel dieser Arbeit wendete ich die oben beschriebene „*mapping by sequencing*"-Methode an, um ein Gen zu identifizieren, welches die Sprossverzweigung der Kulturgerste kontrolliert. Ich konnte die Acyl-CoA N-Acyltransferase *MANY NODED DWARF1* (*MND1*), welche eine 8-bp große Insertion aufweist und damit die konservierte N-Acyltransferasedomäne unterbricht, als Kandidatengen für den Starkbestockungslocus *mnd1* bestimmen. Daraufhin bestätigte ich das Kandidatengen durch Komplementationstests mit unabhängigen Mutantenlinien, welche ebenfalls Mutationen im *MND1* Gen tragen. Ausführliche

Bonitierungen der *mnd1* Mutante auf makro- und mikroskopischer Ebene zeigten, dass *MND1* ein wichtiger Repressor des vegetativen Wachstums und damit entscheidend für die Koordination des Übergangs zur Reproduktionsphase ist. Die Verlängerung der vegetativen Entwicklungsphase und ein verkürztes Phyllochron führten zu einer stark erhöhten Anzahl von Blättern in der Mutante. Die erhöhte Anzahl der Blätter korrelierte mit einer erhöhten Anzahl an Achselknospen und ist damit grundlegend für den stark bestockten Phänotypen der *mnd1* Mutante. Des Weiteren charakterisierte ich die Bildung von Seitentrieben an elongierten Nodien des Haupthalmes und an der Basis der Infloreszenz. Durch rasterelektronenmikroskopische Aufnahmen von Infloreszenzen zeigte ich, dass die Unterbindung des Deckblattwachstums an unteren Nodien der Ähre in der Mutante fehlte und dass an diesen Stellen Blütenmeristeme in vegetative Meristeme umgewandelt wurden. Die molekulare Analyse zeigte, dass *MND1* in den Achselknospenmeristemen junger Blätter und in der Meristemvaskulatur des Hauptsprossapikalmeristems (SAM) während des Phasenübergangs vom vegetativen zum reproduktiven Wachstum exprimiert wurde. Weiterhin zeigten genomweite Transkriptionsanalysen von Infloreszenzgeweben in drei Stadien der frühen reproduktiven Entwicklung, dass Gene verantwortlich für die Zellteilung, Entwicklung und Abwehrmechanismen in der Mutante konsistent fehlexprimiert waren. Auch die Expression wichtiger Regulatorgene der Blühinduktion, wie Homolge des *LEAFY* und des *TERMINAL FLOWER1* Gens, und homöotische Blütenentwicklungsgene zeigten Veränderungen in ihrer Expression in der Mutante. Durch phylogenetische Analysen bestimmte ich das MND1 Homolog in Reis, welches die Transkription von Genen durch Regulation der Acetylierung an Histon H4 steuert. Zukünftig sind weitergehende Studien erforderlich, um die funktionelle Konservierung zwischen *MND1* und seinem nächsten Homolog in Reis zu bestimmen und Zielgene des *MND1* Gens zu identifizieren, damit dieser Signalweg zur Steuerung der Bestockung in Gerste vollständig entschlüsselt werden kann.

Zusammengefasst beschreibt diese Arbeit die Identifizierung zweier mutmaßlicher epigenetischer Modifikatoren, VRS3 und MND1, welche die Expression von Genen im SAM und in Infloreszenzen regulieren und damit starke pleiotrope Effekte in der Spross- und Ährenarchitektur der Gerste hervorrufen. Während das *VRS3* Gen die Expression bekannnter Zeiligkeitsgene reguliert, bestimmt das *MND1* Gen die Expressionsdomänen von Zellzyklusgenen als auch die Expression von Genen verantwortlich für die Blühinduktion und der Ährenentwicklung. Die vorliegende Studie vertieft das aktuelle Verständnis der genetischen Mechanismen, welche die Ähren- und Sprossarchitektur der Kulturgerste kontrollieren und somit wertvoll sind für die züchterische Verbesserung des Ertrags in Gerste.

2 Introduction

Food security is one of the major global needs. Due to the growing world population and changing diets, the demand for agricultural products is increasing rapidly. However, increasing food production is facing several challenges including less arable land, climate change and water scarcity (Godfray et al., 2010). Therefore, increasing the yield of a crop plant is a key measure for ensuring food security. One central component determining the yield of a plant is its shoot architecture. The most prominent example for shoot architecture transformation as adaptation to human needs is the domestication of modern maize (*Zea mays*) (Doebley et al., 2006). Maize derives from its wild progenitor Teosinte (*Zea mays* ssp. *Parviglumis*), which is characterized by a highly branched shoot architecture and low yield. In contrast, domesticated maize typically develops only one to two small branches carrying the female inflorescence, known as the ear, and harboring significantly more kernels than Teosinte. Furthermore, selective breeding for architectural traits was a prerequisite for the first Green Revolution during which dwarfism genes were introduced into crops such as rice and wheat (Hedden, 2003). As consequence, these crop plants were able to carry higher yielding inflorescences and showed more resistance to lodging. Hence, modification of shoot architectures can be beneficial for yield and fitness of a plant.

Among the top four cereal crop species, barley (*Hordeum vulgare* L.) is ranked after maize, rice and wheat and is cultivated worldwide with a yearly yield of 144 Mt (USDA 2017). In most industrialized countries, barley is primarily used for malt and beer production, but also cultivated as a resource for animal feed. Furthermore, it is of high relevance as a human staple food mainly in Southwest Asia and Northern Africa (von Bothmer et al., 2003). Recently, new interest in barley as a component of healthy food products has arisen due to barley's beneficial dietary effects such as the improvement of the glycemic index and the reduction of blood cholesterol and pressure (Baik and Ullrich, 2008). It thus remains of great importance to improve yield of elite barley cultivars to match the world's growing demand by targeting desirable shoot architecture traits.

2.1 The Barley Plant Architecture

In barley, the final shoot and inflorescence architecture of a mature plant is reached after completion of three major growth phases: (i) the vegetative, (ii) the reproductive and (iii) the grain filling phase (Newman and Newman, 2008). Especially the first two phases are governed by the activity of the shoot apical meristem (SAM). The vegetative phase begins with the germination of the seed during which the SAM is protected through the sheath-like coleoptile. Leaf primordia are initiated at the flanks of the SAM in a distichous manner. They develop into leaves consisting of the basal tabular leaf sheath followed by the leaf blade. Together with its associated axillary bud, node and internode, a leaf comprises a phytomer segment and stacks of phytomers result in a vegetative stem unit (McMaster, 2005). Reiterative formation of additional stems, so called tillers, of a barley

plant is encompassed by the outgrowth of axillary buds from the leaf axil located at the plant base (crown). Hereby, axillary meristems have the same potential as the SAM to produce phytomers and finally grain bearing spikes. The irreversible transition from the vegetative to the reproductive phase marks the end of leaf primordia initiation through the differentiation of the SAM into an inflorescence meristem. Hence, shoot architecture is largely determined by the first phase of development, the vegetative growth phase.

The beginning of the second major growth phase of barley, the reproductive development, is characterized by the successive formation of double ridges alternating distichously along the elongating inflorescence rachis (Kellogg et al., 2013). Whereas the development of the lower ridge, harboring the cryptic bract primordium, is suppressed, the triple-spikelet primordium (TSP) in the upper ridge develops further. Briefly, the TSP differentiates into three spikelet meristems (one central and two lateral), of which each produces a floret meristem. A quantitative scale has been introduced by Waddington et al. (1983) to characterize developmental stages of the reproductive shoot apex based on the morphological changes of the SAM and the carpel of its most advanced flower. In the last growth phase, the grain filling phase, barley can be visually classified into two row-type appearances of the spike. Two-rowed barley cultivars only develop central spikelets, which produce the grain, while the corresponding lateral spikelets do not develop complete flowers. In six-rowed cultivars, all three spikelets develop flowers, are fertile and produce grains. Consequently, yield and fitness of a barley plant are determined on the one hand by tillering, as basis for the spike number per plant, and on the other hand by the row-type affecting the grain number per plant (Evans, 1993). However, negative correlations between tillering, the row-type and thus the number of seeds produced restricts the genetic improvement of yield (Kjaer and Jensen, 1996). Moreover, the genetic regulators and molecular pathways underlying these two agronomically important traits are not well characterized in barley. It is therefore of great importance to isolate genes underlying traits such as tillering and spike row-type. Secondly, studying the corresponding gene functions and underpinning the molecular pathways will facilitate a better understanding on how barley shoot architecture is established. Finally, these genetic insights can serve as foundation to investigate the genetic correlation between tillering, spike row-types and their effects on yield.

2.2 Barley Mutants and Genomic Resources for Gene Identification Strategies

The identification of genes and networks controlling shoot architecture is a prerequisite for the targeted manipulation of the trait in crop plants. An unbiased and powerful methodology to discover new genes responsible for the manifestation of a certain trait is the forward genetics approach. This discovery process seeks to identify the gene controlling a characteristic trait in mutant individuals. In barley research, scientists profit from a collection of more than 12,000 documented morphological and physiological mutants which mutations either occurred spontaneously or were induced first by X-rays in the 1920s (Stadler. 1928) followed by neutrons and later by the application

of various chemicals (Lundqvist, 2009). These mutations occurred in different genetic backgrounds and the mutants were isolated under various environments and climatic conditions from all around the world. Major efforts have been undertaken to transfer many of the mutant loci into the common genetic background of cultivar (cv.) Bowman. This was achieved by repeated reciprocal backcrosses allowing for comparative studies between different mutants and facilitating mapping strategies. Nomenclature rules for the assignment of locus names and gene symbols to barley mutants were published in the Barley Genetics Newsletter (BGN) (Franckowiak et al., 1997). Furthermore, the BGN provides a detailed description of the genetic stock and releases updates on the individual mutant lines. Mutants are grouped based on their most prominent feature, as sometimes pleiotropic phenotypes were observed. They are divided according to the following characters: (i) reproduction, (ii) gametic and zygotic formation, (iii) kernel development and distribution, (iv) seedling development, (v) vegetative growth, (vi) environmental stress responses and (vii) nutritional quality factors (Lundqvist and Franckowiak, 2003).

Among these categories of mutant phenotypes, several shoot architecture mutant lines can be found. For example, row-type mutants (reproduction group) show different degrees of lateral spikelet development and the corresponding mutant loci have been termed *six-rowed spike* (*vrs*), *hexastichon* (*hex-v*) or *intermedium spike* (*int*) based on their origin and phenotype (Franckowiak et al., 1997; Lundqvist, 2014). This group includes *vrs3* and *int-a* mutants, which originate from a two-rowed cultivar and were shown to be allelic (Lundqvist and Lundquist, 1988). They are characterized by a spike phenotype in between two- and six-rowed where the upper half of the spike appears to be six-rowed and enlarged lateral spikelets are found at the base of the spike which do not set seed. In addition, the *vrs3*/*int-a* mutants are characterized by the development of two awns in central spikelets, arising from the lemma and palea. Due to the changed spike architecture, backcross-derived *vrs3*/*int-a* mutants in cv. Bowman showed smaller kernels and a reduction in yield. Another example of shoot architecture mutants include those with decreased or increased numbers of tillers per plant (vegetative growth group). Most tillering mutants show additional pleiotropic effects on other plant development traits (Lundqvist and Franckowiak, 2003). The *many noded dwarf* (*mnd*) mutants produce numerous thin tillers with narrow leaves and short internodes. Especially *mnd1* mutants show further pleiotropic phenotypes, namely additional aerial tillers at uppermost tiller nodes which produce small spikes themselves (Harlan and Pope, 1922). Under field conditions, *mnd1* mutants are smaller than wild-type plants, however exceed their parent's height when grown under greenhouse conditions. The specific impact on yield is not known for *mnd1* mutants, however spikes are about half of the size of wild-type and additional vegetative branches arise from lower rachis node which often producing no fertile flowers. Even though the mutant phenotypes are characterized to a certain extent, the underlying genes of these shoot architectural mutants, including *vrs3*/*int-a* and *mnd1*, have not been identified so far.

The identification of causal mutations in barley is hampered by the large genome size and suppressed recombination. Barley is a diploid plant (2n = 14) with a genome size of 5.3 Gb, which

is forty times larger than the Arabidopsis genome with a size of 125 Mb (The Arabidopsis Genome Initiative, 2000). The first partly ordered draft sequence assembly of barley was published in 2012 together with the prediction of 26,159 high-confidence (HC) genes (International Barley Genome Sequencing Consortium, 2012). This assembly consists of a physical map (4.98 Gb) of which most assembled sequence contigs were anchored to a high-resolution genetic map. However, highly abundant repetitive elements and low meiotic recombination in pericentromeric regions were limiting the whole genome sequence assembly. Recently, an updated version of the barley reference has been published which incorporates chromosome confirmation capture sequencing (Hi-C) data (Mascher et al., 2017). This third-generation mapping approach is based on ligation of DNA in its natural three-dimensional folded state and subsequent sequencing reveals DNA fragments in short- and long-range proximity. Constructed 4,265 non-redundant sequence scaffolds, obtained from sequencing of more than 80,000 bacterial artificial chromosomes (BACS) and subsequent clustering of overlapping BACS, were placed onto the seven chromosomes of barley using the high-resolution genetic map, an optical map and Hi-C data. This recent genome comprises 39,734 HC gene models and serves as important resource for comprehensive genetic and genomic studies in barley including cloning of genes in forward genetic approaches. In 1997, the first barley gene cloned was *Mlo*, a powdery mildew resistance gene (Büschges et al., 1997). Since then, gene identification in barley mutants resulted in more than 40 cloned genes (summarized in Hansson et al., 2018). The major gene identification strategy in these studies was map-based cloning. This strategy relies on the construction of a genetic map, indicating the location of the gene relative to molecular markers. However, these mapping intervals can be large and harbor many genes, especially in regions with reduced recombination frequencies. Thus, further fine-mapping in larger populations is required to increase the genetic resolution around the gene of interest resulting in high costs, time and labor investment. Next, the physical map between the flanking markers is explored resulting in a list of candidate genes. Last, these genes need to be sequenced to reveal the mutation that is likely to cause the observed mutant phenotype followed by the confirmation using transgenic or alternative approaches. Since the implementation of next generation sequencing (NGS) technologies, new fast forward genetic approaches for the identification of mutations have been developed. The exome capture platform has been established in barley and allows in depth sequencing for selective enrichment of coding DNA sequences (Mascher et al., 2014; Pankin et al., 2014). Recently, a technique called MutChromSeq was introduced by Sánchez-Martín et al. (2016), in which only the chromosome of interest is sequenced resulting in the identification of causative mutations. However, these strategies can have disadvantages. For example, map-based cloning is restricted by recombination frequencies hampering the identification of genes in regions with low meiotic events such as centromeres. In case of exome-enriched re-sequencing, only a selected set of genomic DNA is targeted, which might not reveal the underlying mutation. It thus remains important to explore new gene mapping approaches for cloning of genes that are involved in the manifestation of desired and important

traits. In future, as sequencing is getting less expensive and analysis of NGS data sets is made fast and efficient, the number of identified developmental genes is going to increase further.

2.3 Aims and Approaches

The overall objective of the present study is the detailed phenotypic and genetic characterization of induced shoot architecture mutants in barley. For this purpose, I analyzed the *six-rowed spike3* (*vrs3*) mutant with altered spikelet development and consequently spike morphology. Further I investigated the *many noded dwarf1* (*mnd1*) mutant, a high tillering mutant with pleiotropic phenotypes including increased leaf production, reduced plant height and spike length.

For both investigated mutants I followed three major objectives:

1. To better understand the developmental and morphological effects of the mutant loci *vrs3* and *mnd1*, I endeavored a detailed phenotypic characterization of the mutant lines. Particularly with regard to the high tillering mutant *mnd1*, I described the pleiotropic effect of this mutant locus on different shoot architecture traits.

2. An essential goal of the present study was to identify the candidate mutations underlying the loci of *vrs3* and *mnd1*. Therefore, I aimed at the development of a fast and inexpensive method for gene identification based on RNA sequencing and analysis of allelic mutants. Rough location of the causative genes was achieved by sequencing backcross-derived mutant lines resulting in the identification of the introgression regions. Candidate genes were selected based on sequence variations and confirmed using allelic mutants.

3. Finally, I aimed at a molecular characterization of the mutants by examining differentially expressed transcripts in developmental series of inflorescences. The genetic network controlling the barley row-type was further elucidated in additional row-type mutants which were subjected to whole transcriptome analysis.

2.4 Literature Cited

Baik B, Ullrich SE (2008) Barley for food: Characteristics, improvement, and renewed interest. J Cereal Sci **48**: 233–242

Von Bothmer R, van Hintum T, Knüpffer H, Sato K (2003) Diversity in Barley (Hordeum vulgare), 7th ed. Elsevier Ltd

Büschges R, Hollricher K, Panstruga R, Simons G, Wolter M, Frijters A, Daelen R Van, Lee T Van Der, Diergaarde P, Groenendijk J, et al (1997) The Barley Mlo Gene: A Novel Control Element of Plant Pathogen Resistance. Cell **88**: 695–705

Doebley JF, Gaut BS, Smith BD (2006) The Molecular Genetics of Crop Domestication. Cell **127**: 1309–1321

Evans LT (1993) Crop evolution, adaptation and yield. Cambridge University Press: New York

Franckowiak JD, Lundqvist U, Konishi T (1997) New and revised names for barley genes. Barley Genet Newsl **26**: 4–8

Godfray HCJ, Beddington JR, Crute IR, Haddad L, Lawrence D, Muir F, Pretty J, Robinson S, Thomas SM, Toulmin C (2010) Food Security: The Challenge of Feeding 9 Billion People. Science **327**: 812–818

Hansson M, Komatsuda T, Stein N, Muehlbauer GJ (2018) Molecular Mapping and Cloning of Genes and QTLs. The Barley Genome. Springer, Cham, pp 139–154

Harlan H V, Pope MN (1922) Many-noded dwarf barley. J Hered **13**: 269–273

Hedden P (2003) The genes of the Green Revolution. Trends Genet **19**: 5–9

International Barley Genome Sequencing Consortium (2012) A physical, genetic and functional sequence assembly of the barley genome. Nature **491**: 711–716

Kellogg EA, Camara PEAS, Rudall PJ, Ladd P, Malcomber ST, Whipple CJ, Doust AN (2013) Early inflorescence development in the grasses (Poaceae). Front Plant Sci **4**: 250

Kjaer B, Jensen J (1996) Quantitative trait loci for grain yield and yield components in a cross between a six-rowed and a two-rowed barley. Euphytica **90**: 39–48

Lundqvist U (2009) Eighty years of Scandinavian barley mutation genetics and breeding. Induc. plant Mutat. genomics era. Food and Agriculture Organization of the United Nations, Rome, pp 39–43

Lundqvist U (2014) Scandinavian mutation research in barley – a historical review. Hereditas **151**: 123–131

Lundqvist U, Franckowiak JD (2003) Diversity of barley mutants. Divers. barley. Elsevier Ltd, pp 77–96

Lundqvist U, Lundquist A (1988) Induced intermedium mutants in barley: origin, morphology and inheritance. Hereditas **108**: 13–26

Mascher M, Gundlach H, Himmelbach A, Beier S, Twardziok SO, Wicker T, Radchuk V, Dockter C, Hedley PE, Russell J, et al (2017) A chromosome conformation capture ordered sequence of the barley genome. Nature **544**: 427–433

Mascher M, Jost M, Kuon J-E, Himmelbach A, Aßfalg A, Beier S, Scholz U, Graner A, Stein N (2014) Mapping-by-sequencing accelerates forward genetics in barley. Genome Biol **15**: R78

McMaster GS (2005) Phytomers, phyllochrons, phenology and temperate cereal development. J Agric Sci **143**: 137–150

Newman RK, Newman CW (2008) Barley for food and health: Science, technology, and products. John Wiley & Sons

Pankin A, Campoli C, Dong X, Kilian B, Sharma R, Himmelbach A, Saini R, Davis SJ, Stein N, Schneeberger K, et al (2014) Mapping-by-sequencing identifies HvPHYTOCHROME C as a candidate gene for the early maturity 5 locus modulating the circadian clock and photoperiodic flowering in barley. Genetics **198**: 383–396

Sánchez-Martín J, Steuernagel B, Ghosh S, Herren G, Hurni S, Adamski N, Vrána J, Kubaláková M, Krattinger SG, Wicker T, et al (2016) Rapid gene isolation in barley and wheat by mutant chromosome sequencing. Genome Biol **17**: 221

The Arabidopsis Genome Initiative (2000) Analysis of the genome sequence of the flowering plant Arabidopsis thaliana. Nature **408**: 796

Waddington SR, Cartwright PM, Wall PC (1983) A Quantitative Scale of Spike Initial and Pistil Development in Barley and Wheat. Ann Bot **51**: 119–130

3 Six-Rowed Spike3 (VRS3) Is a Histone Demethylase That Controls Lateral Spikelet Development in Barley

The following manuscript was published in Plant Physiology® in August, 2017.

Authors:

G. Wilma van Esse,*[,a,b,c] Agatha Walla,*[,a,b,c] Andreas Finke,[a] Maarten Koornneef,[a,d] Ales Pecinka,[a] and Maria von Korff[a,b,c]

*These authors contributed equally to this article.

Affiliations:

[a]Department of Plant Breeding and Genetics, Max Planck Institute for Plant Breeding Research, 50829 Köln, Germany

[b]Institute for Plant Genetics, Heinrich-Heine-Universität Düsseldorf, 40225 Düsseldorf, Germany

[c]Cluster of Excellence in Plant Sciences, Heinrich-Heine-Universität Düsseldorf, 40255 Düsseldorf, Germany

[d]Laboratory of Genetics, Wageningen University and Research, 6708 PB Wageningen, The Netherlands

Contributions:

Agatha Walla, G. Wilma van Esse, Maarten Koornneef and Maria von Korff conceived and designed the experiments. Agatha Walla, G. Wilma van Esse and Andreas Finke performed the experiments. Agatha Walla, G. Wilma van Esse, Ales Pecinka and Maria von Korff analyzed the data. Agatha Walla, G. Wilma van Esse and Maria von Korff wrote the article.

Six-Rowed Spike3 (VRS3) Is a Histone Demethylase That Controls Lateral Spikelet Development in Barley[1][OPEN]

G. Wilma van Esse,[a,b,c,2,3] Agatha Walla,[a,b,c,2] Andreas Finke,[a] Maarten Koornneef,[a,d] Ales Pecinka,[a] and Maria von Korff[a,b,c,4]

[a]Department of Plant Breeding and Genetics, Max Planck Institute for Plant Breeding Research, 50829 Köln, Germany
[b]Institute for Plant Genetics, Heinrich-Heine-Universität Düsseldorf, 40225 Düsseldorf, Germany
[c]Cluster of Excellence in Plant Sciences, Heinrich-Heine-Universität Düsseldorf, 40255 Düsseldorf, Germany
[d]Laboratory of Genetics, Wageningen University and Research, 6708 PB Wageningen, The Netherlands

ORCID IDs: 0000-0001-5012-2346 (G.W.v.E.); 0000-0002-7759-4869 (M.K.); 0000-0002-6816-586X (M.v.K.).

The complex nature of crop genomes has long prohibited the efficient isolation of agronomically relevant genes. However, recent advances in next-generation sequencing technologies provide new ways to accelerate fine-mapping and gene isolation in crops. We used RNA sequencing of allelic *six-rowed spike3* (*vrs3*) mutants with altered spikelet development for gene identification and functional analysis in barley (*Hordeum vulgare*). Variant calling in two allelic *vrs3* mutants revealed that *VRS3* encodes a putative histone Lys demethylase with a conserved zinc finger and Jumonji C and N domain. Sanger sequencing of this candidate gene in independent allelic *vrs3* mutants revealed a series of mutations in conserved domains, thus confirming our candidate as the *VRS3* gene and suggesting that the row type in barley is determined epigenetically. Global transcriptional profiling in developing shoot apical meristems of *vrs3* suggested that VRS3 acts as a transcriptional activator of the row-type genes *VRS1* (*Hv.HOMEOBOX1*) and *INTERMEDIUM-C* (*INT-C*; *Hv.TEOSINTE BRANCHED1*). Comparative transcriptome analysis of the row-type mutants *vrs3*, *vrs4* (*Hv.RAMOSA2*), and *int-c* confirmed that all three genes act as transcriptional activators of *VRS1* and quantitative variation in the expression levels of *VRS1* in these mutants correlated with differences in the number of developed lateral spikelets. The identification of genes and pathways affecting seed number in small grain cereals will enable to further unravel the transcriptional networks controlling this important yield component.

Identification of genomic variation is crucial for unraveling the relationship between genotype and phenotype and provides important insights into the genetic basis of agronomic traits in crop plants. Many crop species, including wheat (*Triticum aestivum*) and barley (*Hordeum vulgare*), are characterized by large genomes with regions of reduced recombination. The isolation of genes underlying important agronomic traits is therefore difficult and time consuming. However, next-generation sequencing (NGS) technologies and the generation of genomic reference sequences in these crops are providing new ways to accelerate the genetic analysis of traits. Whole-genome or targeted resequencing has been employed to aid in the fine mapping and identification of causal polymorphisms collectively termed as NGS-enabled genetics. Mapping by sequencing was first applied in the model species Arabidopsis (*Arabidopsis thaliana*; Schneeberger et al., 2009; James et al., 2013). This procedure is based on genome-wide resequencing of phenotypic bulks of mutant F2 individuals to fine-map the gene of interest. Mapping-by-sequencing based on whole-exome capture or RNA sequencing to reduce genome complexity has also been successfully applied for fine mapping in wheat and barley (Trick et al., 2012; Pankin et al., 2014; Liller et al., 2017). Although mapping by sequencing has proven successful to identify candidate genes, it still requires a substantial effort in generating and phenotyping large mapping populations. Furthermore, additional variation in the background may obscure the phenotypic effect of allelic variation at the target gene and mapping resolution may still be low in parts of the genome with low recombination.

An elegant method for gene identification without a segregating population is based on the analysis of multiple allelic mutants. Although the mutagenic treatment may affect many genes in a single genome, it is usually

[1] This research was funded by the German Cluster of Excellence on Plant Sciences (CEPLAS) EXC1028, the Priority Program (SPP1530, Flowering time control: from natural variation to crop improvement) and the Max Planck Society.

[2] These authors contributed equally to the article.

[3] Current address: Laboratory of Molecular Biology, Wageningen University and Research, 6708 PB Wageningen, The Netherlands.

[4] Address correspondence to korff@mpipz.mpg.de.

The author responsible for distribution of materials integral to the findings presented in this article in accordance with the policy described in the Instructions for Authors (www.plantphysiol.org) is: Maria von Korff (korff@mpipz.mpg.de).

A.W., G.W.v.E., M.K., and M.v.K. conceived and designed the experiments; A.W., G.W.v.E., and A.F. performed the experiments; A.W., G.W.v.E., A.P., and M.v.K. analyzed the data; A.W., G.W.v.E., and M.v.K. wrote the article.

[OPEN] Articles can be viewed without a subscription.

www.plantphysiol.org/cgi/doi/10.1104/pp.17.00108

only one gene or a very small set of genes that carry severe changes within all independent allelic mutants. Whole-genome sequencing of allelic mutants in Arabidopsis and rice (*Oryza sativa*) has successfully revealed candidate genes for the variant phenotype without any prior mapping (Nordström et al., 2013). To date, this approach has not been applied to the complex genomes of crops, presumably because of the lack of high-quality physical maps and the difficulty of distinguishing true allelic variants from homologous genes.

In barley, large collections of developmental and morphological mutants represent a valuable resource for gene identification and characterization (Druka et al., 2011). These have been generated by physical and chemical mutagenesis since the early 20th century to explore the potential of mutation breeding in crop improvement (Ahloowalia et al., 2004; Lundqvist, 2014). Primary mutants were induced or discovered in different cultivars, which after mutagenesis contained a different spectrum of background mutations. Therefore, many mutant loci were introgressed into the common genetic background Bowman by repeated back-crossing and phenotypic selection (Druka et al., 2011). This resulted in a large collection of introgression lines (ILs) in the cultivar (cv) Bowman with a relatively small genetic interval originating from the donor that contains the mutated locus. In addition, many of these mutant phenotypes were intercrossed to identify allelic mutant series for different morphological, developmental, and physiological traits. The collection has proven particularly valuable for studying the genetic control of plant and spike architecture (Druka et al., 2011; Koppolu et al., 2013; Liller et al., 2015).

In cereals, plant and spike architecture influence the number of seeds, one of the most important yield component traits. The spike of barley forms a triple spikelet meristem with one central spikelet meristem and two lateral spike meristems. The seeds on the barley spike can be arranged either in two or six rows. In the two-rowed spike, only the central spikelet is fertile, while in the six-rowed spike, all three spikelets give rise to seeds. The genes underlying the *six-rowed spike* (*vrs*) loci *vrs1* and *vrs4* have been identified as key inhibitors of lateral spikelet development, and their loss of function leads to the development of six-rowed spikes. *VRS1* encodes a HD-ZIP transcription factor (Hv.Hox1; Komatsuda et al., 2007). *VRS4* encodes a LATERAL ORGAN BOUNDARY transcription factor that is homologs to the maize (*Zea mays*) *RAMOSA2* (*RA2*) and acts upstream of *VRS1* (Koppolu et al., 2013). In addition, a number of row-type mutants display an *intermedium spike* (*int*) phenotype with varying two- or six-rowed patterns. These intermedium (*int/vrs*) mutants show enlarged lateral florets which may or may not develop into kernels, depending on the position on the spike and the environment (Lundqvist and Lundqvist, 1987, 1988b).

More than 130 intermedium mutants have been isolated, of which 60 were shown to be mutated in one of nine genes (Gustafsson and Lundqvist, 1980). The most frequent intermedium mutant is *int-c*, which has been identified as a barley homolog of *TEOSINTE-BRANCHED1* (Ramsay et al., 2011), a TCP transcription factor and major domestication related gene affecting shoot branching in maize (Studer et al., 2011; Studer and Doebley, 2011). Double mutants of different *int* loci lead to typical six-rowed plants, suggesting that *int* genes and *VRS1* might interact in the same pathway (Lundqvist et al., 1988a, 1988b; Lundqvist and Lundqvist, 1988a). In a comprehensive analysis, we have classified 36 different row-type mutants based on their shoot and spike architecture (Liller et al., 2015). Allelic *vrs3/int-a*, *int-c*, *vrs1*, and *vrs4* mutants and derived introgression lines showed comparable macroscopic phenotypes, such an increase in the number of seeds per spike and a reduction in tiller number at maturity compared to their two-rowed wild-type parents. Taken together, phenotypic studies have shown that *int-a*, *int-c*, *vrs1*, and *vrs4* are genetically separate loci, which likely interact to control lateral spikelet development in barley. These row-type mutants now provide a valuable resource to identify the underlying mutations and investigate the molecular network controlling spikelet development and fertility. The causative genes and mutations for *vrs1*, *vrs4*, and *int-c* are known, while the gene underlying the *vrs3* locus has so far not been identified.

We performed RNA sequencing of developing spike meristems in the allelic *vrs3.f/int-a.1* mutants, and in addition in *vrs1*, *vrs4.k*, and *int-c*, all introgressed into cv Bowman (Druka et al., 2011). We demonstrate that RNA sequencing of allelic and epistatic mutants provides a powerful method for simultaneous gene isolation and functional analysis in barley.

RESULTS

Variant Calling on RNA Sequencing Reads Reveals a Candidate Gene for the *vrs3/int-a* Mutation

Our first aim was to determine the size and location of the introgressions in the two independent ILs carrying the allelic *vrs3.f* and *int-a.1* mutations (Lundqvist et al., 1988a). Both mutants exhibit fertile lateral spikelets resulting in an increased number per spike when compared to cv Bowman (Fig. 1; Supplemental Fig. S1), corroborating previous reports (Lundqvist and Lundqvist, 1988b; Koppolu et al., 2013; Liller et al., 2015). The development of additional lateral spikelets, which mainly occurred at the middle part of the spike, was not associated with a significant change in rachis internode number (Supplemental Fig. S1, A and B).

We hypothesized that the causal gene is likely located within the introgressed regions common to both ILs. In addition, our objective was to identify the gene variants underlying the row-type phenotype (Fig. 1) in both allelic mutants. To accomplish this, we sequenced total RNA extracted from the main shoot apex (MSA) when the lemma and stamen primordium started to develop (Waddington stages W3.0–W3.5). At this stage, the first floral organ primordia differentiate and the stem

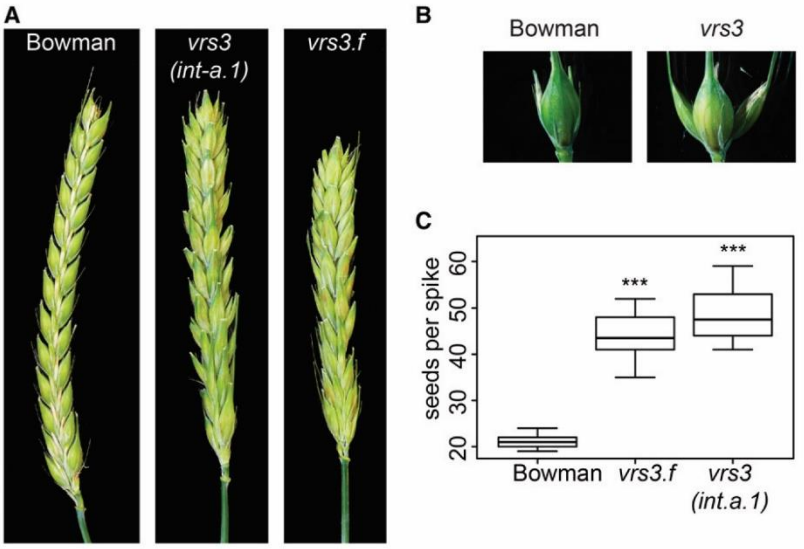

Figure 1. Spike phenotype of *vrs3* plants. A, The intermedium row-type phenotype of *vrs3*, which exhibits fertile lateral spikelets at the upper part of the spike. The awns were removed from the spike to visualize the difference between the mutant and wild type. B, In cv Bowman, only the central spikelet is developed; in the upper part of *vrs3* the central and lateral spikelets give rise to seeds. C, *vrs3*(*int-a*) and *vrs3.f* mutants have a significantly increased seed number per spike when compared to the wild type. Significant differences were determined with a one-way ANOVA, $P \leq 0.01$, $n = 10$ spikes.

elongation is initiated. Moreover, initial differences between six-rowed *vrs* mutants and wild type are clearly visible (Koppolu et al., 2013). RNA sequencing was carried out in the ILs, the backcross recipient cv Bowman and cv Bonus, the parental line of *int-a.1*. Hakata2, the original parent of *vrs3.f*, was not available for sequencing. Reads obtained from RNA sequencing of the MSA tissue were mapped to a combined set of high confidence (HC) and low confidence (LC) predicted coding sequences of cv Morex (International Barley Genome Sequencing Consortium, 2012). The reads were mapped to the barley reference using Burrows Wheeler Aligner (BWA)-MEM (Langmead and Salzberg, 2012; Li, 2013) resulting in a mapping rate of 80%.

Mapping quality filtered reads obtained from BWA-MEM alignments were subjected to variant calling. After stringent filtering of putatively false positive single nucleotide polymorphisms (SNPs), resulting variants of each mutant line were compared to variants obtained from cv Bowman. This comparison resulted in alleles specific to each mutant line and thus revealed the size, number, and position of the introgressions in the ILs. The mutant line *vrs3.f* contained three introgressions on chromosome 1H, 2H, and 4H, while the *int-a.1* mutant carried four introgressions on chromosome 1H, 6H, and 7H (Fig. 2). We detected an overlap between the introgressions in *vrs3.f* and *int-a.1* located on chromosome 1H in the interval of 35.69 cM to 52.55 cM. The region comprises 2075 HC and LC genes. This target interval is useful to delimit the number and position of possible candidate genes. However, the chromosomal position of genes may not be correct. We therefore considered all genetic differences between the ILs and the parental lines regardless of their genomic position. Polymorphisms shared between any of the two ILs and Morex were excluded as candidates for the *vrs3*/*int-a* phenotype. Furthermore, variants obtained from the *int-a.1* mutant were compared to the *int-a.1* parental line cv Bonus. Only seven genes carried unique nonsynonymous mutations that differentiated *int-a.1* from cv Bonus, cv Bowman, and cv Morex (Table I; Supplemental File S1). Mutations differentiating *vrs3.f* from cv Bowman and cv Morex were detected in 196 genes. From those genes only one gene, MLOC_69611.1, carried a unique mutation in *int-a.1* and *vrs3.f* (Table I). Both MLOC_69611.1 alleles in the mutant lines carry deletions causing frame shifts (AT > A at position 394 in *vrs3.f*, TGC > T at position 1667 in *int-a.1*). Analysis of the conserved domains of MLOC_69611.1 showed that the gene is a putative histone demethylase containing a zinc-finger as well as a Jumonji (Jmj) C and N domain. The *vrs3.f* mutant contains a deletion of one nucleotide changing the amino acid sequence anterior to the zinc finger domain. *Int-a.1* contains a deletion of two base pairs prior to the JmjN domain of this protein, resulting in a frame shift. Taken together, our variant calling revealed that MLOC_69611.1 carries unique mutations in *vrs3.f* and *int-a.1* resulting in a nonfunctional protein. Therefore, we selected MLOC_69611.1 located on chromosome 1H at 47.52 cM as a prime candidate for the *vrs3* locus.

Several additional allelic variants of *vrs3* are available, most of them originate from x-ray or neutron-induced mutagenesis screens. The candidate gene MLOC_69611.1 was resequenced in 19 independent *vrs3* mutants, obtained from the Nordic Genome Resource Center (http://www.nordgen.org). The candidate gene MLOC_69611.1 contained an indel, causing a frame shift in five genotypes, six genotypes carried a premature stop codon, six genotypes contained a nonsynonymous SNP in or close to conserved domains, and two genotypes carried a nonsynonymous SNP

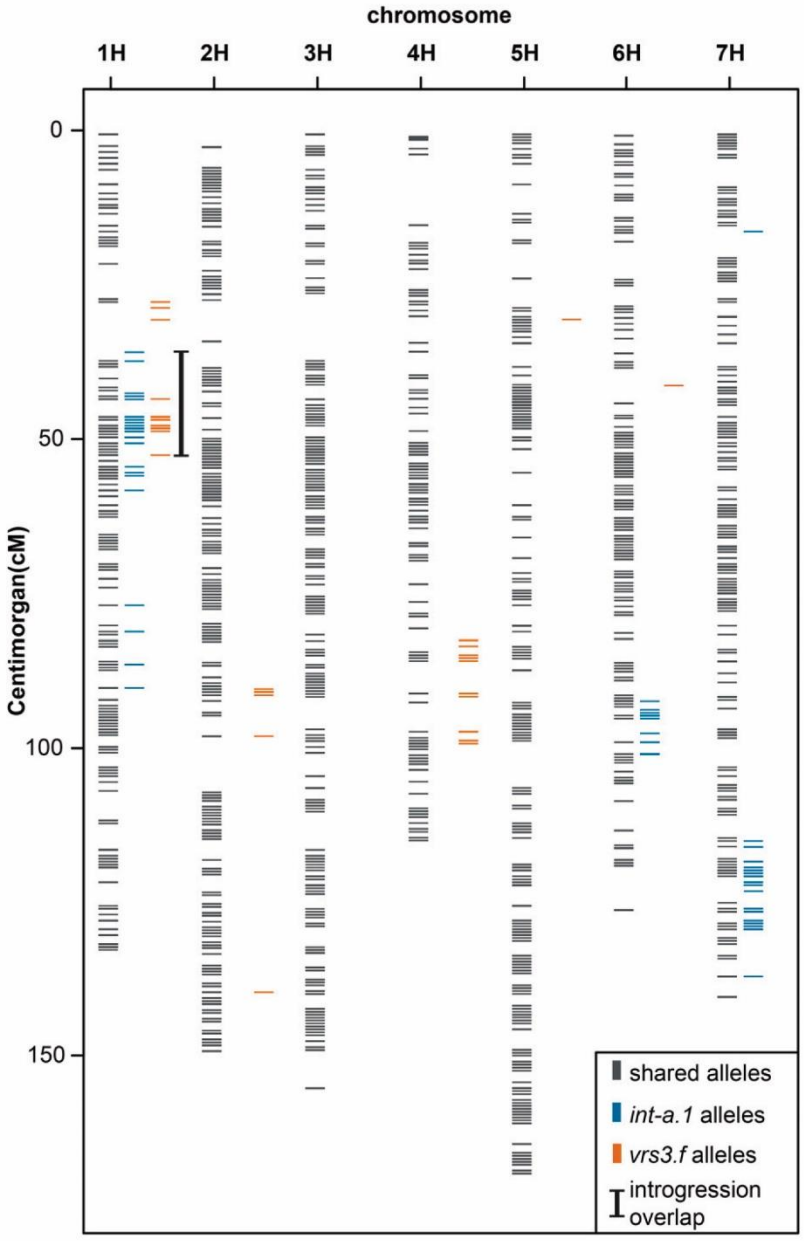

Figure 2. Variant calling in *vrs3.f* and *int-a.1*. Genes carrying mutations in *vrs3.f* and *int-a.1* were identified and placed on the barley POPSEQ map. Introgression regions are detected by variant calling between the respective mutant line and cv Bowman. The overlapping introgression region of *vrs3.f* and *int-a.1* is indicated with a black bar.

close to an intron-exon junction (Fig. 3; Supplemental Table S1). This confirmed that MLOC_69611.1 is indeed the gene underlying the *vrs3* mutant phenotype. Phylogenetic analysis indicated that the MLOC_69611.1 protein shows the highest similarity to the evolutionary conserved JMJD2 group II of JmjC domain-containing proteins (Supplemental Fig. S3). The closest orthologs of MLOC_69611.1 are the Lys-specific demethylases JMJ13 (At5g46910) in Arabidopsis and JMJ706 (Os10g42690) in rice (Supplemental Table S2). Furthermore, comparison of the JmjC domains revealed a 95.97% identity between VRS3 and Os.JMJ706 and an 83.87% identity between VRS3 and At.JMJ13 (Supplemental Table S2). Os.JMJ706 is mainly involved in the removal of a methyl group from the Lys 9 of the histone H3 protein (H3K9me), whereas At.JMJ13 has an H3K27me3 demethylase activity (Sun and Zhou, 2008; Crevillèn et al., 2014).

Table I. *Introgression overview of vrs3.f and int-a.1 mutants*

	vrs3.f		*vrs3(int-a.1)*		*vrs3.f/vrs3(int-a.1)* Overlap	
Introgression intervals	Chromosome	Position (cM)	Chromosome	Position (cM)	Chromosome	Position (cM)
	1H	27.4 to 52.5	1H	35.7 to 58.2	1H	35.7 to 52.6
	2H	90.4 to 97.8	1H	78.8 to 90.2		
	4H	82.7 to 99.2	6H	92.3 to 101.0		
			7H	115.4 to 137.3		
No. of genes in introgression	2639		4046		2075	
Unique nonsynonymous mutations in the ILs	196		7		1 (MLOC_69611.1)	

Comparative Transcriptional Profiling of *vrs3 vrs1, vrs4,* and *int-c* Mutants

Comparative phenotyping of spike architecture in *vrs1*, *vrs3(int-a.1)*, *vrs4.k*, and *int-c.5* revealed that these mutants showed quantitative differences in spikelet development. In *vrs1* and *vrs4.k* plants, the spike was fully six-rowed, whereas in the *vrs3* and *int-c.5* mutants the lower third and upper parts of the spike were two-rowed and the middle of the spike appeared six-rowed (Supplemental Fig. S1). Moreover, both *vrs3* and *vrs4.k* formed additional lateral spikelets, whereas *vrs1* and *int-c.5* did not. To explore the molecular basis of quantitative variation in spikelet development, we performed parallel transcriptional profiling of *vrs1*, *vrs3*, *vrs4.k*, and *int-c.5* mutants in the Bowman background (Supplemental Fig. S2) at W3.5 and W5.0. At the stamen primordium stage (W3.5), the first floral organ primordia start to differentiate. The induction of floret primordia on the inflorescence continues until the awn primordium stage (W5.0). The mutations in *vrs3(int-a.1)* and *int-c.5* are both characterized by a small deletion causing a frame shift in a histone demethylase and an ortholog of *teosinte branched1* (*TB1*), respectively. The *vrs4.k* mutant carries a small deletion causing a nonsense mutation in *Ra2*; and the *vrs1* mutant contains a nonsynonymous SNP in a homeobox (HOX) transcription factor (Komatsuda et al., 2007; Ramsay et al., 2011; Koppolu et al., 2013). We identified transcripts of 30,174 genes at W3.5 and W5.0 (Supplemental Table S3). When compared to cv Bowman, 146 differentially regulated transcripts (DRTs) were identified in *vrs1*, 414 in *vrs4.k*, 524 in *vrs3(int-a.1)*, and 87 in *int-c.5* (Fig. 4A; Supplemental Fig. S4). From the 524 DRTs affected in *vrs3(int-a.1)*, 426 were down-regulated, while only 98 were significantly up-regulated (Supplemental Fig. S4). The high number of repressed versus induced DRTs suggests that VRS3 acts primarily as a transcriptional activator.

To assess whether any of the DRTs identified in *vrs3(int-a.1)* were also affected in *vrs1*, *vrs4.k*, or *int-c.5* and vice versa, a hierarchical cluster analysis (Eisen et al., 1998) was performed. Hierarchical clustering of mutants based on all DRTs grouped *vrs1*, *vrs3(int-a.1)*, and *vrs4.k* together, while *int-c* clustered separately (Fig. 4B). This indicated a high overlap in DRTs among *vrs1*, *vrs3(int-a.1)*, and *vrs4.k*, while expression variation in *int-c* differed from the former. More than 50% of the genes differentially regulated in *vrs1* were also affected in *vrs4.k* and *vrs3(int-a.1)* (Fig. 4A). Among the repressed DRTs in *vrs1*, *vrs4.k*, and *vrs3(int-a.1)*, we detected several His kinases involved in cytokinin and abscisic acid signaling (Supplemental Tables S4 and S5). In addition, PIF helicases, involved in maintenance of genome stability were repressed in the *vrs3(int-a.1)*, *vrs1*, and *vrs4.k*. Furthermore, an ortholog of the Jumonji N/C and zinc finger domain-containing protein: *RELATIVE OF EARLY FLOWERING6* (*REF6*; MLOC_50345.1) was down-regulated in all three mutant genotypes. In Arabidopsis, REF6 acts as a positive regulator of flowering in a FLC-dependent pathway and may play a role in brassinosteroid signaling (Noh et al., 2004; Yu et al., 2008).

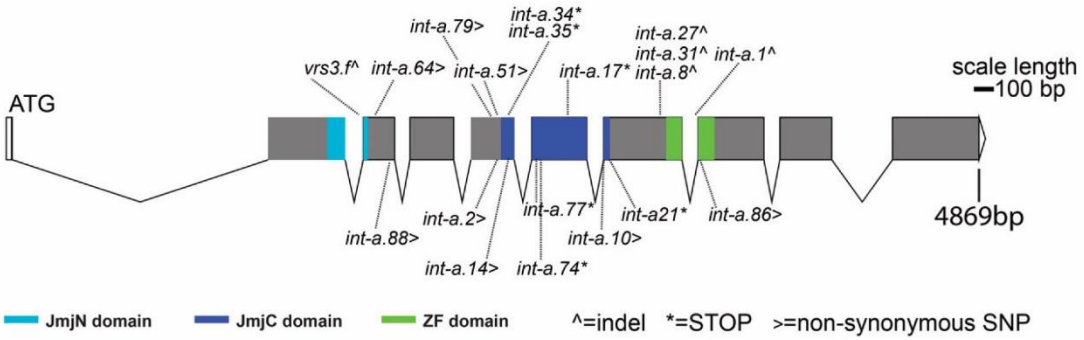

Figure 3. VRS3 is a putative histone demethylase with a Jumonji domain. Gray bars indicate the exons, and the conserved JmjN and JmjC domains are indicated in light blue and dark blue, respectively. The zinc finger (ZF) domain is indicated in green.

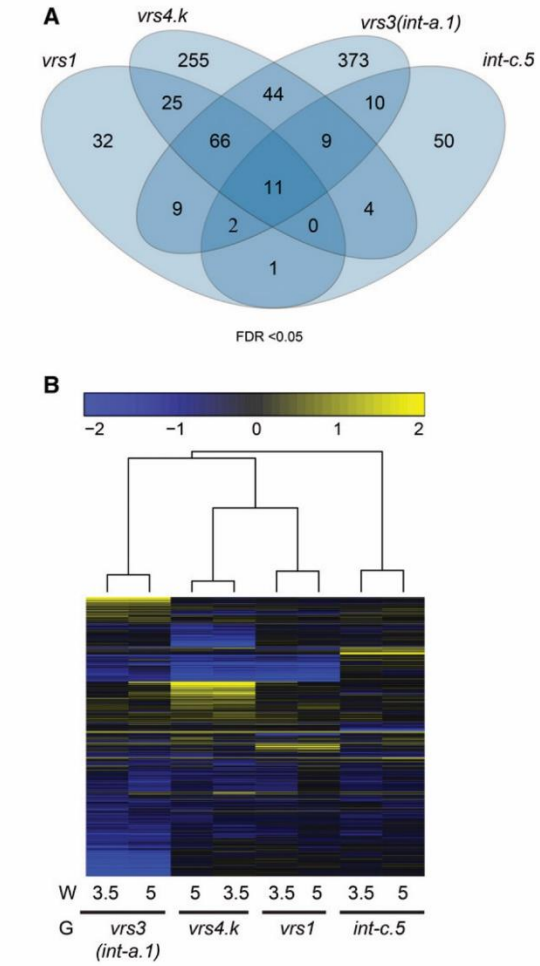

Figure 4. Transcriptional profiling of row-type mutants. A, Venn diagram showing the overlap in differentially regulated genes (FDR 5%) among *vrs1*, *vrs3(int-a)*, *vrs4.k*, and *int-c.5*. B, Hierarchical cluster analysis of all DRTs showing the expression at Waddington stages W3.5 and W5.0 for all four genotypes (G).

Interestingly, *VRS1* (AB259783.1) was down-regulated in *vrs3(int-a.1)*, *vrs4.k*, and *int-c.5*, suggesting that all three genes act as positive regulators of *VRS1* expression in barley. When compared to *VRS1*, which is specifically expressed in the developing inflorescence, *VRS3* shows a more broad expression profile throughout different tissues (Supplemental Fig. S5). RNA sequencing also showed a down-regulation of another HOX-like transcription factor (MLOC_77488.1; hereafter referred to as HOX2) in *vrs3(int-a.1)*, *vrs4.k*, and *int-c.5* (Supplemental Table S4). Taken together, the transcriptional profiling of *vrs3* MSA revealed a high number of down-regulated genes, suggesting that VRS3 is a transcriptional activator. In addition, parallel expression profiling of different row-type mutants revealed that a large subset of DRTs was shared between *vrs1*, *vrs3*, and *vrs4*. Finally, *vrs3*, *vrs4*, and *int-c* were all characterized by a quantitative down-regulation of *VRS1*.

VRS1 and *INT-C* Transcripts Are Reduced in *vrs3*

RNA sequencing revealed that the transcript levels of *VRS1* were lower in *vrs3* mutant plants. To further explore the effect of VRS3 on *VRS1*, *INT-C*, and *VRS4* expression, we performed quantitative real-time PCR (qRT-PCR) at different developmental stages from the initiation of spikelet primordia (W2.0) until early stages of pistil development (W6.0). In wild-type Bowman plants, the expression levels of *VRS1*, *VRS4*, and *INT-C* were upregulated during development to a much higher extent in the wild type compared to the *vrs3* mutant plants (Fig. 5, A–D). This suggested that VRS3 promoted the induction of *VRS1*, *VRS4*, and *INT-C*. RNA sequencing further demonstrated that the transcript levels of *VRS1* were lower in *vrs4* and *int-c* mutant plants. We, therefore, compared the effects of VRS3, VRS4, and INT-C on the expression of *VRS1* using qRT-PCR at the stamen and carpel primordium stages. Expression of *VRS1* was reduced in *vrs3*, *vrs4*, and *int-c* mutants compared to cv Bowman in both stages (Fig. 5E). However, *VRS1* expression levels differed between mutants, the *VRS1* transcript levels were lowest in the *vrs4.k* mutant, followed by *int-c.5*, *vrs3 (int-a.1)*, and *vrs3. f*. *VRS1* expression was also reduced in *vrs3* (*int-a.1)* and *vrs3* (*int-a.64)*, both in the background of cv Bonus and *vrs3 (int-a.8)* in the background of cv Foma. Consequently, we showed that all three genes, *VRS3*, *VRS4*, and *INT-C*, are positive regulators of *VRS1* expression. Interestingly, *INT-C* expression was, like *VRS1*, reduced in both *vrs4* and *vrs3*, suggesting that these genes also act on *INT-C* expression (Fig. 5F).

When *VRS4* expression was analyzed in the different *vrs* and *int-c* mutants at W3.5 and W5.0, a significant reduction of VRS4 expression was only observed in *vrs4.k* in the Bowman background (Supplemental Fig. S6A). This indicates that the effect of *vrs3* on *VRS4* expression were not consistent across stages and genetic backgrounds. Furthermore, a small but significant increase in *VRS3* expression levels was observed in the *vrs4.k* mutant (Supplemental Fig. S6B).

VRS1 is known to determine the row type and its effect is modified by INT-C (Ramsay et al., 2011). We therefore concluded that the quantitative down-regulation of *VRS1* and *INT-C* might be linked to the intermediate row-type phenotype in *vrs3* mutants (Fig. 6).

DISCUSSION

Whole-genome sequencing of allelic variants has been employed to identify candidate genes without prior mapping in model systems such as Arabidopsis and rice with relatively small genomes (Nordström et al., 2013). Because of the genome size of barley, sequencing whole genomes in multiple mutants is not

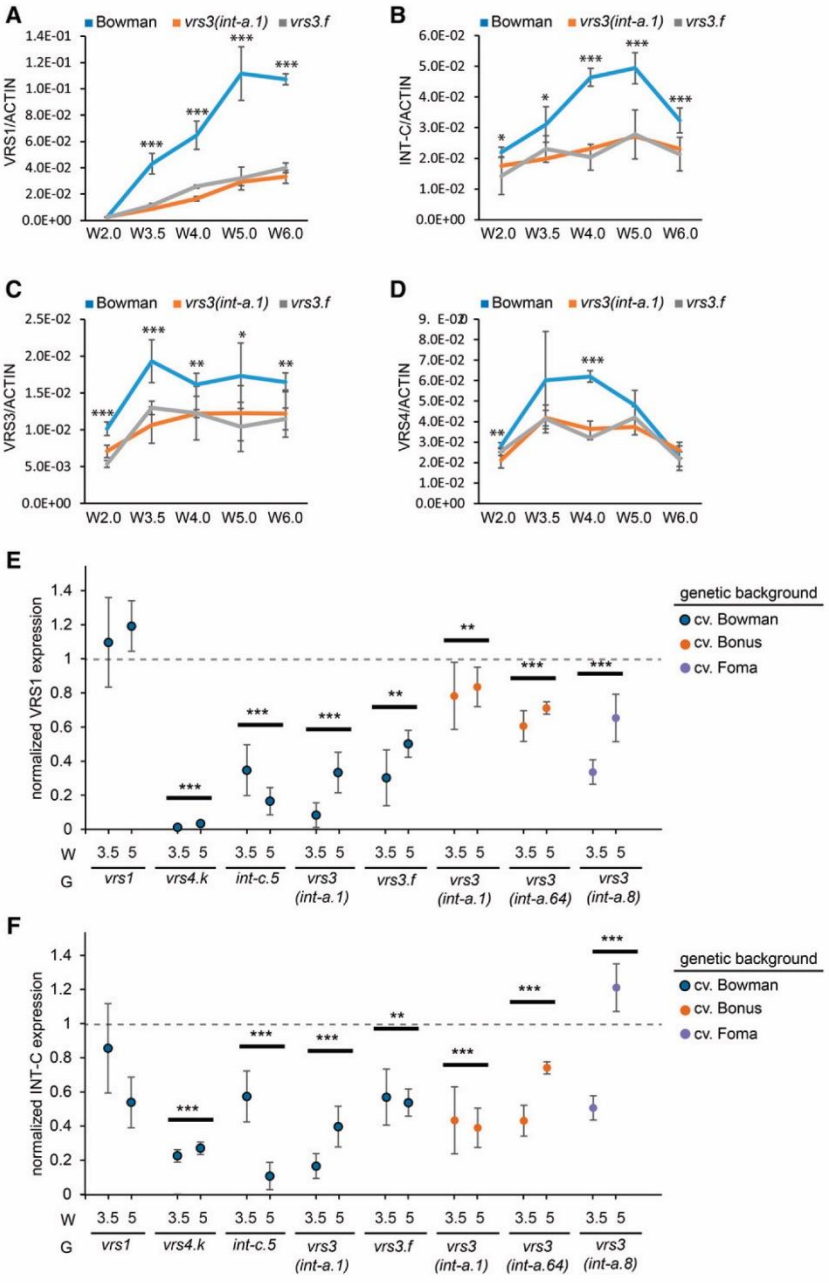

Figure 5. Expression of *VRS1*, *VRS3*, *VRS4*, and *INT-C* in wild type and *vrs3* mutant genotypes. A to D, Expression of *VRS1* (A), *INT-C* (B), *VRS3* (C), and *VRS4* (D) throughout inflorescence development determined with qRT-PCR. Error bars ± SD, $n \geq 3$ replicates. Significant differences per time point are based on a Student's *t* test (Bowman versus *vrs3(int-a.1)* and *vrs3.f* ILs). E and F, Expression of *VRS1* (E) and *INT-C* (F) in various mutant backgrounds (G) at Waddington stages W3.5 and W5.0 determined with qRT-PCR. All expression values were compared to their respective wild-type backgrounds. The gray dashed line represents the corrected value for the wild-type control. Blue dots represent expression in *vrs1*, *vrs4.k*, *int-c.5*, *vrs3(int-a.1)*, and *vrs3.f* ILs in cv Bowman. Orange dots represent expression in *vrs3(int-a.1)* and *vrs3(int-a.64)* in cv Bonus. Purple dots represent *vrs3(int-a.8)* in cv Foma. Significant differences in expression of *VRS1* or *INT-C* in the different mutants compared to the respective wild type across stages was determined using an two-factorial ANOVA with genotype (Bowman versus *vrs3(int-a.1)* and *vrs3.f* ILs) and stage as factors, followed by a post hoc Dunnett's test for multiple comparisons ($n \geq 3$ biological replicates). Asterisks indicate significant differences: $*P \leq 0.1$, $**P \leq 0.05$, $***P \leq 0.01$.

practical due to the cost and the difficulty of interpreting the large datasets. Recently, a method was presented for gene isolation in allelic barley mutants based on flow sorting and sequencing of a single chromosome that carried a known gene for the *eciferum* mutation (Sánchez-Martín et al., 2016). In addition, two stem rust resistance genes, *Sr22* and *Sr45a*, were isolated in wheat using independent ethyl methane sulfonate induced suppressor lines and sequencing of libraries enriched for nucleotide binding and Leu-rich repeats (Steuernagel et al., 2016). These methods enabled the identification of induced mutations without the need for positional fine mapping but still required prior knowledge of the chromosome position (Sánchez-Martín et al., 2016) or of the type of gene affected (Steuernagel et al., 2016). In addition, these methods are technologically and

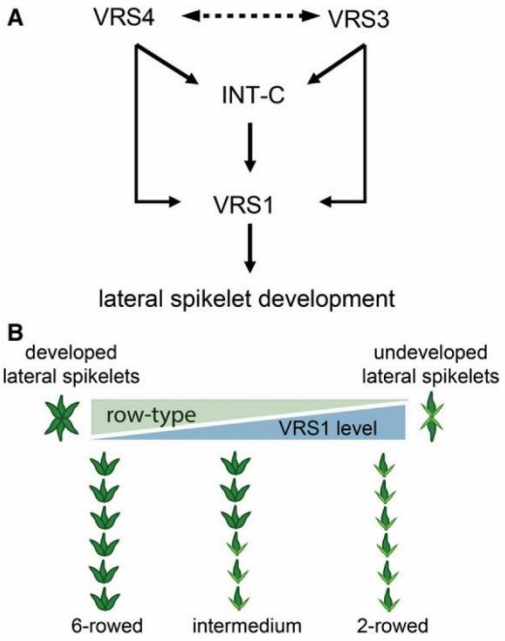

Figure 6. VRS1 expression levels affect lateral spikelet development. A, *VRS1* is significantly down-regulated in all row-type mutants. Similarly, *INT-C* is significantly down-regulated in *vrs3* and *vrs4*, indicating that the latter two act on *INT-C* expression. B, Top-down view on the triple spikelet. *VRS1* expression levels determine lateral spikelet development; in the absence of *VRS1* (*vrs1* or *vrs4* mutants) the spike is fully six-rowed. Intermedium mutants such as *vrs3* and *int-c.5* with partially developed spikelets exhibit reduced expression levels of *VRS1* when compared to the two-rowed wild type, which does not develop lateral spikelets.

computationally demanding. We instead applied RNA sequencing as a cost-efficient and simple method for gene identification without the need for mapping. The availability of allelic introgression lines enabled us to significantly reduce the target interval and thereby reduced the number of possible candidate genes. However, for the identification of the causal gene and sequence variants, we considered all polymorphic genes regardless of their genomic position. This is important when the reference sequence contains errors. It also demonstrates that our method does not rely on the availability of introgression lines or any prior mapping information. The identification of the causative mutation, however, was only possible because the target gene was expressed in the sequenced tissue and the mutation was located in the transcribed part of the gene.

Through RNA and Sanger sequencing of allelic *vrs3* mutants, we were able to identify the candidate gene underlying *vrs3* as a putative histone Lys demethylase with a conserved zinc finger and Jumonji C and N domain. Methylation on the histone H3 Lys 4 and Lys 36 (H3K4 and H3K36, respectively) is often associated with actively transcribed genes, while methylation of H3K9, H3K27, and H4K20 is associated with repressed genes (Kooistra and Helin, 2012). Thus, removal of such methylation by JmjC domain-containing proteins can lead to both transcriptional silencing and activation, respectively. The targets of histone Lys demethylases are genes with diverse functions, which is likely the reason for various developmental phenotypes in JmjC-domain protein mutants. For example, the JmjC domain-containing proteins EARLY FLOWERING6 and REF6, are involved in flowering time control in Arabidopsis (Noh et al., 2004). Moreover, JmjC-mediated histone demethylation at the *FLC* locus at elevated temperature is known to prevent premature early flowering (Gan et al., 2014). In rice, the JMJ703, a histone H3 Lys 4 (H3K4) demethylase, is required for stem elongation and transposon silencing (Chen et al., 2013; Cui et al., 2013). The barley *VRS3* is similar to the JMJD2 group II of Lys demethylases and exhibits a high similarity to the rice JMJ706, which encodes for a histone H3 Lys 9 di- and tri- (H3K9me2 and H3K9me3) demethylase (Sun and Zhou, 2008). The H3K9me2 and me3 are repressive modifications in heterochromatin and euchromatin contexts, respectively, (Liu et al., 2010), suggesting that JMJ706 is necessary for the activation of specific genes (Sun and Zhou, 2008). This scenario may hold true also for VRS3, as suggested by our expression analysis of *vrs3(int-a.1)*. Here, the group of down-regulated DRTs was about 4-fold higher when compared to the up-regulated DRTs. In the context of a putative VRS3 function, the "down-regulation" should be interpreted as absence of activation and "up-regulation" as lack of silencing in the mutant. This hypothesis was further supported by analysis of VRS1 and INT-C expression over development. The induction of both genes was strongly enhanced in the wild type compared to the *vrs3* mutant plants. Thus, we suggest that VRS3 acts as a positive regulator of gene expression, possibly by erasing the repressive methylation at histones of its target genes. How many of the genes identified as misregulated by RNA sequencing are direct targets of VRS3 is currently unknown, but INT-C and VRS1 are the prime candidates, as they showed low transcript amounts in multiple *vrs3* alleles, when compared to wild type and their mutants show similar floral phenotypes. This again leads to functional analogy with rice JMJ706, which regulates floral organ development (Sun and Zhou, 2008). In barley, loss of *VRS3* function results also in an alteration in floral organ number (Lundqvist and Lundqvist, 1988b). JMJ706 affects the histone methylation on the *degenerated hell1* locus, which encodes a putative lateral organ boundaries domain transcription factor (Sun and Zhou, 2008). In our analysis, the LOB-domain transcription factor VRS4 was not consistently down-regulated in the *vrs3* mutants. Vice versa, the *VRS3* expression was not strongly affected in the *vrs4* mutant. Previous studies have demonstrated that in *vrs4* mutants, *VRS1* is significantly down-regulated, placing *VRS4* upstream of *VRS1* (Komatsuda et al., 2007; Sakuma et al., 2013). Whereas expression of *VRS1* was not detected in the

vrs4 mutant, RNA sequencing and qRT-PCR analysis showed that *VRS1* was expressed in *vrs3* but at lower levels compared to Bowman. This could be due to only partial removal of the repressive modification(s) and subsequently weaker transcriptional change as observed for several histone demethylase mutants in Arabidopsis (Yu et al., 2008; Miura et al., 2009; Searle et al., 2010).

VRS1 expression levels in *vrs3*, *vrs4*, and *int-c* mutant genotypes suggested that variation in the development of lateral spikelet between the six-row mutants *vrs1* and *vrs4* and the intermedium mutants *vrs3* and *int-c* was mediated by quantitative variation in *VRS1* expression. No expression of *VRS1* in *vrs4* or nonfunctional *vrs1* alleles resulted in a fully six-row spike, while partial induction of *VRS1* in *vrs3* and *int-c* correlated with an intermedium spike phenotype and partial development of lateral spikelets.

Interestingly, *INT-C* expression was also significantly lower in the *vrs3* mutant. In maize, the HOX transcription factor GRASSY TILLERS1 (GT1) is downstream of TB1 and involved in the shade avoidance pathways (Whipple et al., 2011). GT1 functions mainly during vegetative growth, while VRS1 functions in inflorescence development. However, both have a similar developmental role in preventing the outgrowth of lateral buds/meristem. Therefore, we propose that, in analogy with the maize TB1 and GT1, VRS1 is downstream of INT-C in regulating lateral spikelet development. It remains to be elucidated if VRS3 affect *VRS1* directly or through the transcriptional control of *INT-C*.

CONCLUSION

We presented a fast and efficient method for gene identification with no requirement for recombination or the analysis of mapping populations. This is important when analyzing the large genomes of barley and wheat, which are characterized by extensive regions of suppressed recombination. We identified the gene underlying *vrs3* as a putative histone demethylase with a jumonji domain. Our transcriptional profiling suggested that VRS3 is a regulator of *VRS1* and *INT-C* expression, which controls lateral spikelet development. The *vrs3* locus is well known for its increased seed number per spike, an important yield component in small grain cereals. Unraveling the genetic basis of agronomic traits in crop plants is necessary to further improve crop yield.

MATERIALS AND METHODS

Plant Growth Conditions and Phenotyping

Plants were sown in 96-cell growing trays using "Mini Tray" (Einheitserde) as soil. To equalize germination, the trays were kept in the dark at 4°C for 3 days, after which the seedlings were grown under long-day conditions (16 h, 22°C day; 8 h, 18°C night). The developmental stage of the MSA of *vrs3.f*, *int-a*, *vrs1*, and *vrs4* was determined according to the quantitative scale of Waddington et al. (1983). The quantitative scale by Waddington et al. (1983) is based on the progression of the most advanced floret primordium and carpel of the inflorescence. At the double-ridge stage (W1.5–2.0), the first spikelet primordia on the shoot apex emerge; this specifies a reproductive MSA. The first lemma primordium start to develop at W3.0; at this stage the first differences between two-rowed and six-rowed *vrs* mutants start to occur (Koppolu et al., 2013). The stem elongation and differentiation of the first floral organ primordia occurs at the stamen primordium stage (W3.5). The induction of floral organ primordia continues until the awn primordium stage, which is marked by W5.0.

Plant Material

For the RNA sequencing of the mutants, near-isogenic lines in Bowman background were used. All mutants and parental lines were obtained from the U.S. Department of Agriculture (https://npgsweb.ars-grin.gov/) or from the Nordic Gene Bank (http://www.nordgen.org/). For *VRS3*, two mutants were sequenced: *vrs3.f* (GSHO 2056) and *int-a.1* (GSHO 2055), both backcrossed into the cultivar (cv) Bowman. The *vrs3.f* mutant originates from a gamma-ray-induced mutant in Hakata 2, and the *vrs3(int-a.1)* mutant from an x-ray-induced mutant in cv Bonus. For comparison of *vrs3* with other row-type genes using RNA sequencing, *vrs1*, *vrs4*, and *int-c* mutants were used. The *vrs1* mutant (GSHO 1907), which is a naturally occurring variant in most six-rowed barleys (Druka et al., 2011), has a C 1020 G, resulting in a non-synonymous F075L change. The gamma-ray-induced *vrs4.k* mutant (GSHO 1986) has a C 072 deletion, resulting in a nonsense mutation. The x-ray-induced *int-c.5* mutant (GSHO 2003) carries a C 882 deletion causing a frame shift. These lines were also used for qRT-PCR confirmation. In addition, the *vrs3* mutants *int-a.1* (NGB115419), *int-a.64* (NGB115482), and *int-a.8* (NGB115426) were used to verify down-regulation of *VRS1* and *INT-C* using qRT-PCR. The *int-a.64* originates from an isopropyl methanesulfonate mutagenesis in cv Bonus, and *int-a.8* is an x-ray-induced mutant in cv Foma. The stock numbers and mutagenic agents of the 19 different allelic *vrs3* lines used to verify the selected candidate gene are listed in Supplemental Table S1.

RNA Isolation and Sample Preparation for RNA Sequencing

RNA was isolated from tissue of the MSA harvested from plants grown under long day conditions (16 h, 22°C day; 8 h, 18°C night). MSA tissue was harvested at W3.0 to W3.5 for *vrs3.f* and *vrs3*(*int-a.1*). For *vrs1*, *vrs4.k*, *vrs3*(*int-a.1*), and *int-c.5*, apex tissue was isolated at W3.5 and W5.0. The samples were harvested at the middle of the day, 6 to 8 h before the end of the light period. Before sampling, the developmental stage of the MSA was verified by dissecting three plants per genotype. For sampling the apex, leaves surrounding the MSA were removed manually, and the apex was cut using a microsurgical stab knife (5-mm blade at 15° [SSC#72-1551]). Samples were collected in three individual biological replicates. For each biological replicate, at least 10 MSA were pooled. All MSA harvested for RNA extraction were frozen immediately in liquid nitrogen and stored at −80°C. For RNA isolation, the pooled MSA were ground, dissolved in 500 μL TRIzol reagent (Invitrogen), and incubated for 5 min at room temperature. Next, 100 μL of chloroform was added, and the sample was homogenized, incubated for 2 min, and centrifuged for 15 min at 4°C. After phase separation, isopropanol was added to the aqueous phase, which was subsequently incubated for 10 min at room temperature and further purified using an RNA easy Micro Kit (Qiagen). Before RNA sequencing, the residual DNA was removed using a DNA-free kit (Ambion), and the quality of the RNA was tested using a bio analyzer (Agilent). The Illumina cDNA libraries were prepared according to the TruSeq RNA sample preparation (version 2; Illumina). A cBot (Illumina) was used for clonal sequence amplification and generation of sequence clusters. Single-end sequencing was performed using a HiSeq 2500 (Illumina) platform by multiplexing eight libraries, resulting in ~18 million reads per library. The initial quality control of the raw reads was performed using the FastQC software (version 0.10.1; https://www.bioinformatics.babraham.ac.uk/projects/fastqc/). The adaptors and short reads were trimmed using the Trimmomatic platform and embedded within the trinity pipeline (Grabherr et al., 2011; https://github.com/trinityrnaseq/trinityrnaseq/wiki) using the following default criteria: phred 33, leading and trailing 3, sliding window 4:15, and a minimum read length of 36.

Variant Calling of the RNA Sequencing Reads

The obtained RNA sequencing reads were mapped to a combined set of HC and LC predicted coding sequences of barley (*Hordeum vulgare*) cv Morex (IBGC, 2012) with BWA-MEM (version 0.7.15; Li, 2013). To ensure a high mapping rate even if distantly related barley cultivars are used, a mismatch penalty of 3 was used. PicardTools (version 1.1.00; http://broadinstitute.github.io/picard/) CollectAlignmentSummaryMetrics was applied on resulting SAM files for

evaluation of mappings, and the number of reads mapped with good mapping quality scores (MAPQ > 1) were determined with SAMtools (version 1.1.3; Li et al., 2009). Mapping quality scores indicates the confidence of alignments and uniqueness of the mapping position in the reference with higher values indicating a higher mapping quality. SAM to BAM format conversion was performed with SAMtools, excluding read alignments with a relatively low MAPQ smaller than 1 to maximize the number of mapped reads. Read duplicates were removed with PicardTools MarkDuplicates, and INDEL realignment was performed with GATK (version 3.1-1; McKenna et al., 2010) IndelRealigner to reduce the number of false-positive SNP calls. Resulting alignments were subjected to variant calling with GATK Unifiedgenotyper with a minimum confidence threshold for calling of 30.0 and for emitting of called SNPs of 10.0. Predicted SNP candidates were filtered with GATK Variantfiltration with following thresholds: FS > 30.0, QD < 2.0, MQRankSum < −12.5, ReadPosRankSum < −8.0. Filtered variants with a depth of coverage > 4 and a genotype quality > 30 were taken into consideration, and only homozygous SNPs were of interest in this study. Conserved domains were assigned to HC and LC genes using the NCBI Conserved Domain Database (Marchler-Bauer et al., 2015). The selected candidate was verified using Sanger sequencing on DNA obtained from 19 independent allelic *vrs3/int-a* mutants. The DNA was extracted from freeze-dried leaf material using the Qiagen BioSprint (Qiagen) according to manufacturer's protocol. Fragments for Sanger sequencing were amplified using the primers enlisted in Supplemental Table S6.

Transcriptional Profiling

For transcriptome analysis, we used a combined set of HC and LC predicted coding sequences of barley cv Morex (International Barley Genome Sequencing Consortium, 2012) as reference. Alignment of the reads to the reference was done using BWA-MEM using the same settings as applied for the variant calling. Transcripts per million values were extracted from the BWA-aligned reads using Salmon (Patro et al., 2017). Transcripts with expression levels greater than three counts in three libraries were retained. Tables with raw and normalized transcripts per million values and expression levels are provided as supplemental tables (Supplemental Tables S3 and S4). Differentially regulated reads were called using the R bioconductor package Limma-vroom using a Benjamin & Hochberg adjustment for multiple testing (false discovery rate) for calculation of the adjusted *P* values (FDR values; Ritchie et al., 2015). For expression analysis, an FDR value of 0.05 was used as initial cut-off value for the selection of DRTs. DRTs were extracted per mutant per developmental stage as well as the overall effect, which encompasses all transcripts affected in both W3.5 and W5.0 (Supplemental Fig. S4). Hierarchical cluster analysis was done in R using Pearson correlation coefficients. The overrepresentation analysis of particular GO terms was performed using the R-package TopGo (Alexa et al., 2006). All Venn diagrams were drawn using the R package VennDiagram (Chen and Boutros, 2011).

Results obtained for VRS1(AB259783.1), VRS3(MLOC_69611.1), VRS4 (KC854554), and INT-C(MLOC_70116.1) were verified by performing qRT-PCR using gene-specific primers (Supplemental Table S6). Primer sequences for Hv.ACTIN (AY145451), which was used as control, were used as previously described (Ejaz and von Korff, 2017); VRS4 primers were obtained from Koppolu et al. (2013). MSA tissue of cv Bowman and derived mutant lines *vrs3.f* and *vrs3 (int-a.1)* were harvested at the Waddington stages W2.0, W3.5, W4.0, W5.0, and W6.0 to analyze changes in the expression of *VRS1*, *VRS3*, *VRS4*, and *INT-C* during development. Samples were collected in three individual biological replicates. For each biological replicate, at least 10 MSA were pooled. In addition, MSA tissue was harvested in two to three biological replicates at W3.0 to W3.5 and W5.0 for *vrs1*, *vrs4*, *int-c vrs3.f*, and *vrs3(int-a.1)* mutants in cv Bowman; *vrs3(int-a.1)* and *vrs3(int-a.64)* in cv Bonus; and *vrs3(int-a.8)* in Foma background. The samples were harvested at the middle of the day, 6 to 8 h before the end of the light period. Before sampling, the developmental stage of the MSA was verified by dissecting three plants per genotype. RT-PCR and cDNA synthesis was performed as previously described (Ejaz and von Korff, 2017). Quantification was based on the titration curve for each target gene and normalized against *HvACTIN* as internal control using the LightCycler 480 Software (Roche; version 1.5). Statistical differences were either calculated with a Student's *t* test or a two-factorial ANOVA with genotype and stage as factors, followed by a post hoc Dunnett's test for multiple comparison.

Phylogenetic Analysis

The amino acid sequences of proteins annotated as JmjC domain-containing proteins from barley (*H. vulgare*), rice (*Oryza. sativa*), and Arabidopsis (*Arabidopsis thaliana*) were downloaded from the iTAK database 16.03 (Zheng et al., 2016). A multiple sequence alignment of the retrieved JmjC domain-containing proteins was performed using ClustalO with default parameters (Sievers et al., 2011). The resulting alignment was converted to Phylip format using Alter (Glez-Peña et al., 2010). RAxML 8.2.10 was used to generate a maximum likelihood tree with fixed base frequencies, the GAMMA model, and "autoMRE" as parameter to calculate the optimal number bootstrap repeats (Stamatakis et al., 2008). The automatically determined substitution model was chosen as the "VT" substitution model. The unrooted tree was visualized using Dendroscope 3 (Huson and Scornavacca, 2012), and classification into evolutionary conserved groups was manually performed according to Klose et al. (2006). The JmjC domains of the barley VRS3 protein, and the closest orthologs in rice (JMJ706) and Arabidopsis (JMJ13) were obtained from the NCBI conserved domain database (Marchler-Bauer and Bryant, 2004). ClustalO was used to align and to calculate the pairwise percent identity of the conserved JmjC domains of VRS3, Os.JMJ706, and At.JMJ13 with default settings (Sievers et al., 2011).

Supplemental Data

The following supplemental materials are available.

Supplemental Figure S1. Spike phenotypes of *vrs3*, *vrs1*, *vrs4*, and *int-c* in cv Bowman.

Supplemental Figure S2. Introgression locations of *vrs1*, *vrs4*, and *int-c* in cv Bowman.

Supplemental Figure S3. Phylogenetic relationship of proteins with JmjC domains.

Supplemental Figure S4. Differentially regulated transcripts in *vrs1*, *vrs3*, *int-a.1*, and *int-c.5*.

Supplemental Figure S5. Expression of *VRS3* compared to *INT-C* and *VRS1*.

Supplemental Figure S6. Expression of *VRS3* and *VRS4* determined with qRT-PCR.

Supplemental Table S1. Variants identified in independent *vrs3/int-a* mutants.

Supplemental Table S2. Percentage identity matrix and alignment of the jmjC domains of VRS3, Os.JMJ706, and At.JMJ13.

Supplemental Table S3. All transcripts expressed at W3.5 and W5.0.

Supplemental Table S4. Differentially regulated transcripts in *vrs1*, *vrs3(int-a.1)*, *vrs4.k*, and *int-c.5*.

Supplemental Table S5. GO overrepresentation analysis of genes differentially regulated in the row-type mutants.

Supplemental Table S6. Primers used for in this study.

Supplemental File S1. Variants_VRS3.vcf.

ACKNOWLEDGMENTS

We thank Caren Dawidson, Andrea Lossow, and Kerstin Luxa for excellent technical assistance in the laboratory and greenhouse. Artem Pankin is acknowledged for critically reading this manuscript and performing the phylogenetic analysis.

Received January 30, 2017; accepted June 25, 2017; published June 27, 2017.

LITERATURE CITED

Ahloowalia BS, Maluszynski M, Nichterlein K (2004) Global impact of mutation-derived varieties. Euphytica **135:** 187–204

Alexa A, Rahnenfuhrer J, Lengauer T (2006) Improved scoring of functional groups from gene expression data by decorrelating GO graph structure. Bioinformatics **22:** 1600–1607

Chen H, Boutros PC (2011) VennDiagram: a package for the generation of highly-customizable Venn and Euler diagrams in R. BMC Bioinformatics **12:** 35

Chen Q, Chen X, Wang Q, Zhang F, Lou Z, Zhang Q, Zhou DX (2013) Structural basis of a histone H3 lysine 4 demethylase required for stem elongation in rice. PLoS Genet **9:** e1003239

Cui X, Jin P, Cui X, Gu L, Lu Z, Xue Y, Wei L, Qi J, Song X, Luo M, An G, Cao X (2013) Control of transposon activity by a histone H3K4 demethylase in rice. Proc Natl Acad Sci USA **110:** 1953–1958

Druka A, Franckowiak J, Lundqvist U, Bonar N, Alexander J, Houston K, Radovic S, Shahinnia F, Vendramin V, Morgante M, Stein N, Waugh R (2011) Genetic dissection of barley morphology and development. Plant Physiol **155:** 617–627

Eisen MB, Spellman PT, Brown PO, Botstein D (1998) Cluster analysis and display of genome-wide expression patterns. Proc Natl Acad Sci USA **95:** 14863–14868

Ejaz M, von Korff M (2017) The genetic control of reproductive development under high ambient temperature. Plant Physiol **173:** 294–306

Gan ES, Xu Y, Wong JY, Goh JG, Sun B, Wee WY, Huang J, Ito T (2014) Jumonji demethylases moderate precocious flowering at elevated temperature via regulation of FLC in Arabidopsis. Nat Commun **5:** 5098

Grabherr MG, Haas BJ, Yassour M, Levin JZ, Thompson DA, Amit I, Adiconis X, Fan L, Raychowdhury R, Zeng Q, et al (2011) Trinity: reconstructing a full-length transcriptome without a genome from RNA-seq data. Nat Biotechnol **29:** 644–652

Gustafsson A, Lundqvist U (1980) Hexastichon and intermedium mutants in barley. Hereditas **92:** 229–236

Huson DH, Scornavacca C (2012) Dendroscope 3: an interactive tool for rooted phylogenetic trees and networks. Syst Biol **61:** 1061–1067

International Barley Genome Sequencing Consortium (2012) A physical, genetic and functional sequence assembly of the barley genome. Nature **491:** 711–716

James GV, Patel V, Nordström KJ, Klasen JR, Salomé PA, Weigel D, Schneeberger K (2013) User guide for mapping-by-sequencing in Arabidopsis. Genome Biol **14:** R61

Klose RJ, Kallin EM, Zhang Y (2006) JmjC-domain-containing proteins and histone demethylation. Nat Rev Genet **7:** 715–727

Komatsuda T, Pourkheirandish M, He C, Azhaguvel P, Kanamori H, Perovic D, Stein N, Graner A, Wicker T, Tagiri A, Lundqvist U, Fujimura T, et al (2007) Six-rowed barley originated from a mutation in a homeodomain-leucine zipper I-class homeobox gene. Proc Natl Acad Sci USA **104:** 1424–1429

Kooistra SM, Helin K (2012) Molecular mechanisms and potential functions of histone demethylases. Nat Rev Mol Cell Biol **13:** 297–311

Koppolu R, Anwar N, Sakuma S, Tagiri A, Lundqvist U, Pourkheirandish M, Rutten T, Seiler C, Himmelbach A, Ariyadasa R, Youssef HM, Stein N, et al (2013) Six-rowed spike4 (Vrs4) controls spikelet determinacy and row-type in barley. Proc Natl Acad Sci USA **110:** 13198–13203

Langmead B, Salzberg SL (2012) Fast gapped-read alignment with Bowtie 2. Nat Methods **9:** 357–359

Li H (2013) Aligning sequence reads, clone sequences and assembly contigs with BWA-MEM. arXiv 1303.3997

Li H, Handsaker B, Wysoker A, Fennell T, Ruan J, Homer N, Marth G, Abecasis G, Durbin R; 1000 Genome Project Data Processing Subgroup (2009) The Sequence Alignment/Map format and SAMtools. Bioinformatics **25:** 2078–2079

Liller CB, Neuhaus R, von Korff M, Koornneef M, van Esse W (2015) Mutations in barley row type genes have pleiotropic effects on shoot branching. PLoS One **10:** e0140246

Liller CB, Walla A, Boer MP, Hedley P, Macaulay M, Effgen S, von Korff M, van Esse GW, Koornneef M (2017) Fine mapping of a major QTL for awn length in barley using a multiparent mapping population. Theor Appl Genet **130:** 269–281

Liu C, Lu F, Cui X, Cao X (2010) Histone methylation in higher plants. Annu Rev Plant Biol **61:** 395–420

Lundqvist U (2014) Scandinavian mutation research in barley - a historical review. Hereditas **151:** 123–131

Lundqvist U, Abebe B, Lundqvist A (1988a) Gene interaction of induced intermedium mutations of two-row barley. II. Interaction between the *hex-v* gene and *int* genes. Hereditas **109:** 197–204

Lundqvist U, Abebe B, Lundqvist A (1988b) Gene interaction of induced intermedium mutations of two-row barley. III. Overlapping in dihybrid F2 classification patterns in combinations of recessive *int* genes. Hereditas **109:** 205–214

Lundqvist U, Lundqvist A (1987) An *intermedium* gene present in a commercial six-row variety of barley. Hereditas **107:** 131–135

Lundqvist U, Lundqvist A (1988a) Gene interaction of induced *intermedium* mutations of two-row barley. I. Double mutant recombinants. Hereditas **108:** 133–140

Lundqvist U, Lundqvist A (1988b) Induced *intermedium* mutants in barley: Origin, morphology and inheritance. Hereditas **108:** 13–26

Marchler-Bauer A, Bryant SH (2004) CD-Search: Protein domain annotations on the fly. Nucleic Acids Res **32:** W327–W331

Marchler-Bauer A, Derbyshire MK, Gonzales NR, Lu S, Chitsaz F, Geer LY, Geer RC, He J, Gwadz M, Hurwitz DI, Lanczycki CJ, Lu F, et al. (2015) CDD: NCBI's conserved domain database. Nucleic Acids Res **43:** D222–D226

Mayer KF, Waugh R, Brown JW, Schulman A, Langridge P, Platzer M, Fincher GB, Muehlbauer GJ, Sato K, Close TJ, Wise RP, Stein N; International Barley Genome Sequencing Consortium (2012) A physical, genetic and functional sequence assembly of the barley genome. Nature **491:** 711–716

McKenna A, Hanna M, Banks E, Sivachenko A, Cibulskis K, Kernytsky A, Garimella K, Altshuler D, Gabriel S, Daly M, DePristo MA (2010) The Genome Analysis Toolkit: a MapReduce framework for analyzing next-generation DNA sequencing data. Genome Res **20:** 1297–1303

Miura A, Nakamura M, Inagaki S, Kobayashi A, Saze H, Kakutani T (2009) An Arabidopsis jmjC domain protein protects transcribed genes from DNA methylation at CHG sites. EMBO J **28:** 1078–1086

Noh B, Lee SH, Kim HJ, Yi G, Shin EA, Lee M, Jung KJ, Doyle MR, Amasino RM, Noh YS (2004) Divergent roles of a pair of homologous jumonji/zinc-finger-class transcription factor proteins in the regulation of Arabidopsis flowering time. Plant Cell **16:** 2601–2613

Nordström KJ, Albani MC, James GV, Gutjahr C, Hartwig B, Turck F, Paszkowski U, Coupland G, Schneeberger K (2013) Mutation identification by direct comparison of whole-genome sequencing data from mutant and wild-type individuals using k-mers. Nat Biotechnol **31:** 325–330

Pankin A, Campoli C, Dong X, Kilian B, Sharma R, Himmelbach A, Saini R, Davis SJ, Stein N, Schneeberger K, von Korff M (2014) Mapping-by-sequencing identifies HvPHYTOCHROME C as a candidate gene for the early maturity 5 locus modulating the circadian clock and photoperiodic flowering in barley. Genetics **198:** 383–396

Patro R, Duggal G, Love MI, Irizarry RA, Kingsford C (2017) Salmon provides fast and bias-aware quantification of transcript expression. Nat Methods **14:** 417–419

Ramsay L, Comadran J, Druka A, Marshall DF, Thomas WT, Macaulay M, MacKenzie K, Simpson C, Fuller J, Bonar N, Hayes PM, Lundqvist U, et al. (2011) INTERMEDIUM-C, a modifier of lateral spikelet fertility in barley, is an ortholog of the maize domestication gene TEOSINTE BRANCHED 1. Nat Genet **43:** 169–172

Glez-Peña D, Gómez-Blanco D, Reboiro-Jato M, Fdez-Riverola F, Posada D (2010) ALTER: program-oriented conversion of DNA and protein alignments. Nucleic Acids Res **38:** W14-8

Ritchie ME, Phipson B, Wu D, Hu Y, Law CW, Shi W, Smyth GK (2015) *limma* powers differential expression analyses for RNA-sequencing and microarray studies. Nucleic Acids Res **43:** e47

Sakuma S, Pourkheirandish M, Hensel G, Kumlehn J, Stein N, Tagiri A, Yamaji N, Ma JF, Sassa H, Koba T, Komatsuda T (2013) Divergence of expression pattern contributed to neofunctionalization of duplicated HD-Zip I transcription factor in barley. New Phytol **197:** 939–948

Sánchez-Martín J, Steuernagel B, Ghosh S, Herren G, Hurni S, Adamski N, Vrána J, Kubaláková M, Krattinger SG, Wicker T, Doležel J, Keller B, et al (2016) Rapid gene isolation in barley and wheat by mutant chromosome sequencing. Genome Biol **17:** 221

Schneeberger K, Ossowski S, Lanz C, Juul T, Petersen AH, Nielsen KL, Jørgensen JE, Weigel D, Andersen SU (2009) SHOREmap: simultaneous mapping and mutation identification by deep sequencing. Nat Methods **6:** 550–551

Sievers F, Wilm A, Dineen D, Gibson TJ, Karplus K, Li W, Lopez R, McWilliam H, Remmert M, Söding J, Thompson JD, Higgins DG (2011) Fast, scalable generation of high-quality protein multiple sequence alignments using Clustal Omega. Mol Syst Biol **7:** 539

Searle IR, Pontes O, Melnyk CW, Smith LM, Baulcombe DC (2010) JMJ14, a JmjC domain protein, is required for RNA silencing and cell-to-cell movement of an RNA silencing signal in Arabidopsis. Genes Dev **24:** 986–991

Stamatakis A, Hoover P, Rougemont J (2008) A rapid bootstrap algorithm for the RAxML Web servers. Syst Biol **57:** 758–771

Steuernagel B, Periyannan SK, Hernández-Pinzón I, Witek K, Rouse MN, Yu G, Hatta A, Ayliffe M, Bariana H, Jones JD, Lagudah ES, Wulff BB (2016) Rapid cloning of disease-resistance genes in plants using mutagenesis and sequence capture. Nat Biotechnol **34:** 652–655

Studer AJ, Doebley JF (2011) Do large effect QTL fractionate? A case study at the maize domestication QTL teosinte branched1. Genetics **188:** 673–681

Studer A, Zhao Q, Ross-Ibarra J, Doebley J (2011) Identification of a functional transposon insertion in the maize domestication gene tb1. Nat Genet **43:** 1160–1163

Sun Q, Zhou DX (2008) Rice jmjC domain-containing gene JMJ706 encodes H3K9 demethylase required for floral organ development. Proc Natl Acad Sci USA **105:** 13679–13684

Trick M, Adamski NM, Mugford SG, Jiang CC, Febrer M, Uauy C (2012) Combining SNP discovery from next-generation sequencing data with bulked segregant analysis (BSA) to fine-map genes in polyploid wheat. BMC Plant Biol **12:** 14

Waddington SR, Cartwright PM, Wall PC (1983) A quantitative scale of spike initial and pistil development in barley and wheat. Ann Bot **51:** 119–130

Whipple CJ, Kebrom TH, Weber AL, Yang F, Hall D, Meeley R, Schmidt R, Doebley J, Brutnell TP, Jackson DP (2011) *grassy tillers1* promotes apical dominance in maize and responds to shade signals in the grasses. Proc Natl Acad Sci USA **108:** E506–E512

Yu X, Li L, Li L, Guo M, Chory J, Yin Y (2008) Modulation of brassinosteroid-regulated gene expression by Jumonji domain-containing proteins ELF6 and REF6 in Arabidopsis. Proc Natl Acad Sci USA **105:** 7618–7623

Zheng Y, Jiao C, Sun H, Rosli HG, Pombo MA, Zhang P, Banf M, Dai X, Martin GB, Giovannoni JJ, Zhao PX, Rhee SY, et al. (2016) iTAK: A program for genome-wide prediction and classification of plant transcription factors, transcriptional regulators, and protein kinases. Mol Plant **9:** 1667–1670

4 *Many noded dwarf1* (*MND1*) Is an Acyl-CoA N-acyltransferase That Regulates Inflorescence Architecture and Shoot Branching in Barley

This chapter is a manuscript in preparation for submission.

Authors:

Agatha Walla [a,b,c], G. Wilma van Esse [d], Gwendolyn K. Kirschner [b], Rüdiger Simon [b], Maria von Korff [a,b,c]

Affiliations:

[a]Department of Plant Breeding and Genetics, Max Planck Institute for Plant Breeding Research, 50829 Köln, Germany

[b]Institute for Plant Genetics, Heinrich-Heine-Universität Düsseldorf, 40225 Düsseldorf, Germany

[c]Cluster of Excellence in Plant Sciences, Heinrich-Heine-Universität Düsseldorf, 40255 Düsseldorf, Germany

[d]Laboratory for Molecular biology, Wageningen University and Research, 6708 PB Wageningen, The Netherlands

Contributions:

Agatha Walla, G. Wilma van Esse, Rüdiger Simon and Maria von Korff conceived and designed the experiments. Agatha Walla and G. Wilma van Esse performed the field experiments. Agatha Walla conducted the phenotypic analysis. Agatha Walla and G. Wilma van Esse conducted the RNA sequencing experiment and Agatha Walla and G. Wilma van Esse analyzed the data. Allelism tests, gene resequencing, qPCR experiments and phylogenetic analysis were performed by Agatha Walla. Gwendolyn K. Kirschner conducted the in-situ hybridization and protein localization experiments. Agatha Walla wrote the manuscript with help from G. Wilma van Esse and Maria von Korff.

4.1 Abstract

Shoot architecture in cereal crops is determined by tillering (shoot branching) and spike morphology, both of which are major determinants of yield. However, the molecular control of shoot architecture during development remains poorly understood in the temperate cereal crops barley and wheat. Here, we show that the barley high-tillering mutant *many noded dwarf1* (*mnd1.a*) is characterized by pleiotropic changes in tillering, plant height, leaf number and size and inflorescence morphology. The increased tillering phenotype correlated with the supernumerary production of phytomers which were initiated during the extended vegetative growth phase of *mnd1.a*. After the induction of spikelet primordia, cryptic bracts on the inflorescences grew into leaf-like organs coinciding with the reversion of floral meristems to branch meristems. Our analysis suggests that *mnd1.a* is a heterochronic mutant with a prolonged juvenile phase which overlaps with the adult reproductive phase. Using a mapping by RNA sequencing approach, we found that the *HvMND1* gene encodes an acyl-CoA N-acyltransferase which is predominately expressed in developing axillary meristems and young developing inflorescences. Exploration of the expression network modulated by *HvMND1* revealed the differential expression of many key developmental genes, including MADS-box transcription factors, phase transition genes, such as *LEAFY* and *TERMINAL FLOWER1*, and genes of the cell cycle machinery. Our data suggest that *HvMND1* plays a significant role in the coordinated regulation of phase transition by promoting reproductive growth, thus governing the overall shoot architecture of barley and impacting crop yield.

4.2 Introduction

Shoot architecture, which encompasses all above-ground organs including the number and location of branches, is essential for the function, diversification and fitness of plants. During the Green Revolution, the modification of shoot architecture in cereals such as wheat, barley and rice resulted in a massive increase in grain yield (Hedden, 2003). This achievement was only possible through selective breeding for alleles that modified traits such as plant height and stem thickness, which resulted in the development of lodging-resistant semi-dwarf plants (Peng et al., 1999; Spielmeyer et al., 2002). To date, shoot architecture remains one of the most important yield components targeted for crop improvement in cereals, but the molecular basis is not well understood.

The development of the shoot is controlled by the shoot apical meristem (SAM), which gives rise to all above-ground organs including inflorescences and tillers, the grain-bearing branches of monocots. During vegetative growth, the SAM initiates leaf primordia on its flanks, which later develop into leaves connected to the stem via a node, comprising a phytomeric unit (McMaster, 2005). In most grasses, axillary meristems (AMs) are initiated in the leaf axils of un-elongated internodes at the plant base (Oikawa and Kyozuka, 2009; Kebrom et al., 2013). Generally, the AMs have the same developmental potential as the SAM and therefore may develop into secondary branches. First, an AM develops into an axillary bud (AB) which subsequently either remains dormant or grows out to form a secondary tiller, including its leaves, stem, the inflorescence, and a succession of tertiary tillers (Schmitz and Theres, 2005). Hence, tiller development is regulated at three different steps: at the initiation of AMs in the leaf axil, during the formation of ABs via the development of the meristem-protecting prophyll, and as ABs grow out to form tillers (Doust, 2007). The initiation and outgrowth of shoot branches are controlled by a complex regulatory network including genetic, hormonal and environmental factors, which have been well studied in several plants species including *Arabidopsis thaliana*, tomato and rice (reviewed by Schmitz and Theres, 1999; Domagalska and Leyser, 2011; Liang et al., 2014). For example, the establishment of axil identity in Arabidopsis is regulated by genes such as *CUP-SHAPED COTELYDON* (*CUC*) *1–3* (Aida et al., 1999; Takada et al., 2001; Vroemen et al., 2003) and *LATERAL ORGAN BOUNDERIES* (*LOB*) (Shuai et al., 2002). In addition, the maintenance of meristem formation in both Arabidopsis and tomato is governed by the *LATERAL SUPPRESSOR* (*LAS*) gene (Schumacher et al., 1999; Greb et al., 2003). In the model monocot species rice *MONOCULM1* (*MOC1*), an ortholog of *LAS* with generally conserved function, is a major regulator of tiller development (Li et al., 2003). Loss-of-function mutations in *MOC1* result in rice plants that develop only the main culm without any tillers. Major branch developmental genes such as the rice homeobox gene *OSH1* and *FINE CULM 1* (*FC1*), an ortholog of maize *TEOSINTE BRANCHED1* (*TB1*), are downstream targets of MOC1. *OSH1* is a marker of indeterminate cells in rice and a homolog of Arabidopsis *SHOOT MERISTEMLESS* (*STM*) and *KNOTTED1* in maize (Jackson et al., 1994; Long et al., 1996). *TB1*, which encodes a class II Teosinte branched1/Cincinnata/proliferating cell factor (TCP)-domain transcription factor, was originally

identified as a major domestication-related gene in maize (Doebley et al., 1997). *TB1* and its homologs in other species like Arabidopsis *BRANCHED1* (*BRC1*) and *BRC2* (Aguilar-Martinez et al., 2007), rice *FC1* (Takeda et al., 2003), barley *INTERMEDIUM-C* (*INT-C*) (Ramsay et al., 2011) and sorghum *SbTB1* (Kebrom et al., 2006) encode regulators that can inhibit bud outgrowth dependent on hormonal and environmental cues. However, *TB1* not only regulates shoot branching in grasses, but also inflorescence development (Lewis et al., 2008; Ramsay et al., 2011; Choi et al., 2012). Unlike *MOC1* and *TB1*, there are also several genes that do not show a conserved function in the regulation of AM initiation and AB outgrowth. For example, the maize *BARREN STALK FASTIGIATE1* (*BAF1*) gene, encoding a putative transcriptional regulator with an AT-hook binding motif, is thought to be involved in chromatin remodeling with no clear ortholog in Arabidopsis (Gallavotti et al., 2011). *BAF1* plays a role in not only AM initiation, but also demarcates the boundary region of the developing AM. Taken together, targeting genes that control shoot branching is not straightforward because they are only partially conserved between species and often exhibit pleiotropic effects on other traits such as inflorescence development.

Despite major progress towards the identification of genes regulating AM initiation and outgrowth in model species like Arabidopsis and rice, our knowledge of the genetic mechanisms controlling shoot branching in barley is still fragmented. The discovery of genes regulating these traits is facilitated by the large collection of monofactorial recessive mutations, many of which have been backcrossed to the cultivar Bowman to generate near isogenic lines (Bossinger et al., 1992; Franckowiak et al., 1996). These collections contain many mutants with altered tiller number and represent a valuable resource to the detection of the underlying genes. For example, the mutant phenotype of the *low number of tillers1* (*lnt1*) mutation, with a reduced tiller and seed number per spike, encodes the BELL-like homeodomain transcription factor JuBel2 (Dabbert et al., 2010). A high-tillering phenotype accompanied by small spikes harboring fewer and smaller seeds was described for the *many noded dwarf6* (*mnd6*) mutant (Bregitzer et al., 2014; Mascher et al., 2014). The *mnd6* mutation corresponds to the deletion of an entire gene encoding a cytochrome P450 enzyme (Mascher et al., 2014). Furthermore, the gene corresponding to the *semi-brachytic1* (*uzu1*) mutant was identified as a brassinosteroid hormone receptor, orthologous to the Arabidopsis *BRASSINOSTEROID-INSENSITIVE1* gene (Chono et al., 2003). However, further studies are required to identify candidate genes representing the tillering mutant collection to understand the genetic regulatory networks that coordinate shoot architecture in barley.

Here we characterized the pleiotropic phenotype of allelic barley high-tillering mutant plants. We demonstrate that these mutants are altered in the timing of vegetative and reproductive phase transitions, the number of leaves, tillers, and nodes and inflorescence morphology. We applied a mapping by RNA sequencing approach to identify *HvMND1*, an acyl-CoA N-acyltransferase, underlying the *mnd1.a* locus. We characterized the expression profile in the *mnd1.a* mutant to gain insight into its potential role in the developmental regulation of shoot architecture and recorded that HvMND1 function modulates networks associated with cell proliferation and expression of floral homeotic genes.

4.3 Results

4.3.1 MND1 Regulates Shoot Branching and Inflorescence Development

We investigated the macro- and microscopic phenotypes of the *many noded dwarf1.a* (*mnd1.a*) mutant, which was originally identified as a high-tillering mutant in a mixed field of wheat and barley (Harlan and Pope, 1922). We scored plant height, flowering time and yield in the original mutant line in cultivar (cv.) Mesa, where the *mnd1.a* mutation had occurred spontaneously, and its backcross-derived near-isogenic line in cv. Bowman as well as in the parental lines in outdoor experiments over two consecutive years. For simplicity, we will hereafter refer to the mutants as *mnd1.a* (M) for the original mutant line and *mnd1.a* for the backcross-derived line in cv. Bowman. The *mnd1.a* mutants in both backgrounds were stunted and exhibited a high-tillering phenotype (Figure 1A-C) in agreement with previous reports (Harlan and Pope, 1922; Bregitzer et al., 2014). Moreover, both *mnd1.a* mutant lines flowered significantly later than the corresponding wild-type plants. Whereas the wild-type cultivars flowered ~73 days after seedling emergence, flowering occurred after 86 days or later in the mutant lines (Figure 1D). Although the mutants were 40 % shorter than the corresponding wild-types, they nevertheless produced significantly more vegetative biomass (Figure 1E). The thousand grain weight (TGW) was lower in both mutants (Figure 1F) due to 20 % smaller kernels caused by a decrease in seed width and length (Figure S 1ABC). Additionally, the spike length and the number of seeds per spike were significantly lower in the mutants compared to the corresponding wild-type plants (Figure 1GH). Consequently, the *mnd1.a* mutation increased the vegetative biomass, but reduced the generative biomass given the smaller seed size and seed number.

Since the *mnd1.a* mutants exhibited a delay in flowering time, we further investigated the timing of spikelet initiation and inflorescence development. We therefore monitored the development of the main shoot apical meristem (SAM) in cv. Bowman and the derived introgression line under inductive long day (LD) conditions according to the Waddington scale (Figure 2A). The Waddington scale is a quantitative scale for barley and wheat development based on the morphogenesis of the shoot apex and the carpel of its most advanced flower (Waddington et al., 1983). A reproductive shoot apical meristem is specified by the emergence of the first spikelet primordia at the double ridge stage (W2.0). The first floral organ primordia differentiate and stem elongation starts at the stamen primordium stage (W3.5). During the last stage of the Waddington scale (W10.0), the most advanced floret undergoes anthesis and pollination. In the *mnd1.a* mutant, SAM development was delayed when compared to cv. Bowman, which is in line with the late-flowering phenotype observed in outdoor experiments (Figure 2A). Whereas cv. Bowman initiated the first spikelet primordia (W2.0) 1.5 weeks after emergence (WAE), the *mnd1.a* mutant transitioned to this phase three WAE. Additionally, inflorescence development in the mutant was delayed further, in particular between the stamen primordium stage (W3.5) and pollination (W10.0). Given that the vegetative phase of meristem development was prolonged in the *mnd1.a* mutant, we monitored the number

of leaves on the main shoot (Figure 2B). Five WAE, no further leaves appeared on the main shoot in cv. Bowman plants, and the plants flowered with approximately six leaves. In contrast, the *mnd1.a* mutant showed a steady increase in leaf number throughout development until nine WAE, when the experiment was terminated. The supernumerary leaves produced on the main shoot correlated with an increase in the number of elongated internodes (Figure S 2A). However, *mnd1.a* mutant plants did not only initiate leaf primordia for a longer period, the appearance of successive leaves on the main culm was also faster (Figure 2B). The time between the emergences of two successive leaves was 5.61 days in cv. Bowman plants, whereas *mnd1.a* mutant plants developed two successive leaves in only a 2.56 day interval (Table S 1). Nevertheless, the plastochron, which is the leaf initiation rate, was not changed between cv. Bowman and *mnd1.a* (Table S 1) corroborating previous results (Bregitzer et al., 2013). This demonstrates that the *mnd1.a* mutation caused a shorter phyllochron resulting in the overproduction of phytomers due to the prolonged vegetative development. In addition, the lengths and widths of the leaf blades and the lengths of the leaf sheaths were significantly reduced as shown for the first three fully-developed leaves (Figure 2CD, Figure S 2C). The short leaf phenotype coincided with an earlier termination of leaf growth of the first leaf (L1) in the mutant compared to the equivalent leaf in cv. Bowman (Figure S 2B). To determine whether the shorter leaves in the mutant were caused by a change in cell elongation or proliferation, we examined the adaxial epidermal cells of the first leaf in both genotypes. No differences were found for the average cell length (Figure 1E, Figure S 2DE) but cells located over veins next to sclerenchyma and lateral cells were enlarged in the mutant (Figure S 2DE). Consequently, the shorter leaves in the mutant were not caused by a reduction in cell size, but likely resulted from a lower cell number.

To determine whether the high tiller number was linked to the development of additional leaves, we dissected tiller development at defined developmental stages in the wild-type and mutant plants. Significantly more tillers were already observed on the main shoot at the glume primordium stage (W3.0) in the *mnd1.a* mutant compared to cv. Bowman (Figure 2F). At the awn primordium stage (W5.0), cv. Bowman had developed two to three tillers whereas the main shoots of the *mnd1.a* mutant had established more than 40. We then analyzed the pattern of axillary bud formation in each leaf axil at three different stages of early development (Figure 3A and Figure S 3A). For this purpose, the leaf axil of each leaf larger than 0.3 mm on the main culm was examined for the presence or absence of an axillary bud (AB) or tiller. We classified ABs as young when they were surrounded by only the first leaf, or as mature when they were enclosed in more than one leaf and secondary ABs had potentially formed. As bud outgrowth progressed, we further classified tillers into young tillers with only one visible shoot, and mature tillers if secondary side shoots were apparent. At one WAE, one to two more leaves were produced in the *mnd1.a* mutant compared to cv. Bowman. However, *mnd1.a* and wild-type plants produced the same relative number of ABs per leaf axil, but these were further developed in *mnd1.a* than in cv. Bowman. At three WAE, cv. Bowman plants did not form further leaves on the main culm due to the initiation of spikelet primordia and termination of the vegetative program. In contrast, the *mnd1.a* mutant continued to

form leaves or leaf-like structures until five WAE when spikelets were initiated (Figure S 3A). However, the ratio of AB to leaf number remained the same at three WAE for the mutant and wild-type. This indicated that the high number of ABs in the *mnd1.a* mutant was a consequence of the increased leaf number. Moreover, AB formation continued during inflorescence development and was observed at aerial nodes in the *mnd1.a* mutant, whereas leaf axils at elongated internodes remained without AB formation in cv. Bowman (Figure 3AB and Figure S 3A). In *mnd1.a* plants, ABs did not form in a region restricted to some of the elongated internodes below the SAMs, however, young ABs formed below and at the base of the inflorescence (Figure 3CD and Figure S 3A). The development of such aerial ABs was observed starting at early reproductive stages of inflorescence development, after the reproductive transition (W3.0–W3.5) (Figure 3C). The morphology of the young aerial ABs was identical to ABs at the plant base, with leaf primordia enclosing a vegetative shoot meristem. Aerial ABs initiated leaves, underwent stem elongation, developed inflorescences, and eventually set seeds (Figure 3D).

To investigate in the origin of the ABs at the base of inflorescences in the *mnd1.a* mutant, we compared the morphology of developing inflorescences in wild-type and mutant plants at the lemma primordium stage (W3.0), the stamen primordium stage (W3.5) and the awn primordium stage (W5.0) by scanning electron microscopy (SEM). We found that the previously described aerial ABs at the inflorescence base were present at all analyzed stages in the *mnd1.a* mutant (Figure 4). These branch meristems were still vegetative at the stamen primordium stage of the SAM, but initiated spikelet primordia when the SAM had transitioned to the awn primordium stage. Particularly, we found that bract suppression was disturbed in *mnd1.a* mutant inflorescences. In cv. Bowman, bract growth at the collar and rachis nodes was suppressed, but in the *mnd1.a* mutant leaf-like structures classed as floral bracts and known as third outer glumes (Houston et al., 2012) were subtending the triple-spikelet primordia at the rachis nodes (Figure 4). Eventually, bracts at the basal rachis nodes expanded and were able to enclose the spike, whereas bracts at the upper rachis nodes were not visible in maturing *mnd1.a* spikes (Figure 5A). Moreover, the rachis internodes were elongated at the location of bract outgrowth, causing the *mnd1.a* spikes to adopt an accordion-shaped morphology (Figure 5A). SEM analysis further revealed that the development of lateral spikelets was impaired in the *mnd1.a* mutant. At W3.0, lateral spikelet meristems were less developed in the mutant than in the wild-type. At later developmental stages (W3.5 and W5.0) it became apparent that some lateral floral meristems failed to initiate after the differentiation of the corresponding lateral glume primordia, especially at the basal region of the inflorescence. However, central spikelets without lateral spikelets developed like wild-type central spikelets. Indeed, in mature *mnd1.a* spikes lateral spikelets were missing in particular at the base of the inflorescence where bracts grew out (Figure 5B). In addition to branches at the base of the *mnd1.a* inflorescences, we also observed the occasional formation of ABs in the axils of flag leaves (Figure 5A). Consequently, reduced bract suppression at lower rachis nodes, the reversion of spikelet meristems to branch meristems, and the initiation of ABs in flag leaf axils, contributed to a highly-branched shoot architecture in the *mnd1.a* mutant. Moreover, we observed differences in

inflorescence length and spikelet numbers between the *mnd1.a* mutant and cv. Bowman (Figure S 3BC). The length of *mnd1.a* inflorescences was comparable to wild-type inflorescences when spikelet primordia initiated (W2.0). During reproductive inflorescence development (W3.5 to W6.0), the inflorescences of *mnd1.a* plants were smaller than their wild-type counterparts, and the rate of spikelet initiation was reduced. At W6.0, cv. Bowman plants had initiated an average of 34 spikelets, compared to 24 in *mnd1.a* mutants. The lower number of spikelets in the *mnd1.a* mutant was also caused by the reversion to branch meristems at the basis of inflorescences as described above, and confirms the small spike phenotype with reduced seed set that was observed for *mnd1.a* plants in field trials (Figure 1H).

Taken together, we have demonstrated that the *mnd1.a* mutant produced more leaves and tillers than wild-type plants due to i) a longer vegetative growth period, ii) faster leaf outgrowth, iii) formation of ABs at aerial nodes and iv) reduced bract suppression and floral reversion. Consequently, the mutation underlying the *mnd1.a* locus is a major pleiotropic modifier of barley shoot and inflorescence architecture.

4.3.2 Identification of the Gene Underlying the *mnd1.a* Locus

Previous genotyping of the backcross-derived *mnd1.a* line with a SNP array revealed two introgressions on chromosomes 2H and 7H as putative locations for the *HvMND1* gene (Druka et al., 2011). With the purpose to map the gene, determine the polymorphism underlying the *mnd1.a* mutation and identify potential targets of the gene in developing inflorescences, we performed a RNA sequencing experiment as previously described (van Esse et al., 2017). We therefore sequenced total RNA from the main inflorescences of the backcross-derived *mnd1.a* mutant and cv. Bowman at three developmental stages, at spikelet initiation (W2.0), at the stamen primordium stage (W3.5) and after awn primordia had emerged and started to elongate (W5.0). During these stages, severe morphological phenotypes were observed in the *mnd1.a* mutant, suggesting that the gene underlying the *mnd1.a* locus was expressed in the selected samples. Furthermore, RNA was extracted and sequenced from leaf-enriched SAM samples at W1.0 of the original parent cv. Mesa for comparison of sequence variation originating from this line. To identify polymorphisms in the sequenced genotypes, all reads from one genotype were pooled regardless of the developmental stage of the SAM, enabling a better coverage of expressed transcripts and ultimately more support for called variants. We compared the variants identified for cv. Bowman and the *mnd1.a* mutant and found 261 polymorphic alleles. By mapping the 261 alleles to the ordered sequence of the barley reference genome (Mascher et al., 2017), we identified two introgression regions on chromosomes 2H and 7H in the backcross-derived *mnd1.a* mutant (Figure 6AB) corroborating previous reports (Druka et al., 2011). To narrow down the list of 261 candidate genes, polymorphisms shared between the *mnd1.a* introgression line, the original parent cv. Mesa and reference cv. Morex were excluded as candidates for the *mnd1.a* phenotype and revealed a total of 56 genes with unique mutations to *mnd1.a* (Figure 6B). Among these, 32 alleles carried non-synonymous mutations, 10 mutations were located in a conserved domain, and only 2 were

predicted to be functionally important according to the PROVEAN score (cutoff of –2.5) (Choi and Chan, 2015, Table S 2). The candidate gene located within the introgression region on chromosome 2H encodes a ribosomal L12 family protein (HORVU2Hr1G029240), whereas the candidate gene located within the introgression on chromosome 7H encodes an acyl-CoA N-acyltransferase superfamily protein (HORVU7Hr1G113480.3). The ribosomal L12 family protein carried an amino acid substitution in its conserved ribosomal protein L7/L12 domain, and the acyl-CoA N-acyltransferase superfamily protein carried a frameshift mutation due to an 8-bp insertion in the *mnd1.a* mutant allele (Figure 6C). This insertion was located in the first of three exons at the beginning of the conserved N-acetyltransferase domain, leading to a mistranslation and a premature stop codon. To confirm the mutations obtained from the RNA sequencing reads, we Sanger sequenced both candidate genes in cv. Bowman, cv. Mesa, the backcross-derived *mnd1.a* line and in the original *mnd1.a* mutant in cv. Mesa (Table S 3). The 8-bp insertion in the acyl-CoA N-acyltransferase was detected in both *mnd1.a* mutant lines, but was absent from the parental cultivars. However, we only detected the candidate polymorphism in the ribosomal L12 family protein in the backcross-derived *mnd1.a* line and not in the original *mnd1.a* mutant nor in the parental cultivars. Because the ribosomal L12 family protein polymorphism was not shared between both *mnd1.a* mutant lines, we appointed the acyl-CoA N-acyltransferase as candidate underlying the *mnd1.a* locus. To test this hypothesis, we made use of two independent mutant lines, *many branched* (*mbd*) in the background of cv. ZOH, and *MHOR198* in the background of cv. HOR3069. Both mutants were late flowering and produced aerial branches like the *mnd1.a* mutant (Figure 7, Figure S 4, Table S 4 and Table S 5). We performed complementation experiments by crossing *mnd1.a* with either the *mbd* or *MHOR198* mutant. Compared to the parental wild-type cultivars, the resulting F1 progeny was late flowering and characterized by prolific tiller production, more nodes and the presence of aerial branches (Figure 7, Figure S 4, Table S 4 and Table S 5). Consequently, the *mbd* and *MHOR198* mutants were allelic to *mnd1.a.* Sequencing the two candidate genes in the *mbd* and the *MHOR198* lines revealed no mutation in the L12 family protein, while the candidate acyl-CoA N-acyltransferase gene was deleted in *mbd* and carried a 2-bp insertion in the second exon causing a frame-shift mutation in MHOR198. We therefore concluded that the *mnd1.a* phenotype is caused by a loss-of-function mutation in the acyl-CoA N-acyltransferase in the three allelic *mnd1.a* mutant lines.

The maximum-likelihood analysis of the phylogeny of HvMND1 homologs extracted by BLAST search defined a MND1-family clade comprising the barley *MND1* gene along with 57 MND1-like proteins from nine monocots, nine dicots and the spikemoss *S. moellendorffii*. The MND-like proteins from the angiosperms fell into the two monophyletic clades of dicots and monocots. The tree topology was indicative of a series of independent duplications of the *MND*-like genes within the *Poaceae* clade (Figure S 5). In barley, a recent duplication event was observed resulting in *HvMND1* and its closest paralog HORVU5Hr1G071620.1 located on chromosome 5H. The previously identified GNAT-like acyltransferase (*OsglHAT1*, LOC_Os06g44100.1) (Song et al., 2015) is the closest homolog of HvMND1 in rice (74.81 % amino acid identity), and is located in a

syntenic region on chromosome 6 (Mayer et al., 2011). In the *Arabidopsis* genus, we identified three homologs of HvMND1*,* all coding for acyl-CoA N-acyltransferase (NAT) superfamily proteins, including the ethylene response gene *HOOKLESS1*, which is essential for seedling growth (Lehman et al., 1996).

4.3.3 *HvMND1* Transcript Localization

The localization of *HvMND1* transcripts in cv. Bowman SAMs, inflorescences and crown tissue was investigated by mRNA in situ hybridization. We observed distinct *HvMND1* expression foci at the abaxial base of young developing leaves, which persisted through all investigated stages of vegetative (W1.0-W1.5) and reproductive (W2.0, W3.5, W5) SAM development (Figure 8A-D). This expression pattern was also observed in young axillary buds, where *HvMND1* transcripts localized to the abaxial base of young leaves enclosing the axillary meristem (Figure 8B). In addition, we detected *HvMND1* expression in SAMs undergoing the transition from vegetative to reproductive development (W2.0) with *HvMND1* transcripts localizing broadly to the vasculature of the developing inflorescence, but not in vegetative SAMs nor in later stages of inflorescence development. We verified the localization of *HvMND1* expression in cv. ZOH and tested for expression in the derived deletion mutant *mbd* as well as in the cv. Bowman derived *mnd1*.a mutant line at spikelet initiation (W2.0). The localization of *HvMND1* mRNA was comparable between the *mbd* parental background cv. ZOH and cv. Bowman (Figure S 7). *HvMND1* expression was not detected in inflorescences of the *mnd1.a* and *mbd* mutants at W2.0 (Figure S 7GH). Furthermore, cellular localization of HvMND1 was investigated using infiltrated tobacco leaves transiently expressing HvMND1 fused to GFP. We found that HvMND1 was localized in the nucleus and cytoplasm of the tobacco cells (Figure S 7I). The spatial and temporal expression of *HvMND1* was further investigated by quantitative RT-PCR in different plant tissues of cv. Bowman and in a developmental series of inflorescences in cv. ZOH. In cv. Bowman, *HvMND1* expression was detected in the crown tissue of 3-days-old seedlings, and in the nodes of the uppermost elongated internode segment of plants at W3.5 (Figure S 8A). In the roots of 3-days-old seedlings, *HvMND1* expression levels were close to the detection limit whereas it was not expressed in fully-expanded leaves. Moreover, *HvMND1* expression was detected in the leaf-enriched SAM samples of cv. ZOH at all sampled stages from vegetative SAMs to young developing inflorescences (Figure S 8B). In summary, *HvMND1* was expressed in leaf axils at axillary meristem initiation zones close to the SAM and in the vasculature of SAMs undergoing floral transition but was absent or showed low expression in other plant organs.

4.3.4 Transcriptional Profiling by RNA Sequencing

To determine the molecular function and potential target genes of *HvMND1*, we investigated transcriptional changes in developing inflorescences in cv. Bowman and the backcross-derived *mnd1.a* mutant. For this purpose, the whole transcriptome data set used for the candidate gene identification was screened for transcripts that were differentially expressed between the genotypes

in leaf-enriched inflorescence tissues at early reproductive developmental stages (W2.0, W3.5 and W5.0). A principal component analysis (PCA) of all expressed transcripts in cv. Bowman and the *mnd1.a* mutant revealed that the developmental stage explained most of the variance (PC1, 34 % of the total variance) followed by the genotype (PC2, 11.73 % of the total variance) (Figure S 6). Transcripts expressed at spikelet initiation (W2.0) clustered separately from those expressed in inflorescences at W3.5 and W5.0. Similarly, the hierarchical cluster analysis of differentially expressed transcripts (DETs) showed that DETs at W2.0 grouped separately from those at W3.5 and W5.0, which were more similar in terms of their expression profile (Figure 8E). Furthermore, the number of DETs increased with developmental stage, and the largest number was observed at the awn primordium stage (W5.0). At W2.0 and W3.5, only 160 and 192 DETs were found, respectively, whereas 1032 DETs were observed at W5.0 (Figure 8F). The large number of DETs at W5.0 corresponded to a strong phenotypic differentiation between *mnd1.a* and cv. Bowman inflorescences. At this stage, floral meristems had reverted to branch meristems, and bracts had grown out in the *mnd1.a* mutant. At W2.0 and W3.5, the number of downregulated DETs (89 and 89, respectively) was similar to the number of upregulated DETs (71 and 103, respectively). In contrast, there were more upregulated DETs (754) than downregulated DETs (278) at W5.0.

We discovered a core set of DETs for all three developmental stages in the *mnd1.a* mutant consisting of 43 transcripts (Figure 8F). Out of the 23 upregulated core DETs, 20 showed no or very low expression levels in the inflorescence of cv. Bowman and were clearly expressed in the *mnd1.a* mutant. Conversely, twelve out of the 19 DETs downregulated at all stages exhibited no or very low expression levels in *mnd1.a* but were strongly expressed in the wild-type inflorescences. Genes only expressed in the inflorescence of the *mnd1.a* mutant included, for example, ribonucleoside-diphosphate reductase large subunit genes (RNRs) (HORVU2Hr1G065760.1, HORVU3Hr1G089710.1) (Figure S 9), governing the conversion of ribonucleotides to deoxyribonucleoside triphosphates (dNTPs) which is essential for DNA replication and represents a key reaction in proliferating cells (Burke and Lupták, 2018). We further recorded the upregulation of a RING/U-box superfamily protein (HORVU7Hr1G107430.1) (Figure S 9) belonging to the group of E3 ubiquitin ligases of which many are key players in cell cycle control (Deshaies and Joazeiro, 2009). Similarly, transcripts of two F-box superfamily proteins (HORVU1Hr1G088190.2 and HORVU6Hr1G082230.1) were exclusively expressed in *mnd1.a* inflorescences (Figure S 9). F-box proteins are bound by E3 ubiquitin ligases conferring substrate specificity for the phosphorylation directed proteolysis through the 26S proteasome during cell cycle regulation (Vierstra, 2009). Furthermore, two receptor kinase genes (HORVU2Hr1G037740.1 and HORVU7Hr1G115940.2) were only expressed in the inflorescences of the *mnd1.a* mutant (Figure S 9) whereas the receptor kinase HORVU7Hr1G118610.6 was only expressed in cv. Bowman inflorescences (Figure S 10). Receptor kinases are key signaling proteins and implicated in cell division, cellular differentiation, and morphogenesis (De Smet et al., 2009). Moreover, transcripts with roles in plant development were also primarily upregulated in the *mnd1.a* mutant and included a basic-leucine zipper (bZIP) transcription factor (TF) family protein (HORVU1Hr1G072090.1) (Figure S 9). This bZIP TF is

similar to the flowering BHLH transcriptional activators that are known to bind to E-box *cis*-elements for example in the promotor of the flowering time gene *CONSTANS* in Arabidopsis (Ito et al., 2012). Moreover, exclusively in *mnd1.a* inflorescences we recoded the expression of two *FAR-RED IMPAIRED1* (*FAR1*) genes (HORVU0Hr1G038960.25 and HORVU4Hr1G014170.1) (Figure S 9), which have multiple roles in plant development including light signal transduction and meristem as well as floral development (Wang and Wang, 2015; Liu et al., 2016). Interestingly, we observed no transcripts of a Lysine-specific demethylase 5D (HORVU2Hr1G045000.1) in apices of the *mnd1.a* mutant, but in the inflorescences of cv. Bowman (Figure S 10). Functions of Lysine-specific demethylases include the demethylation of lysine residues on histones regulating chromatin structure and thereby gene expression. For example, expression of the central floral homeotic genes *FLOWERING LOCUS T* (*FT*) and *FLOWERING LOCUS C* (*FLC*), and thereby flowering, is regulated by histone methylation in Arabidopsis (Jiang et al., 2007; Jeong et al., 2009). Furthermore, several transcripts involved in biotic and abiotic defense were partly or completely downregulated in *mnd1.a* inflorescences as for example three putative nucleotide-binding site leucine-rich repeat (NBS-LRR) resistance genes (HORVU7Hr1G111650.1, HORVU7Hr1G117570.5 and HORVU7Hr1G120020.16) (Figure S 10). These results suggest that the *mnd1.a* mutation caused changes in the tissue specific expression of genes, which show functions in cell cycle control, development and defense across all three developmental stages.

We further investigated transcriptional changes for each developmental stage separately to identify transcripts that linked to the stage specific phenotypic differences between wild-type and mutant plants (Table S 6). We found an enrichment of photosynthesis related DETs in *mnd1.a* inflorescences at the spikelet initiation stage (W2.0). For example, several genes encoding for chlorophyll a-b binding proteins, which are part of the light-harvesting complex (LHC), and for photosystem I (PSI) and II (PSII) subunits were upregulated in the *mnd1.a* mutant compared to cv. Bowman. The LHC in plant chloroplasts functions as a light receptor capturing and delivering excitation energy to PSI and PSII (Jansson, 1994). Notably, these expression changes in photosynthesis related genes coincide with the de-repression of inflorescence bract development followed by the outgrowth of bracts into leaf like structures in the mutant. In *mnd1.a* inflorescences at the stamen primordium (W3.5) and awn primordium stage (W5.0), we observed misexpression of several genes, which are implicated in developmental control such as the upregulation of four *LIGHT-DEPENDENT SHORT HYPOCOTYLS* (*LSH*) genes (HORVU2Hr1G089190.3, HORVU3Hr1G088000.1, HORVU6Hr1G058340.3 and HORVU6Hr1G088790.1). Members of the LSH protein family are known suppressors of organ differentiation in boundary regions in Arabidopsis (Takeda et al., 2011). Furthermore, we found seven barley *MADS-box* (*BM*) genes, which were downregulated in *mnd1.a* inflorescences at W3.5 and W5.0. *MADS-box* genes encode floral homeotic TFs that are involved in flower development and vegetative organogenesis (Davies and Schwarz-Sommer, 1994; Trevaskis et al., 2007). These *BM* genes included barley homologs of floral patterning genes, as for example an *AP1*-like (*HvBM8, HORVU2Hr1G063800*) and a *SEP*-like gene (*SEP1*, *HORVU5Hr1G095710*) differentially regulated at the stamen primordium

stage. Moreover, we observed a strong upregulation of two *TERMINAL FLOWER 1* (*TFL1*)-like genes in *mnd1.a* shoot apices (HORVU2Hr1G072750.4, HORVU4Hr1G078770.1). *TFL1*-like genes have been studied in great detail in Arabidopsis, rice and tomato, and were shown to be key repressors of flowering time and regulators of shoot architecture (Shannon and Meeks-Wagner, 1991; Bradley et al., 1996; Pnueli et al., 1998; Nakagawa et al., 2002). Among the identified *TFL1*-like DETs, we found the barley homolog of *Antirrhinum CENTRORADIALIS* (*HvCen*), an important regulator of seasonal flowering and growth habit which has been targeted during barley improvement (Comadran et al., 2012). With the onset of the early reproductive development (W3.5), we found reduced transcript levels for a *LEAFY* (*LFY*, HORVU2Hr1G102590.2) homolog in *mnd1.a* apices. *LFY* is involved in the initiation of floral meristems in Arabidopsis (Weigel et al., 1992) and *LFY* homologs in rice regulate flowering time, as well as tillering and panicle branching (Rao et al., 2008). The upregulation of floral repressors (*TFL1-like*, *LSH*) and downregulation of inducers of floral development (*BM*) correlated with the delayed floral development in the *mnd1.a* mutant. In addition, we found several homeobox-leucine zipper protein family genes (*HOX*) to be differentially regulated in developing *mnd1.a* inflorescences at W3.5 and W5.0. Among them, two *WUSCHEL-related HOX* (*WOX*) TF genes (HORVU2Hr1G113820.5, HORVU4Hr1G051530.8) showed higher transcript levels in the mutant. WOX genes confer several regulatory roles in plants including stem cell maintenance, cell proliferation, floral transition and lateral organ formation (Wu et al., 2007; Vandenbussche et al., 2009; Dolzblasz et al., 2016). The barley *HOX* gene *SIX-ROWED SPIKE 1* (*VRS1*) (Komatsuda et al., 2007), a major regulator of lateral spikelet development, was only weakly expressed in *mnd1.a* inflorescences at W5.0, whereas we observed high transcript levels in cv. Bowman during this stage. Another class of highly abundant TFs with regulatory functions in plant growth and development are *TCP* TFs. We observed increased transcript levels for four *TCP* TF family genes in *mnd1.a* inflorescences at W5.0 (HORVU7Hr1G038130.1, HORVU6Hr1G075650.1, HORVU3Hr1G073830.1, HORVU5Hr1G000490.1). Interestingly, we found one *TB1*-like *TCP* TF which showed expression in *mnd1.a* developing inflorescences, but transcripts were absent in cv. Bowman inflorescences at W3.5 and W5.0. *HvMND1* itself showed overall lower transcript levels in mutant apices than in cv. Bowman at all three investigated stages.

Taken together, our transcriptome analysis revealed a core set of DETs consistent for all investigated stages of inflorescence development in the *mnd1.a* mutant. A high proportion of the core DETs showed expression in mutant inflorescences, but transcripts were absent in cv. Bowman, and vice versa. Most of these transcripts are associated with regulatory functions in cell cycle control and development. Furthermore, genes controlling phase change transition, floral meristem identity and floral development were particularly misexpressed during inflorescence development (W3.5 and W5.0) in *mnd1.a*. We therefore hypothesize that *HvMND1* is a regulator of organ specific expression of genes involved in cell proliferation and meristem development. Further, changes in expression of floral homeotic genes correlate with the delayed vegetative to reproductive stage transition and development of *mnd1.a* inflorescences.

4.4 Discussion

Understanding the development of shoot and inflorescence architecture and the underlying molecular mechanisms could facilitate the improvement of yield and fitness in barley breeding programs. However, many genes regulating shoot and inflorescence development show pleiotropic effects, so improving one trait can negatively influence another. Therefore, it is essential to not only identify developmental genes but also dissect their specific roles in plant organ development. This knowledge can be used in future for the targeted improvement of favorable traits. Here we report that loss-of-function mutations at the barley *mnd1.a* locus directly affect multiple shoot architecture traits in a pleiotropic manner and that the corresponding gene encodes an acyl-CoA N-acyltransferase.

4.4.1 *HvMND1* Is a Promoter of Reproductive Growth and Yield

Our analysis showed that in the absence of a functional *HvMND1* gene, the shoot apical meristem (SAM) remained vegetative for a longer period and thereby more leaves were initiated without changing the plastochron. However, leaves in the *mnd1.a* mutant were smaller due to precocious leaf maturation which in turn shortened the phyllochron. We found a clear correlation between the higher number of fast-outgrowing leaves and the number of initiated axillary buds (ABs). We therefore hypothesize that the supernumerary leaves act as a prerequisite for the high-tillering phenotype of the *mnd1.a* mutant. Similar correlations between leaf and tiller numbers have been described in other studies. In rice, loss-of-function mutations in the *PLASTOCHRON1* (*PLA1*) gene, encoding a cytochrome P450 enzyme (Miyoshi et al., 2004), generate a phenotype similar to that of *mnd1.a*. The *pla1* mutant is characterized by stunted growth and supernumerary leaves and internodes, associated with increased shoot branching. Similarly, the barley *many noded dwarf6* (*mnd6*) mutant, which is also caused by a mutation in a cytochrome P450 enzyme, shows abnormal leaf and internode development resulting in a high-tillering plant architecture (Mascher et al., 2014). However, there is not always a positive correlation between leaf and tiller number. For example, the rice *leafy-head2* (*lhd2*) mutant develops more leaves than wild-type plants due to the shortened plastochron and maintenance of a vegetative SAM, but fewer tillers due to the suppression of tiller bud outgrowth (Xiong et al., 2006). In contrast, we observed the enhanced outgrowth of tillers in the *mnd1.a* mutant, not only at the plant base, but also from elongated nodes. *HvMND1* transcripts localized to the abaxial side of young developing leaves, as it has been observed for other genes that control axillary meristem initiation, such as *TILLERS ABSENT1* (*TAB1*), a rice ortholog of the Arabidopsis *WUSCHEL* gene (Tanaka et al., 2015). In contrast to *TAB1*, *HvMND1* acts as a repressor of axillary meristem initiation and mutations in *HvMND1* result in increased AB development leading to basal and aerial tiller outgrowth. We therefore propose that *HvMND1* is a suppressor of vegetative growth including leaf and tiller initials, and mutations in *HvMND1* lead to increased vegetative biomass and shoot branching.

We further showed that loss-of-function mutations at the *mnd1.a* locus resulted in a de-repression of bracts coinciding with the reversion of triple-spikelet meristems to vegetative branch meristems. So far, only a few genetic regulators of bract suppression have been described in barley. The GATA zinc finger transcription factor *THIRD OUTER GLUME1* (*TRD1*) is a repressor of bract outgrowth, and mutations in the *TRD1* gene cause the development of leaf-like structures subtending rachis nodes at basal inflorescences (Houston et al., 2012). Orthologs such as maize *TASSELSHEATH1* (*TSH1*) (Whipple et al., 2010) and *rice NECK LEAF1* (*NL1*) (Wang et al., 2009) show conserved functions with *TRD1*, whereas the Arabidopsis ortholog *HANABA TARANU* (*HAN*) has no bract suppression role but acts as regulator of auxin and cytokinin signaling to restrict boundary domains (Zhao et al., 2004; Whipple et al., 2010). Furthermore, the rice plastochron mutant *pla1* develops ectopic shoots at primary rachis branches, which are subtended by outgrown and enlarged bracts (Miyoshi et al., 2004). Due to the strong effects on associated axillary meristems in bract suppression mutants such as *pla1*, bracts have been proposed to act as signaling centers regulating the fate of the correlated floral meristems (Whipple, 2017). It is therefore possible, that insufficient bract suppression was causal for the indeterminate fate of triple-spikelet meristems and subsequent reversion into branch meristems in the *mnd1.a* inflorescence. In addition, the outgrowth of branches at aerial nodes subtending the inflorescence was indicative of a reduced apical dominance as also indicated by floral reversion and the strong vegetative program of the *mnd1.a* mutant. Moreover, the thousand grain weight (TGW) in *mnd1.a* was reduced due to smaller kernels and the amount of seeds per spike and fertile spikes per plant were decreased when compared to wild-type. We therefore propose, that *HvMND1* is a promoter of reproductive growth in barley governing the reproductive phase transition and thereby positively affects grain yield.

The release of bract outgrowth, spikelet meristem indeterminacy and reduced lateral spikelet development in the *mnd1.a* mutant was only observed at basal inflorescence nodes and these phenotypes gradually diminished towards the apical inflorescence. Interestingly, the strict progression of vegetative followed by reproductive growth was impaired in the *mnd1.a* mutant, where the induction of vegetative structures continued even after the transition to reproductive growth. Similarly, the heterochronic maize mutant *Corngrass1* (*Cg1*), caused by overexpression of *miRNA156*, displayed a prolonged expression of a juvenile developmental program which overlapped with the reproductive developmental program (Poethig, 1988; Chuck et al., 2007). The mutant phenotype of *Cg1* is characterized by the overproduction of leaves and inflorescences with changed floral architecture and abolished bract suppression. In barley, lines overexpressing *miRNA171* likewise show defects in the phase transition and floral meristem determinacy by acting on *miRNA156* transcript levels (Curaba et al., 2013). We conclude that, similar to the *Cg1* gene, *HvMND1* is a positive regulator of juvenile (vegetative) to reproductive phase transition and represses the juvenile growth program.

4.4.2 The Gene Underlying the *mnd1.a* Locus Encodes an Acyl-CoA N-acyltransferase

Using RNA sequencing, we identified an 8-bp insertion in an acyl-CoA N-acyltransferase gene on chromosome 7HL which causes a frameshift and generates a premature stop codon. This mutation was unique to *mnd1.a* mutants and is therefore a promising candidate for the causal mutation. Allelism tests with two independent mutant sources, a whole-gene deletion and a frameshift mutant of this gene, confirmed the candidate as *HvMND1*. The causal mutation in the *mnd1.a* mutant is located upstream of the conserved N-acyltransferase domain and presumably abolishes the function of the protein resulting in the highly-pleiotropic *mnd1.a* phenotype. Acyltransferases are widespread among plants, yeasts and other organisms, and show a range of targets for amino group acetylation. These targets include small molecules such as IAA-related metabolites (Epstein and Ludwig-Müller, 1993), N-termini of larger proteins that are blocked from degradation when acetylated (Driessen et al., 1985), and the lysine residues of histones. The latter are posttranslational modifications of histone tails which result in either permissive or repressive chromatin states modulating gene expression (Chen and Tian, 2007). Our phylogenetic analysis demonstrated that *HvMND1* has three homologs in Arabidopsis, one of which is the functionally characterized *HOOKLESS1* (*HLS1*) gene. *HLS1* is a major regulator of seedling growth which integrates environmental and endogenous hormonal signals to control the formation of the apical hook (Lehman et al., 1996). The molecular function of HLS1 was recently demonstrated, revealing its interaction with the Mediator complex in histone acetylation (Liao et al., 2016). Similarly, it was shown that the closest HvMND1 homolog in rice (OsglHAT1) acetylates histone H4 and associated proteins specify its lysine acetylation spectrum (Song et al., 2015). In our protein localization experiment, we detected HvMND1 proteins not only in the cytoplasm but also in nuclei and thus propose that HvMND1 might act as a regulator of gene expression through the acetylation of histones in the chromatin of specific target genes. However, this hypothesis is based on the assumed functional conservation among HvMND1 homologs and protein localization. Further biochemical studies on acetylation targets of HvMND1 need to be conducted in order to determine its molecular function. Nevertheless, functional conservation between HvMND1 and rice OsglHAT1 is supported by their similar pleiotropic phenotypes. Transgenic knockdown *OsglHAT1* plants were stunted and had smaller seeds reflecting the presence of fewer cells (Song et al., 2015). However, the authors did not report higher leaf and tiller numbers, bract outgrowth or a flowering time phenotype. Our data suggest that *HvMND1* and its paralogue HORVU5Hr1G071620 arose from a recent duplication event in barley, so the regulation of inflorescence development and vegetative growth by HvMND1 may be due to subsequent neofunctionalization. However, it is also possible that the knockdown of *OsglHAT1* was not sufficient to cause such a drastic phenotype as that observed in *mnd1.a* mutants. Interestingly, the spatial and temporal expression profile of *OsglHAT1* is similar to that of *HvMND1* (Song et al., 2015). In both barley and rice, expression was detected on the abaxial side of young developing leaves and only at the onset of reproductive development in developing inflorescences. Additionally, *OsglHAT1* was expressed in bracts but only during the primary and secondary branch differentiation stages of inflorescence development suggesting a

potential function in bract outgrowth repression. In summary, we identified the gene underlying the *mnd1.a* locus as an acyl-CoA N-acyltransferase which might be involved in histone acetylation.

4.4.3 HvMND1 Modulates Expression of Cell Cycle and Floral Homeotic Genes

Comparison of the transcriptomes originating from young developing inflorescences between cv. Bowman and the *mnd1.a* mutant revealed no differential regulation of known barley genes such as *TRD1* and *MND* which cause similar phenotypes to *mnd1.a* when mutated. This suggests, that we identified a novel molecular pathway controlling barley development. We identified a core set of differentially expressed transcripts (DETs) for the *mnd1.a* mutant in which all transcripts showed significant regulation at all three investigated inflorescence development stages (W2.0, W3.5 and W5.0). Interestingly, the majority of the core DETs were expressed in either one of the genotypes but were absent from the other. This implicates, that HvMND1 controls expression of target genes in a tissue specific and temporally coordinated manner. Furthermore, the core DETs showed an enrichment for cell cycle associated transcripts which were upregulated in the *mnd1.a* mutant. Previous studies highlighted the impact of the cell-cycle machinery shaping the plant architecture. For example, tillering in rice is controlled through cell division and growth mediated by cell-cycle-dependent degradation of MOC1 (Xu et al., 2012). Furthermore, the Arabidopsis AP2/EREBP family gene *PUCHI* prevents cell proliferation by controlling the cell cycle and thereby acts on bract suppression and floral fate determination (Karim et al., 2009). However, it remains unclear whether this enrichment in cell cycle genes is due to the highly proliferating and morphologic different inflorescence tissues in comparison to those from cv. Bowman or if HvMND1 is directly balancing cell proliferation and arrest. In the set of core DETs, we further observed expression of two *FAR-RED IMPAIRED1* (*FAR1*) genes exclusively in *mnd1.a* inflorescences. It has been suggested, that the Arabidopsis *FAR1* is involved in the promotion of shoot branching via the strigolactone and cytokinin hormonal regulation (Stirnberg et al., 2012). The *mnd1.a* specific upregulation of these *FAR1* genes indicates, that HvMND1 might repress shoot branching through repression of *FAR1*-related genes in barley. Moreover, transcripts of a Lysine-specific demethylase 5D were absent in *mnd1.a* inflorescences, but present in at all stages in cv. Bowman. Methylation marks at histones, including those at lysine residues, maintain the repression of its target genes and are important for the correct expression of plant developmental genes (Zhang et al., 2007). For example, the Arabidopsis histone demethylase RELATIVE OF EARLY FLOWERING 6 (REF6) promotes flowering through regulation of the expression of floral integrators such as *FLOWERING LOCUS T* (*FT*) and *SUPPRESSOR OF CONSTANS OVEREXPRESSION 1* (*SOC1*) (Noh et al., 2004; Lu et al., 2011). Consequently, the absence of the Lysine-specific demethylase 5D transcript in the *mnd1.a* mutant might impact misexpression of developmental genes resulting in the strong pleiotropic phenotype.

The prolonged vegetative growth phase and the de-repression of bracts at basal inflorescence nodes demonstrated that the vegetative growth continued even after the onset of the reproductive phase. Genetic mechanisms regulating the phase transition from vegetative to reproductive

meristem growth are well studied in Arabidopsis. For example, *LEAFY* (*LFY*) and *TERMINAL FLOWER1* (*TFL1*) act antagonistically in the meristem for the acquisition of a floral meristem fate (Ratcliffe et al., 1998). Studies in rice showed that the ortholog of *LFY*, *RICE FLORICAULA* (*RFL*), confers a delayed transition to reproductive development when its transcript levels are reduced (Rao et al., 2008). Vice versa, overexpression of *RFL* leads to early flowering (Rao et al., 2008). The antagonistic relation between *RFL* and the rice ortholog of *TFL1*, *RCN2*, has also been observed to regulate phase transition in rice. Transcript levels of *RCN2* were increased in *RFL* knockdown plants, together delaying the phase transition of the meristem as observed for *RCN2* overexpression lines (Nakagawa et al., 2002). We found a similar trend of antagonistic expression in our *mnd1.a* transcriptome study. On the one hand, a homolog of the Arabidopsis *LFY* gene, HORVU2Hr1G102590.2, was significantly downregulated in apices at W3.5. On the other hand, two *TFL1*-like genes, HORVU4Hr1G078770.1 and HORVU2Hr1G072750.4, the latter encoding for the barley *CENTRORADIALIS* (*HvCEN*) gene (Comadran et al., 2012), were strongly upregulated at W3.5 and W5.0. Furthermore, *LFY* is known to induce floral homeotic genes including those of the MADS-box transcription factor family (Weigel et al., 1992). These MADS-box transcription factors are involved in many developmental processes including the phase transition, floral meristem determinacy and floral organ identity. In barley, 11 MADS-box genes (BMs) have been identified and some have been characterized in more detail (Schmitz et al., 2000; Trevaskis et al., 2007). For example, overexpression of *BM1* results in the reversion of spikelet meristems to branch meristems at the inflorescence base and late flowering due to an extended reproductive phase (Trevaskis et al., 2007). *BM1* belongs to the *SHORT VEGETATIVE PHASE* (*SVP*)-like clade of *BM* genes and putative interactions of *SVP*-like BMs with *APETALA1*/*FRUITFUL* (*AP1*/*FUL*) BMs have been suggested. In rice, the *AP1*/*FUL*-like genes *OsMADS14* and *OsMADS15* specify meristem identity as well as palea and lodicule identities (Wu et al., 2017). Interestingly, homozygous *os-mads15*;heterozygote *osmads14* double mutants exhibited AB formation at stem nodes, de-repression of bracts and floral reversion in the inflorescence similar to the inflorescence phenotypes we have observed for the *mnd1.a* mutants (Wu et al., 2017). Seven *BM*-like genes, including the *OsMADS15* homolog *BM8*, were significantly downregulated in the *mnd1.a* transcriptome. Consequently, the downregulation of AP1/FUL-like genes by *mnd1.a* might be causal for the de-repression of bracts and outgrowth of tillers at aerial nodes in the *mnd1.a* mutants.

Taken together, we presented a detailed analysis of the pleiotropic phenotypes caused by loss-of-function mutations at the *mnd1.a* locus. These phenotypes included an extended vegetative growth period and consequently a prolonged phase of leaf initiation, rather than any change in the leaf initiation rate (plastochron). A longer vegetative phase together with a shortened phyllochron resulted in a larger number of leaves and a correlated increase in tiller number. We detected *HvMND1* transcripts in leaf axils, suggesting an additional role in the repression of AM or AB initiation for *HvMND1*. Furthermore, continuous tillering, bract outgrowth and reversion of spikelets into branch-like structures at the base of the spike in *mnd1.a* demonstrated that *HvMND1* controls the transition from a juvenile, vegetative to a reproductive developmental program. Such

developmental transitions require the coordinated regulation of a multitude of different processes at many different levels of organization. How this regulation is achieved is a central problem in developmental biology. Here, we propose that *HvMND1,* identified as an acyl-CoA N-acyltransferase, plays a crucial role in this coordinated transition from vegetative to reproductive development in barley. Moreover, the phenotype of the *mnd1.a* mutant is interesting also from an evolutionary perspective. The *mnd1.a* mutant shares several features with the wild progenitor of barley and *Hordeum* species from the secondary and tertiary gene pool, such as a more pronounced vegetative program, prolonged tillering, and a reduced ratio of reproductive to vegetative biomass. Selection and breeding of modern barley may have caused a progressive reduction in the vegetative program or the relative duration of the juvenile and adult phases of shoot development. Since spike size is generally related to the duration of the reproductive phase, human selection for large spikes may have resulted in the suppression of juvenile traits.

4.5 Material and Methods

Plant Material and Cultivation

Seeds of the original *mnd1.a* mutant line in the background of cv. Mesa, the derived backcross line in the background of cv. Bowman, cv. Bowman and cv. Mesa were obtained from the Department of Agriculture of the United States of America (USDA) (Table 1). Seeds of the *mbd* mutant, the parental cultivar ZOH, *MHOR198* and HOR3069 were obtained from the IPK in Gatersleben. The previously identified mutations of both mutant lines are summarized in Table 1.

Table 1 Mutants used in this study. If available, identified mutations or locus allocation of the respective mutants are listed.

Allele	Background	Seed Stock Number	Mutation	obtained from
mnd1.a	Bowman (backcross)	GSHO 2038	unknown, located to chromosome 2H (Druka et al., 2011)	USDA
mnd1.a	Mesa	GSHO 253	unknown, located to chromosome 2H (Druka et al., 2011)	USDA
mbd	ZOH		large deletion on chromosome 7H including HORVU0Hr1G022470, HORVU7Hr1G113500, HORVU7Hr1G113480 (Stein and Guo, unpublished)	IPK
MHOR198	HOR3069	MUT 1479	frameshift mutation in HORVU7Hr1G113480, located to chromosome 7HL (Stein and Guo, unpublished)	IPK
parent	Bowman	PI 483237		USDA
parent	Mesa	CIho 2328		USDA
parent	ZOH			IPK
parent	HOR3069			IPK

Outdoor Plant Cultivation and Phenotyping

The original and backcrossed *mnd1.a* mutant, as well as the respective parental cultivars, were sown in 96-well trays in February 2014 and 2015. Plants germinated in the greenhouse and were transferred to 12 L pots with one plant per pot and at least 16 replicates per genotype. The soil was composed of peat and a clay soil mixture (Einheitserde®, Einheitserdewerke Werkverband e.V., Sinntal-Altengronau, Germany) and was supplemented with long-term fertilizer. Plants were cultivated outdoors (Cologne, Germany), irrigated with a sprinkling robot and fertilized or treated with pesticides, as described previously (Liller et al, 2015). The pots were randomized and arranged in 22 rows, with 54 pots per row placed at a distance of 10 cm. The plots were surrounded by one row of pots with cv. Morex plants to ensure an even planting density for every experimental plant. At 89 days after emergence, plant pictures were taken of one representative plant per genotype. Flowering time was measured in days from plant emergence until appearance of the first awns from

the flag leaf, called tipping. At plant maturity, approximately two weeks before harvest, tiller numbers were counted at the base of each plant and plant height was measured (from soil surface to the base of the uppermost spike). After harvest in the year 2015, whole plants were dried for two weeks, spikes were removed and the vegetative dry weight of each plant was determined. Exemplary spikes for each genotype were scanned. Seed measurements were performed on 40 representative spikes from individual plants per genotype of the 2014 and 2015 outdoor trial. Seed cleaning was performed by hand for each spike individually and measurements were performed using the MARVIN Seed Analyser (GTA Sensorik, Neubrandenburg, Germany) to assess the number of seeds per spike, thousand grain weight (TGW), seed length, width and area.

Greenhouse Cultivation and Phenotyping

For detailed macroscopic phenotyping of the investigated *mnd1.a* mutant, Bowman and the *mnd1.a* near isogenic mutant line were sown in 96-well trays (Einheitserde®, Einheitserdewerke Werkverband e.V., Sinntal-Altengronau, Germany). After stratification for 3 days at 4 °C, plants were cultivated in controlled long-day greenhouse chambers (Bronson Climate b.v., Zaltbommel, The Netherlands) with 16 h light (22 °C, PAR 270 µm/m²s) and 8 h dark (18 °C) day/night cycles. After emergence of the second leaf, plants were transferred to 20-well growing trays. Three days after emergence and subsequently every week after emergence (WAE), five plants per genotype were dissected until the end of the experiment at nine WAE. At each time point, the developmental stage of the shoot apical meristem of the main stem was determined according to the quantitative scale introduced by Waddington et al. (1983) using the stereo microscope Nikon SMZ18 and the NIS-Elements BR software (version 3.4; Nikon Instruments Europe B.V, Amsterdam, The Netherlands). In addition, the number of visible leaves, tillers, and elongated internodes (distance to previous node > 5 mm) were counted at each time point. To study phyllochron in wild-type cv. Bowman and *mnd1.a* mutant plants, leaf emergence rates during the first five WAE were compared. Phyllochron was calculated as the leaf emergence rate^{-1} from the slope of the linear regressions in R (R version 3.3.2; (R Development Core Team, 2011)). We used the tidy function of the ‘broom’ package (Robinson and Hayes, 2018) to extract the significance of the fitted linear regression, the slope (phyllochron) and the standard error. The number of spikelet primordia was counted for main shoot apices at the stage of pistil primordium initiation (W4.0) until the stage of style formation (W6.0). From spikelet initiation (W2.0) until style formation (W6.0), the length of the shoot apical meristem was measured for each plant. For the first three developed leaves, leaf length and width and the corresponding sheath length were determined when leaves were mature. At one, three and five WAE, the number of initiated leaves was counted for five representative plants per genotype. At the same time, each leaf axil was examined for the presence or absence of an axillary bud or tiller. Axillary buds were classified into young ABs (axillary meristem is surrounded by only one leaf) or mature ABs (axillary meristem is enveloped in more than one leaf and potentially secondary ABs were formed). As bud outgrowth progressed we further classified tillers into young tillers with only one shoot visible or mature tillers when secondary side shoots

became apparent. At one, three and five days after germination, the length of the first leaf was measured to investigate the rate of leaf elongation for each genotype. To study the wild-type and *mnd1.a* mutant specific plastochron, the number of all initiated leaves, including leaf primordia, was counted for seedlings one to five days after germination in daily intervals. The plastochron was calculated as the leaf initiation rate^{-1} analogously to the calculation of the phyllochron.

Cell Size Measurements in the Leaf Epidermis

Cell size measurements were conducted on five mature L1 leaves per genotype of three WAE old plants grown under controlled long-day conditions as described above. The length of the leaf blade was determined. A 2 cm interval was marked around at 33 % and 66 % of the leaf blade length, which was thinly brushed with 5 % cellulose acetate dissolved in acetone. After drying, epidermal imprints were carefully removed with tape and attached on microscope slides. The length of five cells at 33 % and 66 % of the leaf blade length of each plant was measured for each of the following cell types: blade lateral cell (lc), blade cell between veins (bv), blade cell between veins and next to lateral cells (bvn), over vein cell (ov), over vein cell and next to sclerenchyma cells (ovs), over vein cell and next to lateral cells (ovn) and cells in the stomatal row (sr) (see Wenzel et al. (1997) for terminology of cell types). A Nikon SMZ18 stereo microscope with the NIS-Elements BR software (version 3.4; Nikon Instruments Europe B.V, Amsterdam, The Netherlands) was utilized for cell measurements.

Scanning Electron Microscopy

Dissected main shoot apical meristems were mounted to a copper specimen holder with freeze-hardening glue and fast-frozen in liquid nitrogen. Using a transfer unit, meristems were moved to an air tight cryo chamber (Emitech K1250X). After sublimation, meristems were chilled and subsequently coated in palladium and gold for imaging. Meristem morphology was observed using a Zeiss Supra 40VP scanning electron microscope. Images were processed with Adobe Photoshop to remove the background of the electron micrographs.

RNA Sample Preparation and RNA Sequencing

inflorescences of main culms from cv. Bowman, cv. Mesa and the backcross-derived *mnd1.a* mutant grown in controlled long-day greenhouse chambers (Bronson Climate b.v., Zaltbommel, The Netherlands) with 16 h light (22 °C, PAR 270 µm/m²s) and 8 h dark (18 °C) day/night cycles were used for RNA isolation. The following stages of inflorescence development were selected: spikelet initiation (W2.0), stamen primordium stage (W3.5) and awn primordium (W5.0). In case of cv. Mesa plants, only vegetative SAM tissue (W1.0) was harvested. Collected tissues included the SAM, its base and small surrounding leaves and were sampled in the middle of the day, 6-7 hours before the onset of the night period. To assure that all samples were collected at correct stages, three plants per genotype were dissected before sampling. At least three separate biological replicates each consisting of a pool of at least 10 meristems were collected. RNA sample preparation, RNA sequencing, quality control and adaptor trimming were performed as described

in van Esse et al. (2017). Additionally, vegetative SAMs (W1.0-W1.5) from cv. Mesa plants grown at the same conditions were harvested and total RNA was extracted. Two biological replicates of cv. Mesa SAMs with at least 10 pooled meristems were subjected to RNA sequencing.

SNP Calling and Candidate Gene Selection

Reads obtained from sequencing the total mRNA of SAMs were mapped to a combined set of high-confidence (HC) and low-confidence (LC) coding sequences of the recent barley genome of cv. Morex (Mascher et al., 2017). For the SNP detection, all reads obtained from one genotype were pooled regardless of the developmental stage of the underlying SAM tissue. The alignments to the reference coding sequences were performed using BWA-MEM (version 0.7.15; (Li, 2013)). Mapped reads were filtered and processed as described in van Esse et al. (2017). Subsequent variant calling was performed using the UnifiedGenotyper of GATK (version 3.6; (McKenna et al., 2010)). Although barley is a diploid plant species, we treated the reads as originating from a haploid species to preclude heterozygous calls and adjust the variant calling to inbreeding plant features. In addition, a minimum phred-scaled confidence threshold for calling and for emitting of SNPs was set to 30.0 and 10.0, respectively. Variants were filtered in a custom R script (R version 3.3.2; (R Development Core Team, 2011)) that only allowed for variants with support of at least 30 in read depth (DP), at least 98 for genotype quality (GQ) and a Phred Quality Score of more than 2000. Introgression regions were defined by comparing filtered variants of *mnd1.a* and cv. Bowman. Candidate genes were selected when a variant observed for *mnd1.a* was not detected in either cv. Bowman, cv. Mesa or the reference of cv. Morex. Pairwise alignments of translated candidate protein sequences were performed using MUSCLE (Edgar, 2004) to reveal non-synonymous variants. Location of conserved domains were assigned using the NCBI Conserved Domain Database (Marchler-Bauer et al., 2015). Further, candidate variants were evaluated by PROVEAN (Protein Variation Effect Analyzer, http://provean.jcvi.org), a software that computationally predicts the influence of single amino acid substitutions on the protein biological function. The pairwise sequence alignment-based score (PROVEN score) measures the change in sequence similarity of a query sequence to a protein sequence homolog before and after introducing an amino acid variation to the query sequence (Choi and Chan, 2015). The mutations in the chosen candidate genes were confirmed using Sanger sequencing using primers listed in Table S 7.

Complementation Tests

Allelism tests were performed through crosses between the backcross-derived *mnd1.a* mutant line in cv. Bowman and the shoot architecture mutants *mbd* and *MHOR198* in cv. ZOH and cv. HOR3069 background, respectively. Plants used for crosses were grown in long-day greenhouses, emasculated and pollinated with pollen from a single plant. Backcross-derived *mnd1.a* mutants were used as pollen donor in this study. The F1 progeny of the two crossing combinations *mbd* x *mnd1.a* and *MHOR198* x *mnd1.a* was genotyped using Sanger sequencing spanning the *mnd1.a* specific eight bp insertion in candidate gene HORVU7Hr1G113480.3 with primers listed in Table S 7. True heterozygous crosses were grown in greenhouse LD conditions

along with the parental mutant lines and the respective genetic background parents. Parental lines and F1 progeny of *MHOR198* x *mnd1.a* crosses were vernalized for eight weeks at 4°C in a plant growing chamber. Flowering time was assessed in days from emergence until tipping; height, tiller number, node number and aerial branching when plants senesced. Plant pictures were taken, when most of the analyzed genotypes were flowering.

Phylogenetic Analysis

To identify homologs of *HvMND1*, we performed a blastp search using the HvMND1 protein sequence as query against peptide sequences from following species: *Aegilops tauschii*, *Arabidopsis thaliana*, *Brachypodium distachyon*, *Carica papaya*, *Cucumis sativus*, *Hordeum vulgare*, *Medicago truncatula*, *Oryza sativa*, *Populus trichocarpa*, *Phaseolus vulgaris*, *Ricinus communis*, *Sorghum bicolor*, *Secale cereal*, *Setaria italica*, *Solanum lycopersicum*, *Selaginella moellendorffii, Triticum aestivum*, *Vitis vinifera*, and *Zea mays*. For barley, the current database of predicted peptide sequences was used (Mascher et al., 2017). For all other species we used the Phytozome 12.1.6 database (Goodstein et al., 2011) to retrieve homologues proteins. Blast results were filtered with an E-value cutoff of 1E-10. We then extracted the coding nucleotide sequences of the homologues proteins, selected only one representative isoform in case of alternative splicing variants and aligned the sequences using MUSCLE (Edgar, 2004) in MEGA version 5 (Tamura et al., 2011) based on translated codons. Visually unaligned leading or trailing nucleotide sequences were removed manually from the multiple sequence alignment. The conversion to phylip format was performed using a stream editor (sed) script. The maximum likelihood tree was generated using RAxML 8.2.10 (fixed base frequencies, GAMMA model and 'autoMRE' for an optimal number of bootstrap repeats) (Stamatakis et al., 2008). Dendroscope 3 (Huson and Scornavacca, 2012) was used for the visualization of the tree, which was rooted using *S. moellendorffii* as outgroup.

Analysis of DETs in the Transcriptomic Data Set of Developing Inflorescences

Whole transcriptome expression analysis was performed on the RNA sequencing reads obtained from main SAM tissues including their base and small surrounding leaves of cv. Bowman and *mnd1.a*. The reads were aligned to the barley high confidence (HC) transcript sequences (Mascher et al., 2017) using the quasi-mapping based mode in Salmon with default settings (Patro et al., 2015). Further processing and read quantification was performed as described in van Esse et al. (2017). Differentially regulated transcripts (DETs) in *mnd1.a* mutants were selected based on adjusted p-values ≤ 0.05 and log2-fold-changes (LogFC) ≤ -1.5 or LogFC ≥ 1.5. Hierarchical clustering of DETs was performed using Pearson correlation coefficients in R. The number of DETs per stage was visualized using the R package 'eulerr' which generates area-proportional Euler diagrams. GO overrepresentation analysis was performed using Blast2GO (version 5.0) (Götz et al., 2008) with the Fisher's Exact Test for significantly enriched GO terms ($p \leq 0.05$). Obtained GO terms were reduced to the most specific terms with the implemented function in Blast2GO.

RNA *in situ* Hybridization and Localization in Tobacco

Probes for detecting the *HvMND1* mRNA were prepared from genomic DNA of the barley cv. Morex from the *HvMND1* start to stop codon (1690 bp), or 861 bp upstream of the stop codon (Exon3). The DNA was cloned into the pGGC000 entry vector of the GreenGate cloning system (Lampropoulos et al., 2013) and then amplified including the T7 and SP6 promoter sites by PCR. RNA probes were built as described in Hejátko et al. (2006). The long RNA probes (1609 bp) were hydrolysed by adding 50 µl carbonate buffer (0.08 M NaHCO3, 0.12 M Na2CO3) to 50 µl RNA probe and incubation at 60 °C for 54 min. On ice, 10 µl 10 % acetic acid, 12 µl sodium acetate and 312 µl EtOH were added, the RNA was precipitated and dissolved in RNase-free dH2O. RNA *in situ* hybridisations were performed on SAMs at the stages W1.0-W1.5, W2.0, W3.5, W5.0 as described in Kirschner et al. (2017). Plant cultivation and sampling time were according to the above described RNA sequencing experiment, however more leaves and plant base remained on the collected SAM samples. Polyvinyl alcohol was added to a final concentration of 10 % to the NBT/BCIP staining buffer. Permanent specimens were created by washing the slides in 50 % EtOH, 70 % EtOH, 95 % EtOH and 100 % EtOH for 2 min each and for 10 s in xylol, and after drying, a few drops of Entellan (Merck) and a cover slip were added. The construction of estradiol inducible expression vectors with GFP as translational fusions at the C terminus for transient expression in tobacco (*Nicotiana benthamiana*) leaves and the transformation of tobacco leaves was described before (Bleckmann et al., 2010). The open reading frame sequence of *HvMND1* (from genomic DNA) was inserted upstream of the fluorophore, without stop codon and in frame with GFP. Nuclei were stained with DAPI (1 µg/ml), plasma membranes were stained with FM1-43FX (Thermo Scientific) (20 µM). Pictures were taken using a plan-neofluar 10x objective with a NA of 0.30 using the Zeiss Axioskop light microscope, and image processing, i.e. stitching, was performed with the Stitching Plugin in Fiji (Preibisch et al., 2009; Schindelin et al., 2012). For imaging of the tobacco leaves, the confocal laser scanning microscope Zeiss LSM780 with a C-Apochromat 40x/1.20 W Korr M27 was used. GFP was excited at 488 nm and emission was detected at 490 – 508 nm, DAPI was excited at 405 nm and detected at 410 – 483 nm, FM1-43FX was excited at 488 nm and detected at 545 – 668 nm.

HvMND1 Expression Analysis Using qRT-PCR

To study the expression of *HvMND1* in different plant tissues in cv. Bowman, as well as in developing meristems of cv. ZOH, qRT-PCR was performed. Wild-type cv. Bowman plants were germinated on Whatman® Cellulose Filter Paper (Sigma-Aldrich) in Petri dishes sealed with parafilm. Enriched seedling crown tissue containing vegetative SAMs surrounded by leaves and whole roots were sampled three days after germination. Plants for leaf and node tissues of cv. Bowman were grown in 96-well trays and SAM development was staged every three days. At W3.5, leaf material from the youngest fully elongated leaves were collected. Additionally, nodes from the uppermost elongated internode located close to the SAM were harvested. For expression analysis of *HvMND1* in cv. ZOH, plants were grown in 96-well trays and leaf-enriched developing inflorescences were collected at W1.0, W2.0, W3.5 and W5.0 as described for the RNA sequencing

experiment. All plants were grown in chambers with 16 h light (22 °C, PAR 270 µm/m²s) and 8 h dark (18 °C) day/night cycles and samples were taken 6-7 hours before the onset of the night period. Three biological replicates per tissue and genotype were collected, each consisting of a pool from three individual plants. The isolation of total RNA, cDNA synthesis and qRT-PCR was performed as described in Campoli et al. (2012). For each sample, two technical replicates were used and quantification was based on the titration curve using the LightCycler 480 Software (Roche, version 1.5). The expression of *HvMND1* was normalized against the geometric mean of the expression of two internal controls: *HvActin* and *HvGAPDH*. All primers used in the qRT-PCR analysis are listed in Table S 7.

4.6 Figures

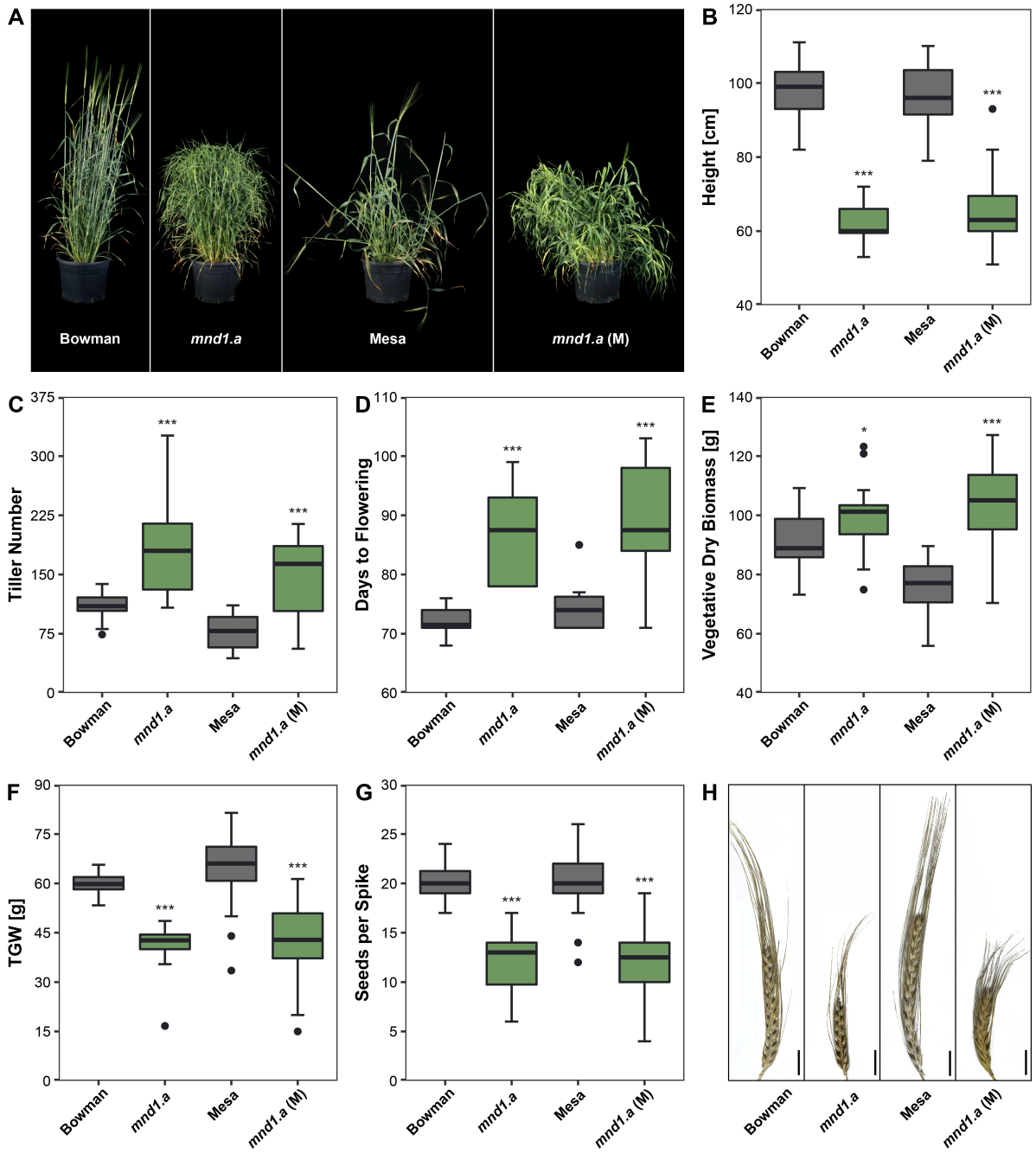

Figure 1 Phenotypic characteristics of adult *mnd1.a* mutants grown under outdoor conditions. **A** Morphology and plant architecture caused by the spontaneous *mnd1.a* mutation in cv. Mesa (*mnd1.a* (M)) and its backcross-derived near isogenic line in cv. Bowman (*mnd1.a*). Comparison of **B** plant height and **C** tiller number between the *mnd1.a* mutants and the corresponding parents representing each genetic background. **D** Flowering time was measured in days until the appearance of the first awns from the flag leaves. **E** Vegetative biomass of whole plants was quantified after senescence and an additional drying period excluding reproductive organs. **F** Thousand grain weight (TGW) was determined using one spike from each plant. **G** Seed set was assessed for individual spikes per genotype. **H** Main spike morphology of wild-type and *mnd1.a* genotypes. Scale bar = 2 cm. Data were obtained from outdoor trials in the consecutive years 2014 and 2015 (n=10–40). Statistical significance was assessed for each mutant and the corresponding genetic background cultivar by a two-tailed unpaired Student's *t*-test (* $p < 0.05$, ** $p < 0.01$, *** $p < 0.001$).

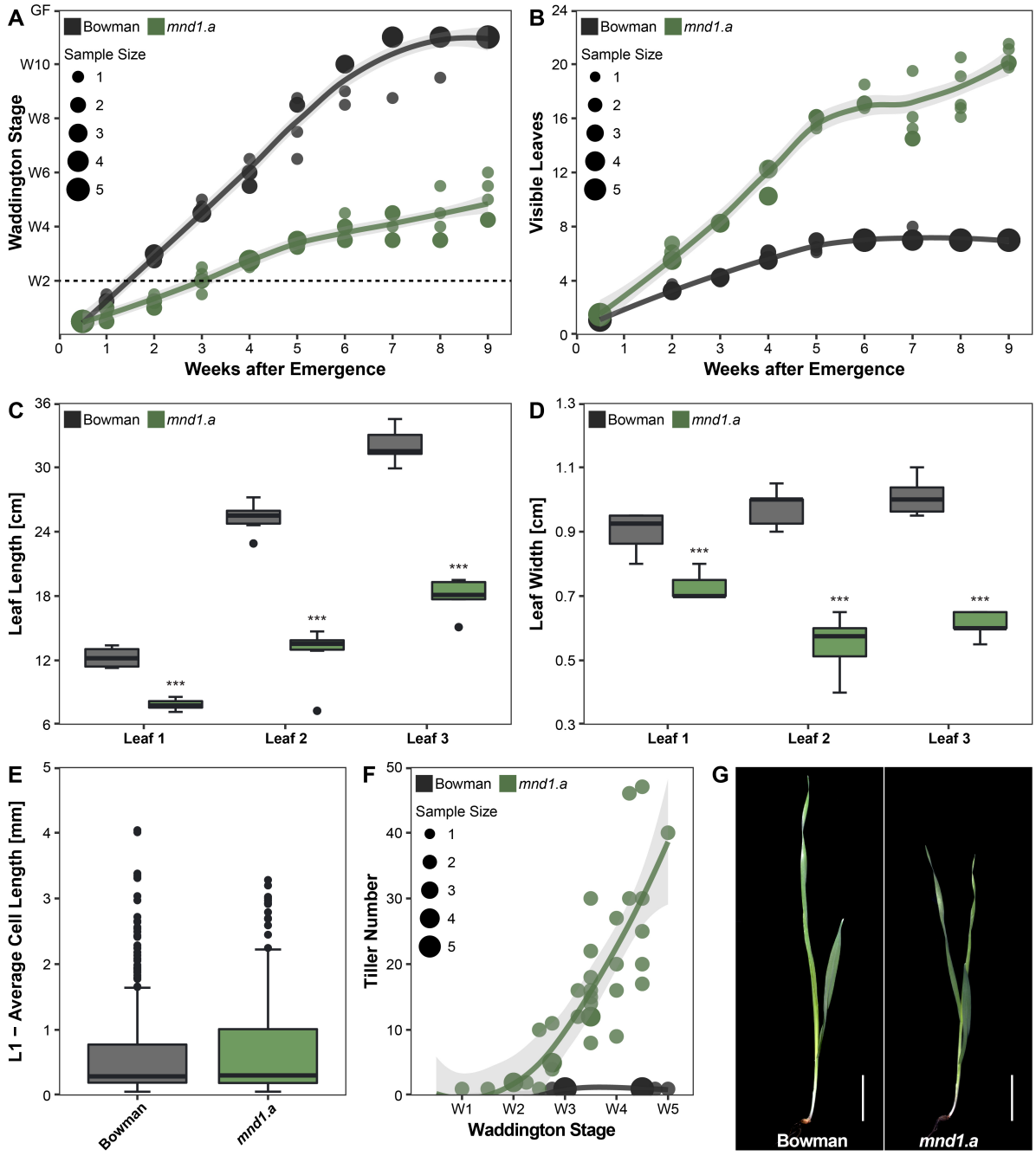

Figure 2 Influence of the *mnd1.a* locus on plant development. A Development of the main shoot apical meristem (SAM) reported in Waddington stages. The dotted line at W2.0 marks the stage of spikelet primordia initiation. **B** Number of visible leaves developed on the main shoot. **C** Leaf length and **D** leaf width of the first three fully developed leaves. Sizes were measured at the longest/broadest position (n ≥ 16). **E** Averaged cell size of all cell types in the adaxial epidermis of the first fully developed leaf (L1) measured according to the method of Wenzel et al. (1997) (n = 350 cells). **F** Number of tillers in *mnd1.a* and cv. Bowman plants according to the SAM developmental stage until W5.0. **G** Bowman and *mnd1.a* seedling morphology at 10 days after emergence grown in a short-day climate chamber. Scale bar = 2 cm. Gray areas around fitted curves indicate the 95 % confidence interval. Statistical significance was assessed by a two-tailed unpaired Student's *t*-test (* $p < 0.05$, ** $p < 0.01$, *** $p < 0.001$). GF: grain filling.

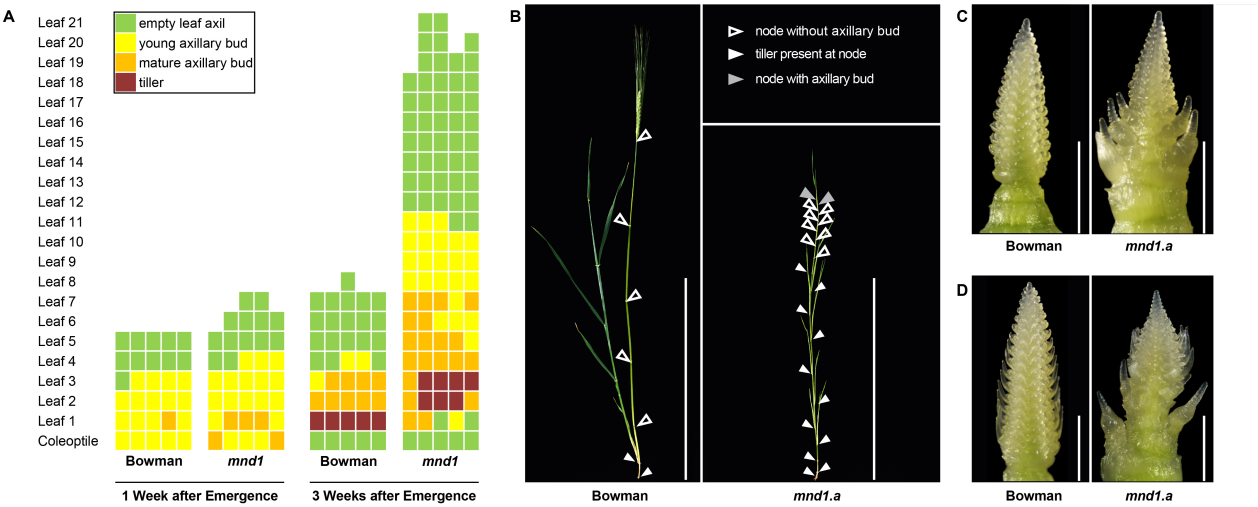

Figure 3 Axillary bud initiation pattern in cv. Bowman and *mnd1.a* mutants. A Schematic representation of axillary bud (AB) formation at 1 and 3 weeks after emergence (WAE) in cv. Bowman and *mnd1.a* mutants. Leaf axils were examined under a binocular microscope. Each column represents a single plant of the respective genotype, and each square represents an individual leaf axil. The bottom row represents the axil of the coleoptile, whereas axils of progressively younger leaves are stacked on top with leaf 1 as the oldest leaf. The absence of AB formation is coded in green, and the presence of ABs is shown in yellow to dark red depending on the developmental status of the axillary shoot. **B** Internode patterning on the main stem and AB and tiller position in cv. Bowman and *mnd1.a* mutants at 7 WAE. Node positions along the main stem are indicated with triangles. Triangle color and shape indicate the presence or absence of ABs or tillers at the corresponding node. The uppermost node in cv. Bowman ends the peduncle. Scale bar = 30 cm. **C** Shoot apical meristem (SAM) phenotype of *mnd1.a* mutants at W3.5. **D** SAM phenotype of *mnd1.a* mutants at W5.0. Leaves around the SAM and ABs were removed for visualization of the phenotype. Scale bar = 1 mm.

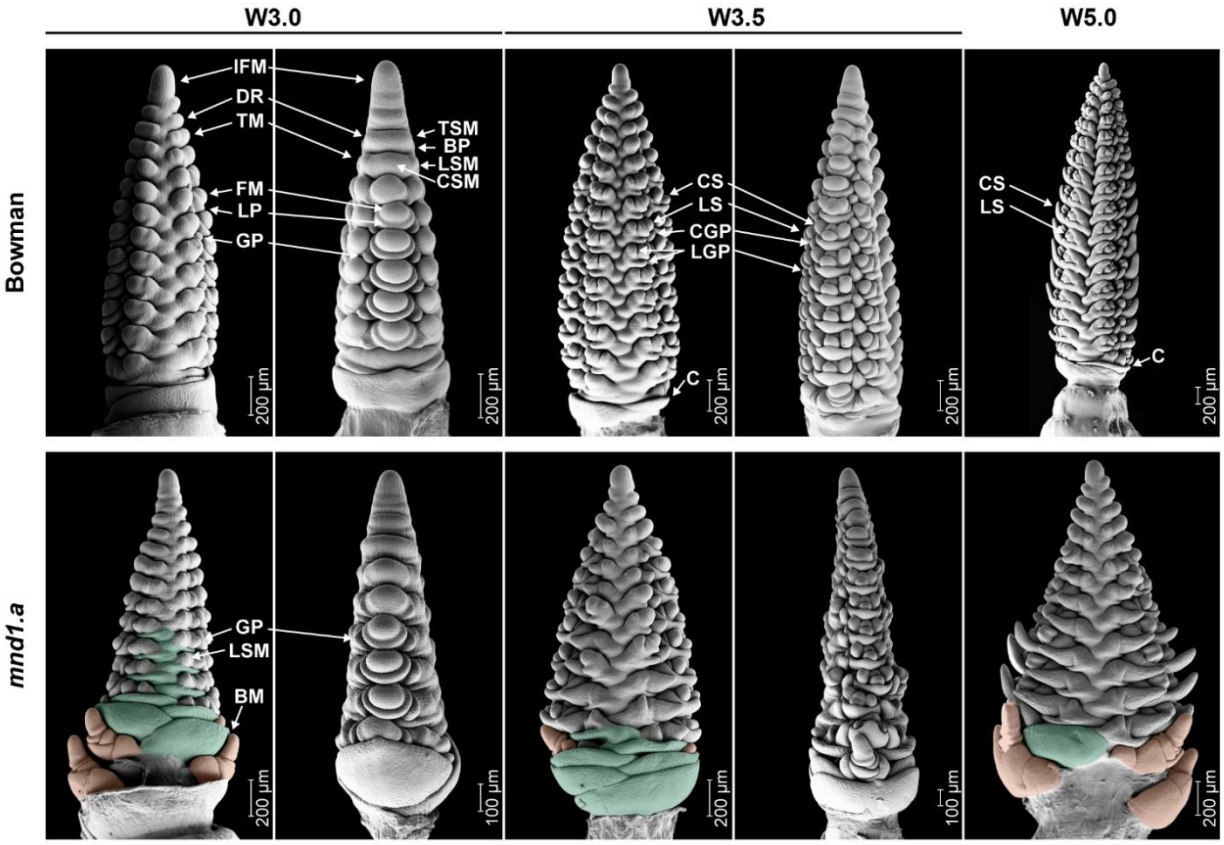

Figure 4 Wild-type and *mnd1.a* mutant inflorescence development. Scanning electron microscopy images of developing inflorescences in cv. Bowman (upper panel) starting from the lemma primordium stage (W3.0) to the stage of stamen primordia initiation (W3.5) until the awn primordium stage (W5.0). The main shoot apical meristems (SAMs) in the *mnd1.a* mutants were investigated at comparable developmental stages (lower panel). Subtending bracts at *mnd1.a* inflorescence bases were removed to expose the spikelet meristem reversion to branch meristems. In frontal angle images, exemplary outgrowing bracts were highlighted in green and branch meristems in orange. Lateral angle images of SAMs were not colored. IFM: inflorescence meristem; DR: double ridge; TM: triple mound; TSM: triple-spikelet meristem; BP: bract primordium; LSM: lateral spikelet meristem; CSM: central spikelet primordium; FM: floral meristem; LP: lemma primordium; GP: glume primordium; CS: central spikelet; LS: lateral spikelet; CGP: central glume primordium; LGP: lateral glume primordia; C: collar; BM: branch meristem.

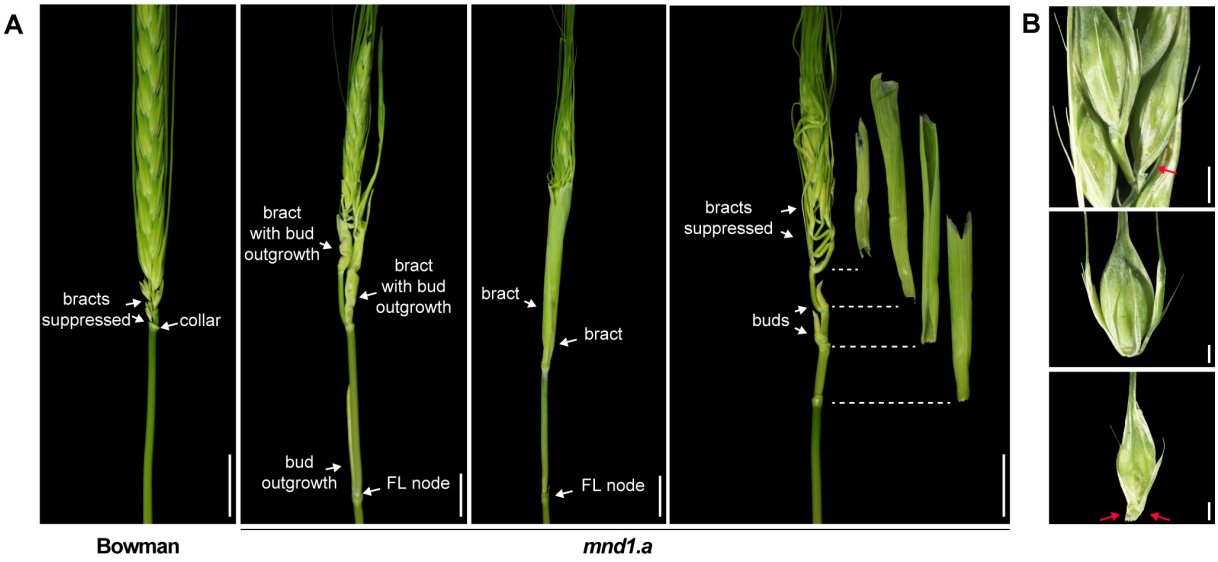

Figure 5 Developing spike morphology in *mnd1.a* mutants. A Bract outgrowth phenotype observed in *mnd1.a* inflorescences. Rudimentary, suppressed bracts and the collar are indicated in the wild-type cv. Bowman inflorescence. Outgrown and suppressed bracts, aerial buds and the flag leaf (FL) node are marked by arrows in *mnd1.a* inflorescences. No collar was formed in the *mnd1.a* mutants, but a bract was present instead. Scale bar = 1 cm. **B** Lateral floret presence/absence phenotype of *mnd1.a* mutants. Top: Basal part of a *mnd1.a* inflorescence. Center and bottom: Spikelets detached from basal *mnd1.a* inflorescences. Red arrows indicate absence of lateral florets. Scale bar = 1 mm.

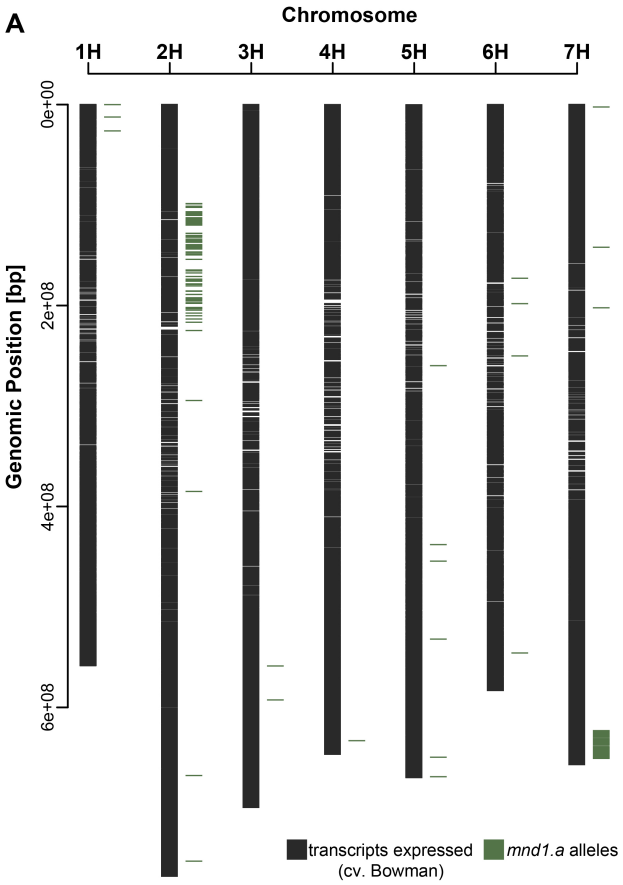

B

Introgression Intervals	Chromosome	Position	No. of Genes
	2H	98.67-224.99	1474
	7H	623.28-650.66	1235

	No. of Genes
***mnd1.a* alleles in cv. Bowman**	261
unique *mnd1.a* alleles	56
unique *mnd1.a* alleles carrying non-synonymous mutations	32

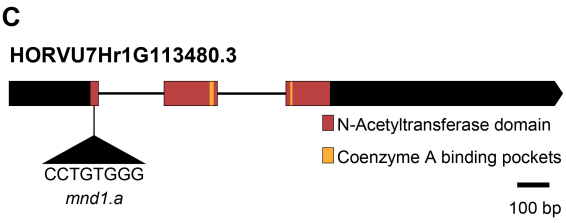

Figure 6 Introgression mapping and candidate gene selection for the *mnd1.a* locus. A Visualization of the *mnd1.a* introgressions introduced to the reciprocal backcross parent cv. Bowman. Black lines represent genes expressed in cv. Bowman in the transcriptome data set with a coverage of least four reads. Alleles originating from the primary *mnd1.a* mutant in cv. Mesa were identified through variant calling on the transcriptome sequencing data and mapped to the barley genome according to the physical distance. **B** Overview of the introgression intervals of the backcrossed-derived *mnd1.a* mutant line and the reduction of candidate genes through filtering steps. **C** Intron-exon organization of the candidate gene underlying the *mnd1.a* locus. The gene contains three exons (boxes) encoding a conserved N-acetyltransferases motif with two coenzyme A binding pockets. The *mnd1.a* allele contains an insertion of 8-bp in the first exon.

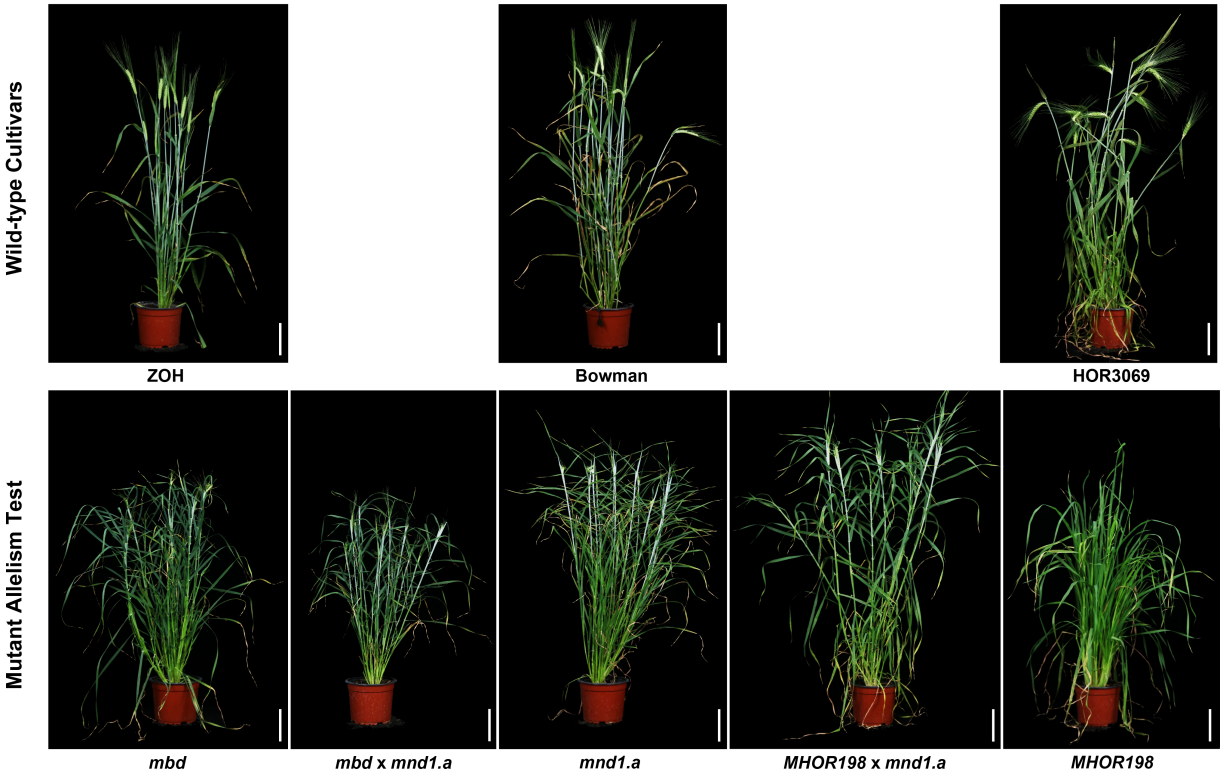

Figure 7 Allelism crosses between the backcross-derived *mnd1.a* line and the putative *HvMND1* mutant lines, *mbd* and *MHOR198*. Plant morphology of the parental cultivars ZOH, Bowman and HOR3069, the corresponding mutant lines *mbd*, *mnd1.a* and *MHOR198* and their corresponding F1 progeny derived from allelism crosses. Pictures show one representative plant from each genotype. Scale bar = 20 cm.

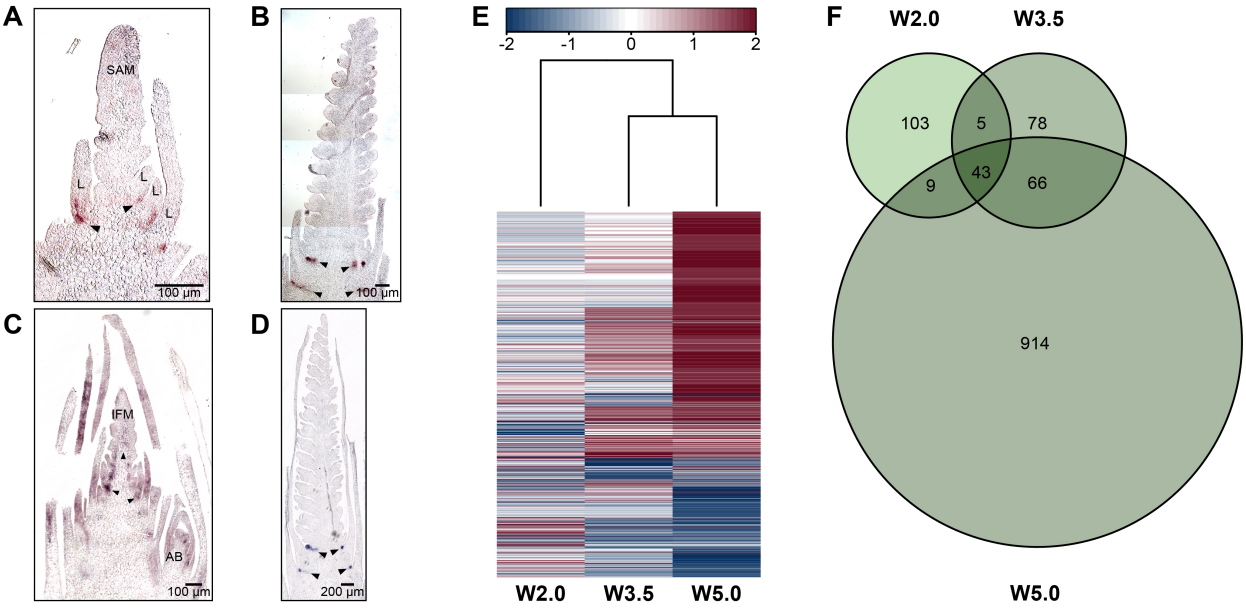

Figure 8 *HvMND1* expression and global transcriptome analysis in developing inflorescences. Longitudinal sections of cv. Bowman shoot apical meristems (SAMs) **A** before floral transition (W1.0-W1.5), **B** at the spikelet primordium initiation stage (W2.0) and **C** the glume (W3.0) and **D** awn primordium stage (W5.0) hybridized with an *HvMND1* antisense probe. Expression of *HvMND1* is restricted to the base at the abaxial site of developing leaves and in the inflorescence at W2.0 (marked by arrows). **E** Hierarchical cluster analysis of differentially expressed transcripts (DETs) identified at three developmental stages of *mnd1.a* inflorescences (W2.0, W3.5 and W5.0). Direction of expression (LogFC compared to corresponding Bowman transcriptome data) is color coded. **F** Number of transcripts differentially regulated at W2.0, W3.5 and W5.0 in the *mnd1.a* mutant and overlap of DETs between the investigated developmental stages of inflorescences. AB: axillary bud; IFM: inflorescence meristem; L: leaf.

4.7 Supplemental Data

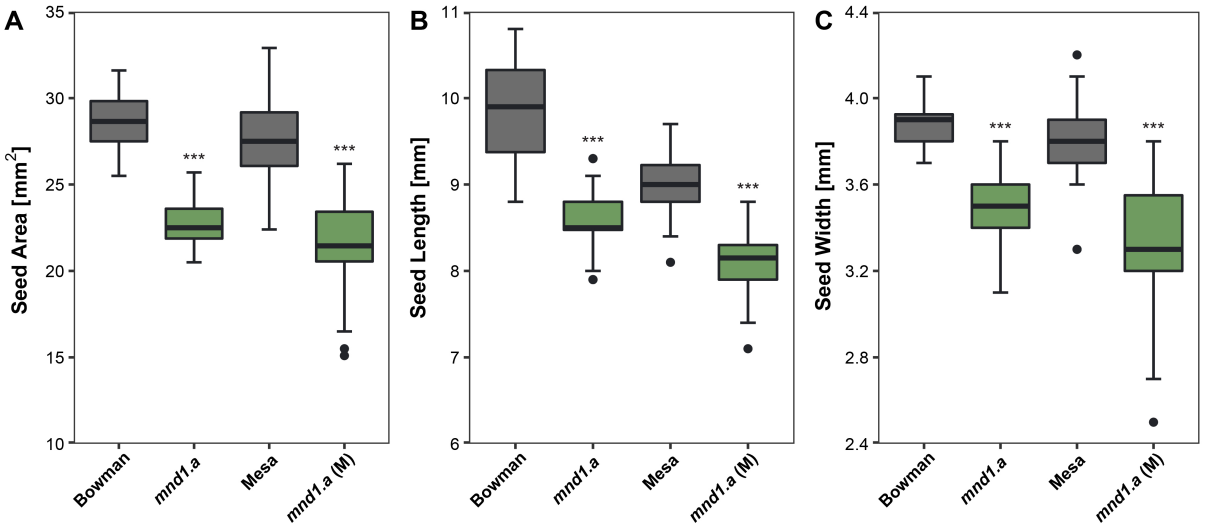

Figure S 1 Seed shape parameters of *mnd1.a* mutants in cv. Bowman and cv. Mesa. A Seed area, **B** seed length and **C** seed width of every fertile seed from single spikes derived from individual plants were measured (n = 40 spikes). Spikes were harvested in two outdoor cultivation experiments in the years 2014 and 2015. Statistical significance was assessed for each mutant and the corresponding genetic background cultivar using a two-tailed unpaired Student's *t*-test (* $p < 0.05$, ** $p < 0.01$, *** $p < 0.001$).

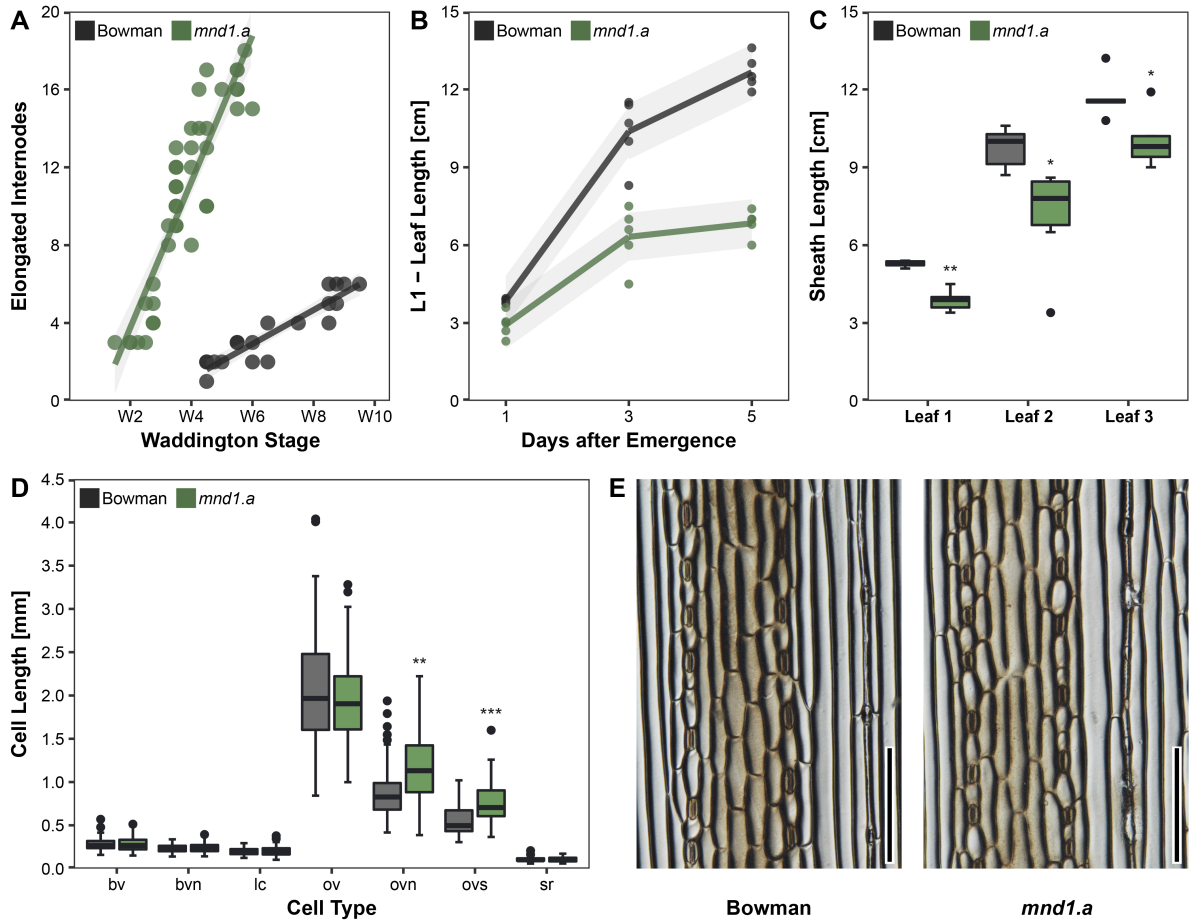

Figure S 2 Internode and detailed leaf phenotype of the backcross derived *mnd1.a* mutant. A Number of internodes along the main culm according to the developmental stage of the shoot apical meristem (SAM). Elongation of internodes was recorded if the distance between two successive nodes exceeded 0.5 cm. **B** Leaf maturation of the first developed leaf in *mnd1.a* mutants and cv. Bowman. Leaf length was measured 1, 3 and 5 weeks after seedling emergence from soil (n = 5). **C** Sheath length of the first three fully developed leaves. Sizes were measured at the longest position of the sheath (n ≥ 16). **D** Individual cell type measurements of the L1 leaf adaxial epidermis at 33 % and 66 % leaf blade according to Wenzel et al. (1997) (n = 50). **E** Light micrograph of imprints of the adaxial leaf epidermis at 33 % leaf blade. Scale bar = 200 µm. Gray areas around fitted curves indicate the 95 % confidence interval. Statistical significance was assessed using a two-tailed unpaired Student's *t*-test (* $p < 0.05$, ** $p < 0.01$, *** $p < 0.001$). bv: between veins; bvn: between veins and next to lateral cell; lc: lateral cell; ov: over vein; ovn: over vein and next to lateral cells; ovs: over vein and next to sclerenchyma; sr: stomatal row.

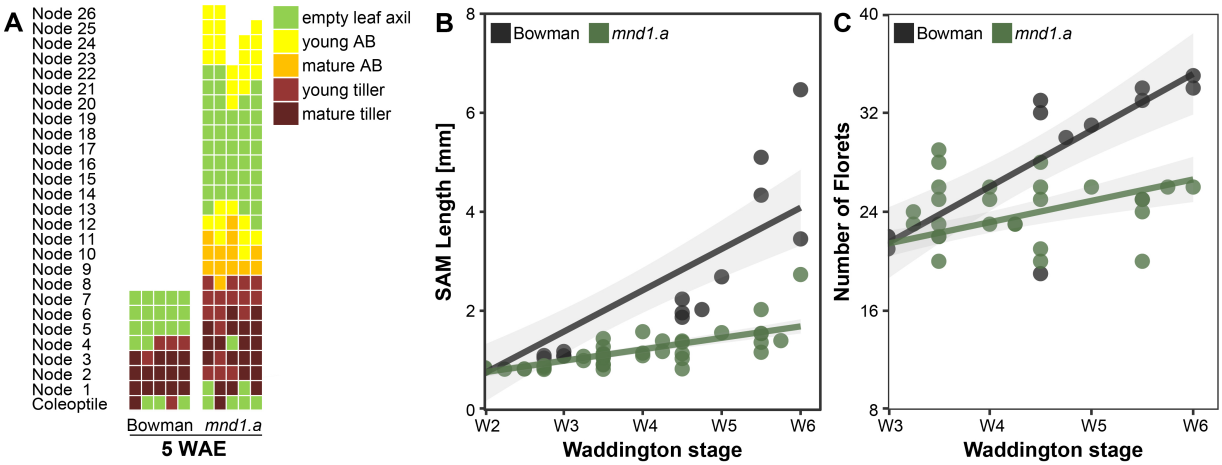

Figure S 3 Bract outgrowth related aerial bud formation in *mnd1.a* mutant plants and impaired shoot apical meristem (SAM) and spike development. A Schematic representation of axillary bud formation of plants at 5 weeks after emergence (WAE). Each column represents a single plant of either cv. Bowman or the *mnd1.a* mutant. Each row shows the presence or absence of axillary buds (ABs) or tiller formation in leaf axils or axils of leaf-like structures at the corresponding node. Bottom rows belong to older nodes, whereas younger nodes are stacked on top. The absence of ABs is shown in green and the presence of ABs is presented in yellow to dark red depending on the developmental status of the AB. **B** Length of cv. Bowman and *mnd1.a* mutant SAMs during the early reproductive development (W2.0–W6.0). **C** Number of initiated florets counted at main SAMs from stage W3.0 until W6.0. Five plants per genotype were dissected weekly after seedling emergence for the first 9 WAE. Gray areas around fitted curves indicate the 95 % confidence interval.

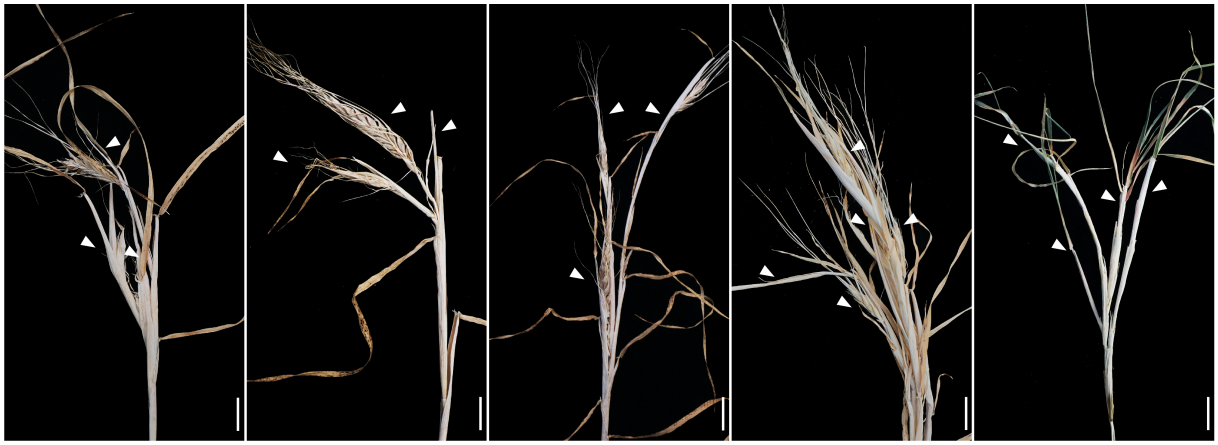

Figure S 4 Aerial shoot branching in *mbd*, *mnd1.a* and *MHOR198* mutants and in the heterozygous F1 progeny of crosses *mbd* x *mnd1.a* and *MHOR198* x *mnd1.a*. Representative branches showing a strong aerial branching phenotype were chosen from individual plants. Each branch, which arose from one culm, is indicated by arrows. Scale bar = 1 cm.

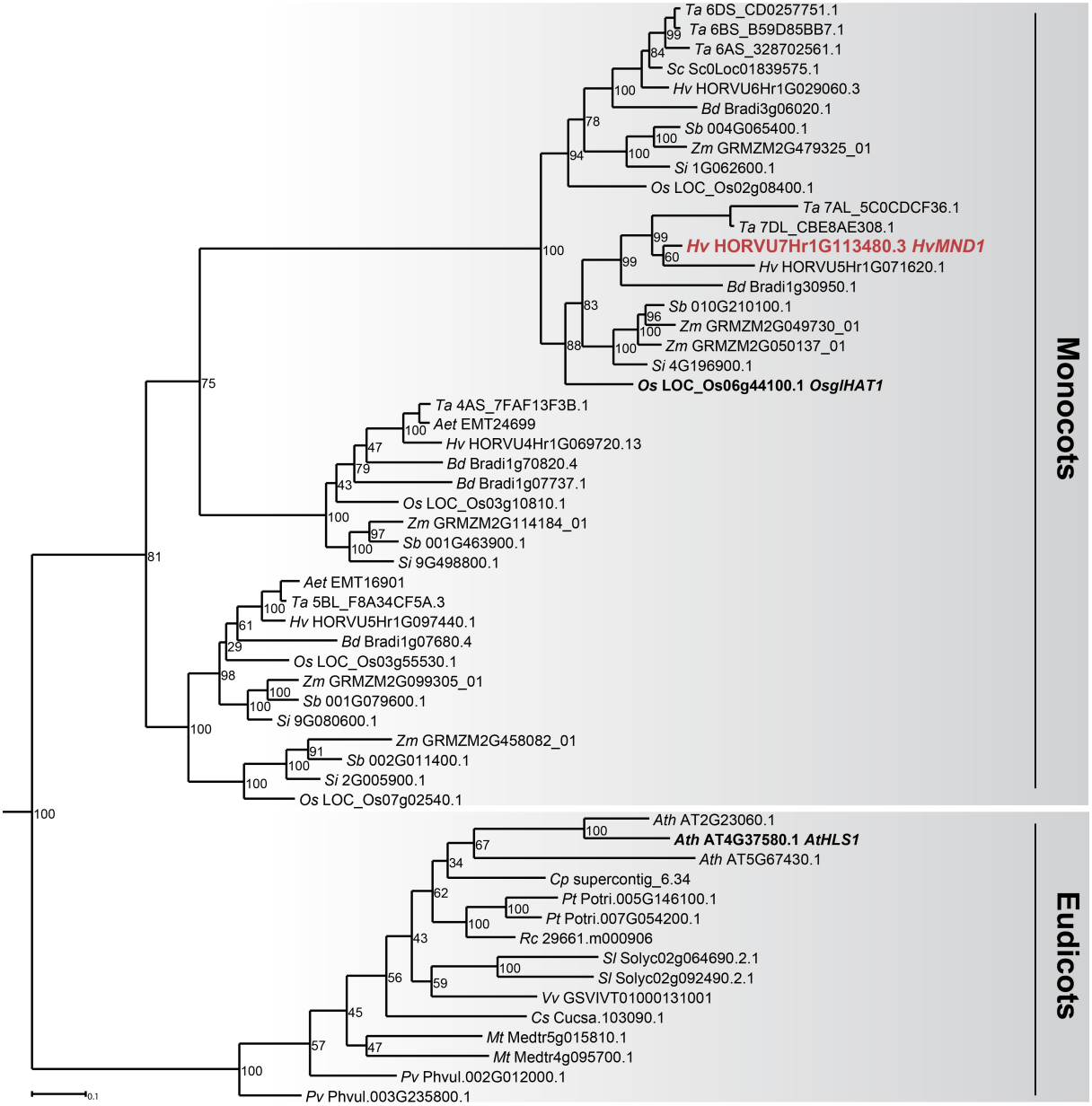

Figure S 5 Maximum likelihood phylogenetic tree of acyl-CoA N-acyltransferase-like genes in 19 monocot and eudicot plant species. Sequences obtained from *Selaginella moellendorffii* were used for rooting. The barley acyl-CoA N-acyltransferase gene described in this study, *HvMND1*, is highlighted in red. Functionally characterized *HvMND1* homologs in rice (*OsglHAT1*) and *A. thaliana* (*AtHLS1*) are marked in bold characters. Bootstrap support (%) is shown at the nodes. Abbreviated species names are given before gene identifiers. *Aet*: *Aegilops tauschii*; *Ath*: *Arabidopsis thaliana*; *Bd*: *Brachypodium distachyon*; *Cp*: *Carica papaya*; *Cs*: *Cucumis sativus*; *Hv*: *Hordeum vulgare*; *Mt*: *Medicago truncatula*; *Os*: *Oryza sativa*; *Pt*: *Populus trichocarpa*; *Pv*: *Phaseolus vulgaris*; *Rc*: *Ricinus communis*; *Sb*: *Sorghum bicolor*; *Sc*: *Secale cereale*; *Si*: *Setaria italica*; *Sl*: *Solanum lycopersicum*; *Ta*: *Triticum aestivum*; *Vv*: *Vitis vinifera*; *Zm*: *Zea mays*. Scale bar = 0.1 substitutions per site.

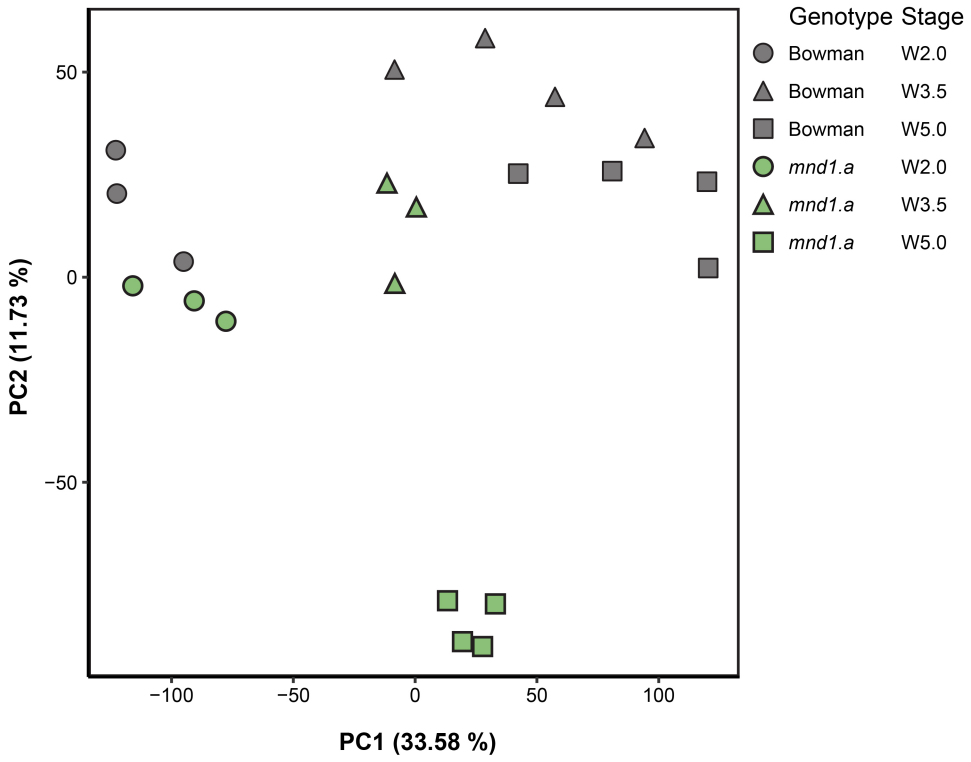

Figure S 6 Principal component analysis (PCA) showing the variation of all differentially regulated transcripts of cv. Bowman and *mnd1.a*. Genotypes and developmental stages of the sampled inflorescence tissues (W2.0, W3.5 and W5.0) are indicated with colors shown in the legend. The fraction of explained variance is given in brackets.

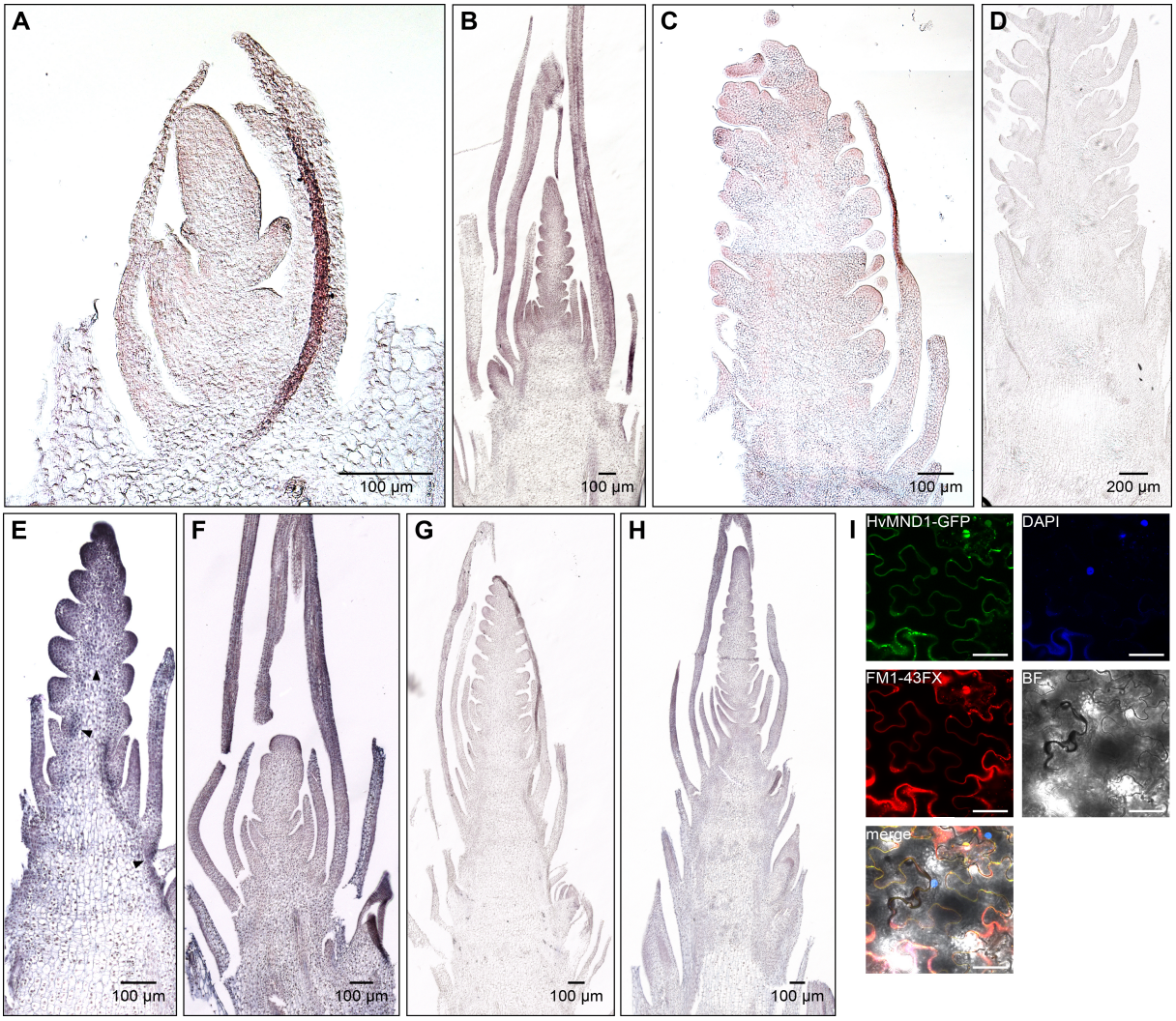

Figure S 7 Corresponding negative controls of the *HvMND1* in situ hybridization experiment and the *HvMND1* transcript localization in cv. ZOH. RNA in situ hybridization experiment using the sense probe of *HvMND1* in cv. Bowman shoot apical meristems at **A** W1.0-W1.5, **B** W2.0, **C** W3.5 and **D** W5.0. **E** In situ localization of *HvMND1* transcripts in wild-type cv. ZOH meristems at W2.0. Transcript loci are indicated with arrows. **F** Sense probe of *HvMND1* in cv. ZOH meristems at W2.0. Antisense *HvMND1* probe showing no transcript localization in **G** *mnd1.a* mutants and **H** *mbd* mutants at W2.0. **I** Localization of the HvMND1-GFP fusion protein in transformed tobacco leaves. Nuclei were stained with DAPI, plasma membranes were stained with FM1-43FX. Scale bar = 50 µm. BF: bright field. GFP: green fluorescent protein; DAPI: 4′,6-diamidino-2-phenylindole.

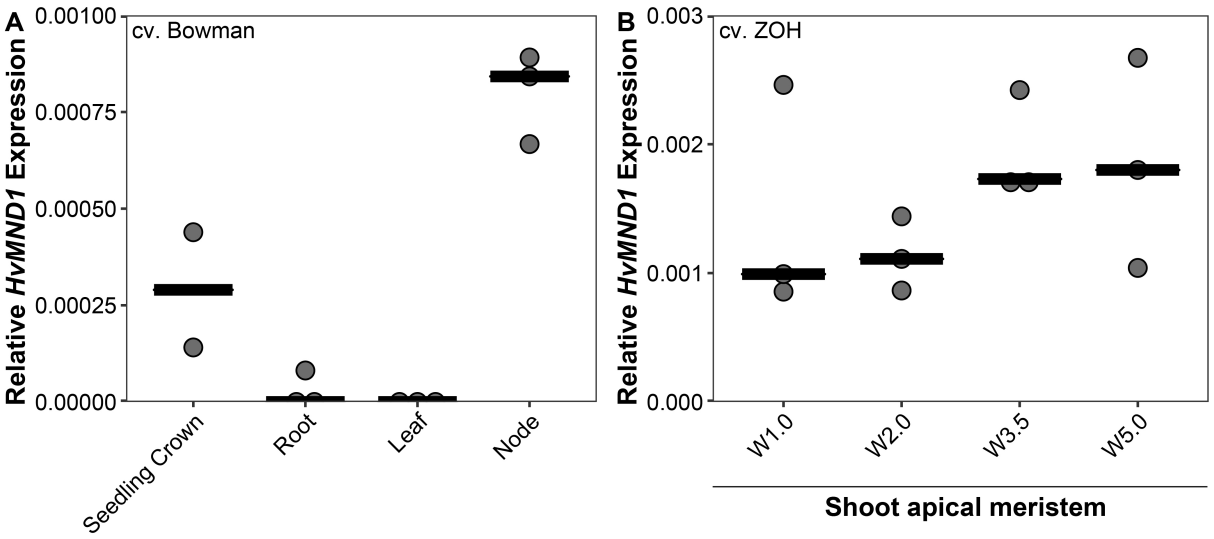

Figure S 8 *HvMND1* expression determined by qRT-PCR. A Relative *HvMND1* expression in cv. Bowman in a selection of different tissues (crown tissue and roots of 3-days-old seedlings, leaf and uppermost elongated node from plants at W3.5). **B** Relative *HvMND1* expression in cv. ZOH measured in the main SAMs at four developmental stages.

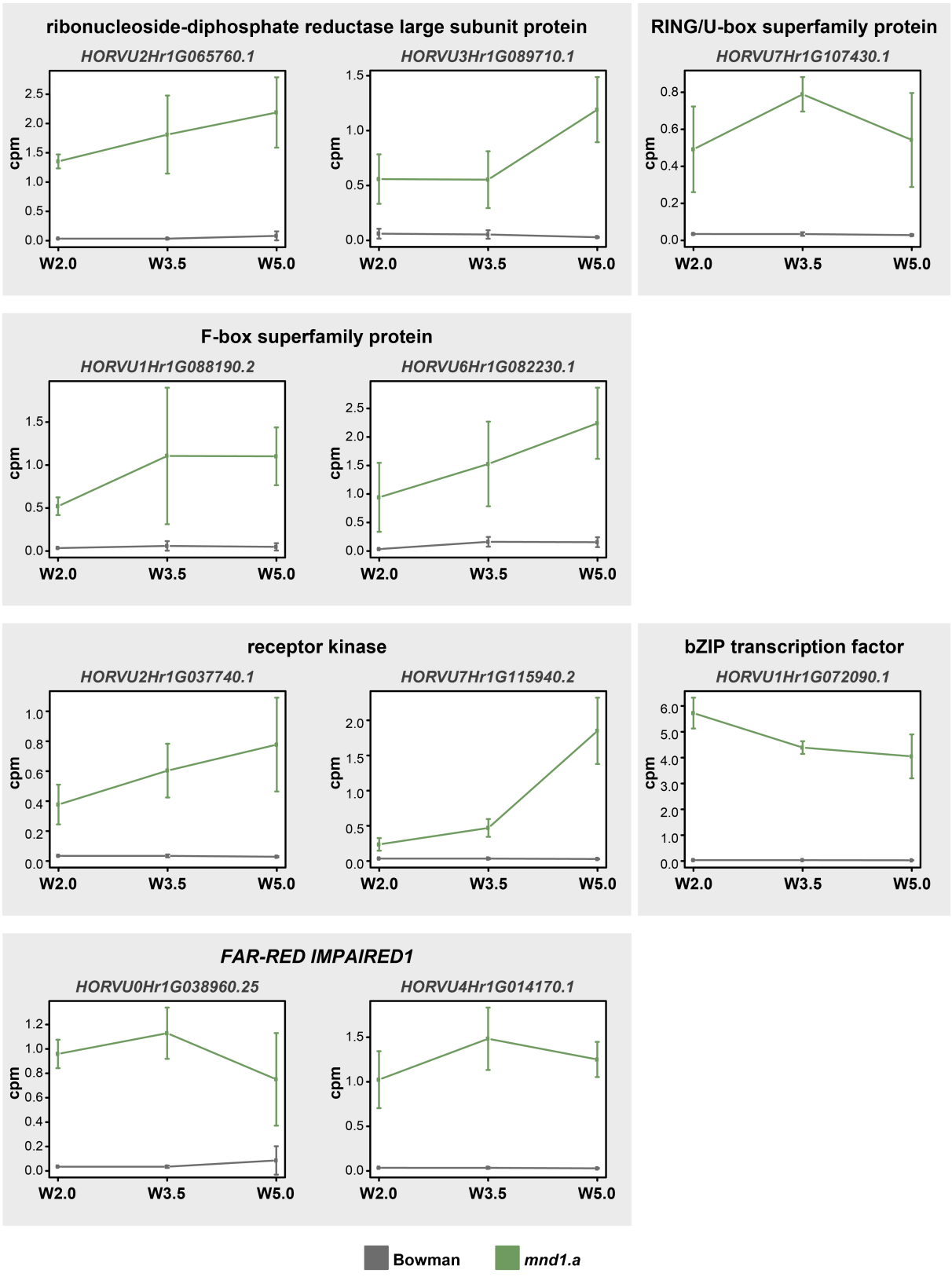

Figure S 9 Selected differentially expressed transcripts which were only expressed in the *mnd1.a* mutants and absent from cv. Bowman. Expression values were extracted from RNA sequencing of leaf-enriched inflorescence samples at three developmental stages: spikelet initiation (W2.0), stamen primordium initiation (W3.5) and awn primordium initiation (W5.0). Selected transcripts belong to the core transcripts showing significant expression changes at all three investigated developmental stages (LogFC ≤ -1.5 or ≥ 1.5, FDR ≤ 0.05). cpm: counts per million.

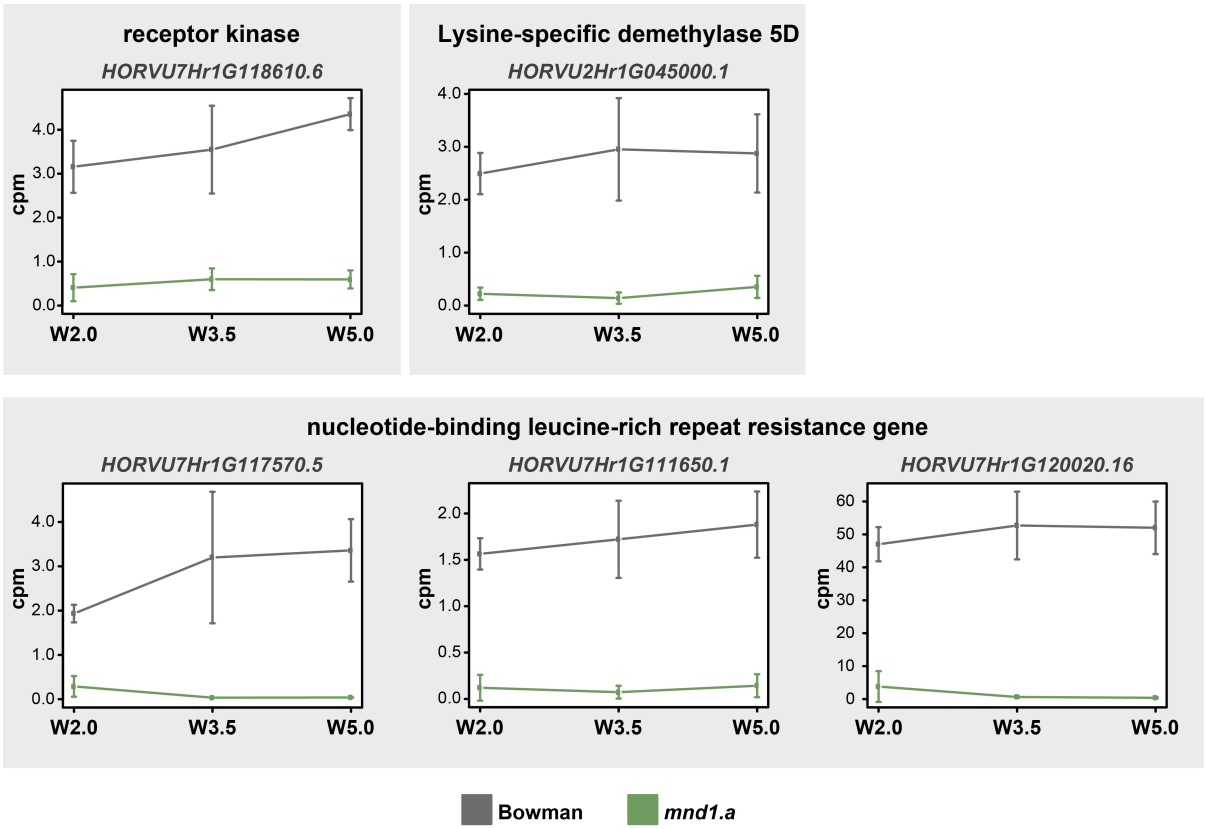

Figure S 10 Selected differentially expressed transcripts which were absent in *mnd1.a* mutants but expressed in cv. Bowman. Expression values were extracted from RNA sequencing of leaf-enriched inflorescence samples at three developmental stages: spikelet initiation (W2.0), stamen primordium initiation (W3.5) and awn primordium initiation (W5.0). Selected transcripts belong to the core transcripts showing significant expression changes at all three investigated developmental stages (LogFC ≤ -1.5 or ≥ 1.5, FDR ≤ 0.05). cpm: counts per million.

Table S 1 Phyllochron and plastochron of cv. Bowman and *mnd1.a* mutant plants. Phyllochron (leaf emergence rate^{-1} for the first five weeks after emergence) and plastochron (leaf initiation rate^{-1} for the first five days after emergence) were calculated from the slope of the fitted linear regression.

Genotype	**Phyllochron**	**SD**	**p-value of regression**	**Plastochron**	**SD**	**p-value of regression**
Bowman	5.61	0.191	1.030E-19	0.86	0.057	1.96E-13
mnd1.a	2.20	0.071	2.640E-20	1.08	0.073	3.54E-13

Table S 2 Non-synonymous mutations assigned to a conserved domain of the corresponding protein in *mnd1.a* backcross-derived mutants identified through mapping by RNA sequencing. Amino acid changes and corresponding functional effects of the protein sequence variation predicted using the PROVEAN tool (Choi and Chan, 2012). * = frameshift mutation leading to a premature stop codon.

Gene	***mnd1.a* mutation effect**	**PROVEAN score**	**Prediction (cutoff= -2.5)**
HORVU2Hr1G031470.2	H429Q	-0.32	Neutral
HORVU2Hr1G040710.1	D416N	-0.47	Neutral
HORVU2Hr1G029240.1	T93M	-5.36	Deleterious
HORVU7Hr1G119810.1	A113V	-0.66	Neutral
HORVU2Hr1G030820.1	R18L	-0.30	Neutral
HORVU2Hr1G029120.5	I764V	-0.244	Neutral
HORVU7Hr1G113480.3	G97*	/	/
HORVU2Hr1G040780.4	T39A	0.079	Neutral
HORVU2Hr1G038480.14	A352_A353delinsSV	0.64	Neutral
HORVU2Hr1G041250.1	S290N	0	Neutral

Table S 3 Resequencing of candidate polymorphisms in the parental lines cv. Bowman and cv. Mesa as well as in the backcross-derived *mnd1.a* mutant (*mnd1.a* (B)) and the original *mnd1.a* mutant in cv. Mesa (*mnd1.a* (M)). Positions of the candidate polymorphisms are given according to their location in the coding sequence of cv. Morex.

Genotype	**HORVU2Hr1G029240.1 Pos. 278**	**HORVU7Hr1G113480 Pos. 264**
Morex	C	G
Bowman	C	G
***mnd1.a* (B)**	T	GCCTGTGGG
Mesa	C	G
***mnd1.a* (M)**	C	GCCTGTGGG

Table S 4 Allelism test between *mnd1.a* and *mbd* mutants in the cv. Bowman and cv. ZOH genetic backgrounds, respectively. Flowering time and shoot architectural traits were measured after plants had flowered and set seed. Values represent mean ± SD (n ≥ 3 plants per genotype).

Genotype	**Days to Tipping**	**Tiller Number**	**Height [cm]**	**Node Number**
Bowman	44.33 [±0.58]	20.67 [±4.16]	78.00 [±3.61]	5.08 [±0.67]
ZOH	34.33 [±0.58]	18.67 [±2.08]	70.00 [±2.65]	4.00 [±0.71]
mnd1.a	61.67 [±1.51]	67.50 [±8.53]	73.83 [±5.85]	16.56 [±2.83]
mbd	49.33 [±0.52]	62.00 [±10.55]	53.00 [±3.79]	12.11 [±0.90]
mbd* x *mnd1.a	40.43 [±1.81]	39.00 [±10.07]	48.00 [±2.77]	9.19 [±1.47]

Table S 5 Allelism test between *mnd1.a* and *MHOR198* in the cv. Bowman and cv. HOR3069 genetic backgrounds, respectively. Flowering time and shoot architectural traits were measured after plants had flowered and set seed. Values represent mean ± SD (n ≥ 3 plants per genotype).

Genotype	**Days to Tipping**	**Tiller Number**	**Height [cm]**	**Node Number**
Bowman	84.50 [±0.58]	15.75 [±1.71]	67.25 [±2.63]	5.08 [±0.67]
HOR3069	124.43 [±20.72]	34.57 [±10.11]	75.86 [±8.13]	5.52 [±0.98]
mnd1.a	103.50 [±6.40]	67.33 [±9.07]	65.00 [±1.00]	13.56 [±2.65]
MHOR198	205.29 [±6.07]	26.86 [±4.14]	92.71 [±7.74]	18.33 [±3.65]
MHOR198* x *mnd1.a	112.00 [±1.63]	44.25 [±4.65]	91.00 [±2.16]	15.67 [±2.10]

Table S 6 Differentially expressed transcripts in developing *mnd1.a* mutant inflorescences. Leaf-enriched inflorescences at the spikelet initiation stage (W2.0), the stamen primordium stage (W3.5) and the awn primordium stage (W5.0) have been collected from cv. Bowman and *mnd1.a* mutants plants and subjected to RNA sequencing. Log-fold changes (Log2FC) and false discovery rates (FDR) derive from comparisons between genotypes per each developmental stage. Annotations of genes have been extracted from Mascher et al. (2017).

Table S 6 can be downloaded using the following URL:

https://www.dropbox.com/s/cfhoe3vuwxmz096/Table_S_6_DETs.xlsx?dl=0

Table S 7 Primer pairs used in this study.

Gene		**Primer sequence (5'→3')**	**Usage**	**Comment**	**Source**
HORVU7Hr1G113480	F	AGCTCCGTATATAATTGGCTCG	Sanger Sequencing	spanning *mnd1.a* 8-bp insertion	
	R	GAAACTCTCACCAGACGCGA			
HORVU7Hr1G113480	F	CAGATAGCCATTGAGAAGGCA	Sanger Sequencing		
	R	GTTTGGTCGGTGGCATTCTT			
HORVU7Hr1G113480	F	AGATGGTCGGCGTCATAAAG	qRT-PCR		
	R	AGCCGGAGGAAGAAGAAGAC			
HORVU2Hr1G029240	F	GGGTGAAAACGCCTCCCATA	Sanger Sequencing		
	R	GACTCTGGATCACTCGAGCG			
AY145451, *HvACTIN*	F	CGTGTTGGATTCTGGTGATG	qRT-PCR		Campoli et al., 2012
	R	AGCCACATATGCGAGCTTCT			
AK362208, *HvGAPDH*	F	GTGAGGCTGGTGCTGATTACG	qRT-PCR		Ejaz and Korff, 2016
	R	AGTGGTGCAGCTAGCATTTGAGAC			

4.8 Literature Cited

Aguilar-Martinez JA, Poza-Carrion C, Cubas P (2007) Arabidopsis BRANCHED1 Acts as an Integrator of Branching Signals within Axillary Buds. Plant Cell **19**: 458–472

Aida M, Ishida T, Tasaka M (1999) Shoot apical meristem and cotyledon formation during Arabidopsis embryogenesis: interaction among the CUP-SHAPED COTYLEDON and SHOOT MERISTEMLESS genes. Development **126**: 1563–1570

Bleckmann A, Weidtkamp-Peters S, Seidel CAM, Simon R (2010) Stem Cell Signaling in Arabidopsis Requires CRN to Localize CLV2 to the Plasma Membrane. Plant Physiol **152**: 166–176

Bossinger G, Rohde W, Lundqvist U, Salamini F (1992) Genetics of barley development: mutant phenotypes and molecular aspects. Barley Genet. Biochem. Mol. Biol. Biotechnol. pp 231–263

Bradley D, Carpenter R, Copsey L, Vincent C, Rothstein S, Coen E (1996) Control of inflorescence architecture in Antirrhinum. Nature **379**: 791–797

Bregitzer P, Lundqvist U, Blake VC (2013) Full Descriptions of barley genetic stocks. Barley Genet Newsl **43**: 48–223

Bregitzer P, Lundqvist U, Carollo Blake V (2014) Barley Genetics Newsletter Vol. 43. Barley Genet Newsl 51–208

Burke CR, Lupták A (2018) DNA synthesis from diphosphate substrates by DNA polymerases. Proc Natl Acad Sci **115**: 980 –985

Campoli C, Drosse B, Searle I, Coupland G, Von Korff M (2012) Functional characterisation of HvCO1, the barley (Hordeum vulgare) flowering time ortholog of CONSTANS. Plant J **69**: 868–880

Chen ZJ, Tian L (2007) Roles of dynamic and reversible histone acetylation in plant development and polyploidy. Biochim Biophys Acta **1769**: 295–307

Choi MS, Woo MO, Koh EB, Lee J, Ham TH, Seo HS, Koh HJ (2012) Teosinte Branched 1 modulates tillering in rice plants. Plant Cell Rep **31**: 57–65

Choi Y, Chan AP (2015) PROVEAN web server: A tool to predict the functional effect of amino acid substitutions and indels. Bioinformatics **31**: 2745–2747

Chono M, Honda I, Zeniya H, Yoneyama K, Saisho D, Takeda K, Watanabe Y (2003) A Semidwarf Phenotype of Barley uzu Results from a Nucleotide Substitution in the Gene Encoding a Putative Brassinosteroid Receptor. Plant Physiol **133**: 1209–1219

Chuck G, Cigan AM, Saeteurn K, Hake S (2007) The heterochronic maize mutant Corngrass1 results from overexpression of a tandem microRNA. Nat Genet **39**: 544–549

Comadran J, Kilian B, Russell J, Ramsay L, Stein N, Ganal M, Shaw P, Bayer M, Thomas W, Marshall D, et al (2012) Natural variation in a homolog of Antirrhinum CENTRORADIALIS contributed to spring growth habit and environmental adaptation in cultivated barley. Nat Genet **44**: 1388–1391

Curaba J, Talbot M, Li Z, Helliwell C (2013) Over-expression of microRNA171 affects phase transitions and floral meristem determinancy in barley. BMC Plant Biol **13**: 6

Dabbert T, Okagaki RJ, Cho S, Heinen S, Boddu J, Muehlbauer GJ (2010) The genetics of barley low-tillering mutants: Low number of tillers-1 (lnt1). Theor Appl Genet **121**: 705–715

Davies B, Schwarz-Sommer Z (1994) Control of floral organ identity by homeotic MADS-box transcription factors. Plant Promot. Transcr. factors. pp 235–258

Deshaies RJ, Joazeiro CA (2009) RING domain E3 ubiquitin ligases. Annu Rev Biochem **78**: 399–434

Doebley J, Stec A, Hubbard L (1997) The evolution of apical dominance in maize. Nature **386**: 485–488

Dolzblasz A, Nardmann J, Clerici E, Causier B, Graaff E Van Der, Chen J, Davies B, Werr W, Laux T (2016) Stem Cell Regulation by Arabidopsis WOX Genes. Mol Plant **9**: 1028–1039

Domagalska MA, Leyser O (2011) Signal integration in the control of shoot branching. Nat Rev Mol Cell Biol **12**: 211–221

Doust AN (2007) Grass architecture: genetic and environmental control of branching. Curr Opin Plant Biol **10**: 21–25

Driessen HPC, De Jong WW, Tesser GI, Bloemendal H (1985) The mechanism of N-terminal acetylation of protein. Crit Rev Biochem **18**: 281–325

Druka A, Franckowiak J, Lundqvist U, Bonar N, Alexander J, Houston K, Radovic S, Shahinnia F, Vendramin V, Morgante M, et al (2011) Genetic Dissection of Barley Morphology and Development. Plant Physiol **155**: 617–627

Edgar RC (2004) MUSCLE: Multiple sequence alignment with high accuracy and high throughput. Nucleic Acids Res **32**: 1792–1797

Epstein E, Ludwig-Müller J (1993) Indole-3-butyric acid in plants: occurrence, synthesis, metabolism and transport. Physiol Plant **88**: 382–389

van Esse GW, Walla A, Finke A, Koornneef M, Pecinka A, von Korff M (2017) Six-Rowed Spike3 (VRS3) Is a Histone Demethylase That Controls Lateral Spikelet Development in Barley. Plant Physiol **174**: 2397–2408

Franckowiak JD, Davis MP, Konishi T, Lundqvist U (1996) Barley Genetics Newsletter Vol. 26. Barley Genet. Newsl. 26:

Gallavotti A, Malcomber S, Gaines C, Stanfield S, Whipple C, Kellogg E, Schmidt RJ (2011) BARREN STALK FASTIGIATE1 Is an AT-Hook Protein Required for the Formation of Maize Ears. Plant Cell **23**: 1756–1771

Goodstein DM, Shu S, Howson R, Neupane R, Hayes RD, Fazo J, Mitros T, Dirks W, Hellsten U, Putnam N, et al (2011) Phytozome: A comparative platform for green plant genomics. Nucleic Acids Res **40**: D1178–D1186

Götz S, García-Gómez JM, Terol J, Williams TD, Nagaraj SH, Nueda MJ, Robles M, Talón M, Dopazo J, Conesa A (2008) High-throughput functional annotation and data mining with the Blast2GO suite. Nucleic Acids Res **36**: 3420–3435

Greb T, Clarenz O, Schäfer E, Müller D, Herrero R, Schmitz G, Theres K (2003) Molecular analysis of the LATERAL SUPPRESSOR gene in Arabidopsis reveals a conserved control mechanism for axillary meristem formation. Genes Dev **17**: 1175–1187

Harlan H V, Pope MN (1922) Many-noded dwarf barley. J Hered **13**: 269–273

Hedden P (2003) The genes of the Green Revolution. Trends Genet **19**: 5–9

Hejátko J, Blilou I, Brewer PB, Friml J, Scheres B, Benková E (2006) In situ hybridization technique for mRNA detection in whole mount Arabidopsis samples. Nat Protoc **1**: 1939

Houston K, Druka A, Bonar N, Macaulay M, Lundqvist U, Franckowiak J, Morgante M, Stein N, Waugh R (2012) Analysis of the barley bract suppression gene Trd1. Theor Appl Genet **125**: 33–45

Huson DH, Scornavacca C (2012) Dendroscope 3: An interactive tool for rooted phylogenetic trees and networks. Syst Biol **61**: 1061–1067

Ito S, Song YH, Josephson-Day AR, Miller RJ, Breton G, Olmstead RG, Imaizumi T (2012) FLOWERING BHLH transcriptional activators control expression of the photoperiodic flowering regulator CONSTANS in Arabidopsis. Proc Natl Acad Sci **109**: 3582–3587

Jackson D, Veit B, Hake S (1994) Expression of maize KNOTTED1 related homeobox genes in the shoot apical meristem predicts patterns of morphogenesis in the vegetative shoot. Development **413**: 405–413

Jansson S (1994) The light-harvesting chlorophyll a b-binding proteins. Biochim Biophys Acta **1184**: 1–19

Jeong JH, Song HR, Ko JH, Jeong YM, Kwon YE, Seol JH, Amasino RM, Noh B, Noh YS (2009) Repression of FLOWERING LOCUS T chromatin by functionally redundant histone H3 lysine 4 demethylases in Arabidopsis. PLoS One **4**: e8033

Jiang D, Yang W, He Y, Amasino RM (2007) *Arabidopsis* Relatives of the Human Lysine-Specific Demethylase1 Repress the Expression of *FWA* and *FLOWERING LOCUS C* and Thus Promote the Floral Transition. Plant Cell **19**: 2975–2987

Karim MR, Hirota A, Kwiatkowska D, Tasaka M, Aida M (2009) A Role for Arabidopsis PUCHI in Floral Meristem Identity and Bract Suppression. Plant Cell **21**: 1360–1372

Kebrom TH, Burson BL, Finlayson SA (2006) Phytochrome B represses Teosinte Branched1 expression and induces sorghum axillary bud outgrowth in response to light signals. Plant Physiol **140**: 1109–1117

Kebrom TH, Spielmeyer W, Finnegan EJ (2013) Grasses provide new insights into regulation of shoot branching. Trends Plant Sci **18**: 41–48

Kirschner GK, Stahl Y, Von Korff M, Simon R (2017) Unique and Conserved Features of the Barley Root Meristem. Front Plant Sci **8**: 1240

Komatsuda T, Pourkheirandish M, He C, Azhaguvel P, Kanamori H, Perovic D, Stein N, Graner A, Wicker T, Tagiri A, et al (2007) Six-rowed barley originated from a mutation in a homeodomain-leucine zipper I-class homeobox gene. Proc Natl Acad Sci **104**: 1424–1429

Lampropoulos A, Sutikovic Z, Wenzl C, Maegele I, Lohmann JU, Forner J (2013) GreenGate - A novel, versatile, and efficient cloning system for plant transgenesis. PLoS One **8**: e83043

Lehman A, Black R, Ecker JR (1996) HOOKLESS1, an Ethylene Response Gene, Is Required for Differential Cell Elongation in the Arabidopsis Hypocotyl. Cell **85**: 183–194

Lewis JM, Mackintosh CA, Shin S, Gilding E, Kravchenko S, Baldridge G, Zeyen R, Muehlbauer GJ (2008) Overexpression of the maize Teosinte Branched1 gene in wheat suppresses tiller development. Plant Cell Rep **27**: 1217–1225

Li H (2013) Aligning sequence reads, clone sequences and assembly contigs with BWA-MEM. arXiv 1–3

Li X, Qian Q, Fu Z, Wang Y, Xiong G, Zeng D, Wang X, Liu X, Teng S, Hiroshi F, et al (2003) Control of tillering in rice. Nature **422**: 618–621

Liang WH, Shang F, Lin QT, Lou C, Zhang J (2014) Tillering and panicle branching genes in rice. Gene **537**: 1–5

Liao C, Lai Z, Lee S, Yun D, Mengiste T (2016) Arabidopsis HOOKLESS1 Regulates Responses to Pathogens and Abscisic Acid through Interaction with MED18 and Acetylation of WRKY33 and ABI5 Chromatin. Plant Cell **28**: 1662–1681

Liu L, Li B, Liu X (2016) FAR-RED ELONGATED HYPOCOTYL3 promotes floral meristem determinacy in Arabidopsis. Plant Signal Behav **11**: e1238545

Long JA, Moan EI, Medford JI, Barton MK (1996) A member of the KNOTTED class of homeodomain proteins encoded by the STM gene of Arabidopsis. Nature **379**: 66–69

Lu F, Cui X, Zhang S, Jenuwein T, Cao X (2011) Arabidopsis REF6 is a histone H3 lysine 27 demethylase. Nat Genet **43**: 715–719

Marchler-Bauer A, Derbyshire MK, Gonzales NR, Lu S, Chitsaz F, Geer LY, Geer RC, He J, Gwadz M, Hurwitz DI, et al (2015) CDD: NCBI's conserved domain database. Nucleic Acids Res **43**: D222–D226

Mascher M, Gundlach H, Himmelbach A, Beier S, Twardziok SO, Wicker T, Radchuk V, Dockter C, Hedley PE, Russell J, et al (2017) A chromosome conformation capture ordered sequence of the barley genome. Nature **544**: 427–433

Mascher M, Jost M, Kuon J-E, Himmelbach A, Aßfalg A, Beier S, Scholz U, Graner A, Stein N (2014) Mapping-by-sequencing accelerates forward genetics in barley. Genome Biol **15**: R78

Mayer KFX, Martis M, Hedley PE, Šimková H, Liu H, Morris JA, Steuernagel B, Taudien S, Roessner S, Gundlach H, et al (2011) Unlocking the Barley Genome by Chromosomal and Comparative Genomics. Plant Cell **23**: 1249–1263

McKenna A, Hanna M, Banks E, Sivachenko A, Cibulskis K, Kernytsky A, Garimella K, Altshuler D, Gabriel S, Daly M, et al (2010) The genome analysis toolkit: A MapReduce framework for analyzing next-generation DNA sequencing data. Genome Res **20**: 1297–1303

McMaster GS (2005) Phytomers, phyllochrons, phenology and temperate cereal development. J Agric Sci **143**: 137–150

Miyoshi K, Ahn B-O, Kawakatsu T, Ito Y, Itoh J-I, Nagato Y, Kurata N (2004) PLASTOCHRON1, a timekeeper of leaf initiation in rice, encodes cytochrome P450. Proc Natl Acad Sci **101**: 875–880

Nakagawa M, Shimamoto K, Kyozuka J (2002) Overexpression of RCN1 and RCN2, rice Terminal Flower 1/Centroradialis homologs, confers delay of phase transition and altered panicle morphology in rice. Plant J **29**: 743–750

Noh B, Lee S, Kim H, Yi G, Shin E, Lee M, Jung K (2004) Divergent roles of a pair of homologous jumonji/zinc-finger–class transcription factor proteins in the regulation of Arabidopsis flowering time. Plant Cell **16**: 2601–2613

Oikawa T, Kyozuka J (2009) Two-Step Regulation of LAX PANICLE1 Protein Accumulation in Axillary Meristem Formation in Rice. Plant Cell **21**: 1095–1108

Patro R, Duggal G, Kingsford C (2015) Salmon: Accurate, Versatile and Ultrafast Quantification from RNA-seq Data using Lightweight-Alignment. bioRxiv 021592

Peng J, Richards DE, Hartley NM, Murphy GP, Devos KM, Flintham JE, Beales J, Fish LJ, Worland AJ, Pelica F, et al (1999) 'Green revolution' genes encode mutant gibberellins response modulators. Nature **400**: 256–261

Pnueli L, Carmel-Goren L, Hareven D, Gutfinger T, Alvarez J, Ganal M, Zamir D, Lifschitz E (1998) The SELF-PRUNING gene of tomato regulates vegetative to reproductive switching of sympodial meristems and is the ortholog of CEN and TFL1. Development **125**: 1979–1989

Poethig RS (1988) Heterochronic mutations affecting shoot development in maize. Genetics **119**: 959–973

Preibisch S, Saalfeld S, Tomancak P (2009) Globally optimal stitching of tiled 3D microscopic image acquisitions. Bioinformatics **25**: 1463–1465

R Development Core Team (2011) R: A Language and Environment for Statistical Computing. R Found Stat Comput. doi: 10.1007/978-3-540-74686-7

Ramsay L, Comadran J, Druka A, Marshall DF, Thomas WTB, MacAulay M, MacKenzie K, Simpson C, Fuller J, Bonar N, et al (2011) INTERMEDIUM-C, a modifier of lateral spikelet fertility in barley, is an ortholog of the maize domestication gene TEOSINTE BRANCHED 1. Nat Genet **43**: 169–172

Rao NN, Prasad K, Kumar PR, Vijayraghavan U (2008) Distinct regulatory role for RFL, the rice LFY homolog, in determining flowering time and plant architecture. Proc Natl Acad Sci **105**: 3646–3651

Ratcliffe OJ, Amaya I, Vincent CA, Rothstein S, Carpenter R, Coen ES, Bradley DJ (1998) A common mechanism controls the life cycle and architecture of plants. Development **125**: 1609–1615

Robinson D, Hayes A (2018) broom: Convert Statistical Analysis Objects into Tidy Tibbles. https://CRAN.R-project.org/package=broom

Schindelin J, Arganda-Carreras I, Frise E, Kaynig V, Longair M, Pietzsch T, Preibisch S, Rueden C, Saalfeld S, Schmid B, et al (2012) Fiji: An open-source platform for biological-image analysis. Nat Methods **9**: 676

Schmitz G, Theres K (2005) Shoot and inflorescence branching. Curr Opin Plant Biol **8**: 506–511

Schmitz G, Theres K (1999) Genetic control of branching in Arabidopsis and tomato. Curr Opin Plant Biol **2**: 51–55

Schmitz J, Franzen R, Ngyuen TH, Garcia-Maroto F, Pozzi C, Salamini F, Rohde W (2000) Cloning, mapping and expression analysis of barley MADS-box genes. Plant Mol Biol **42**: 899–913

Schumacher K, Schmitt T, Rossberg M, Schmitz G, Theres K (1999) The Lateral suppressor (Ls) gene of tomato encodes a new member of the VHIID protein family. Proc Natl Acad Sci **96**: 290–295

Shannon S, Meeks-Wagner DR (1991) A Mutation in the Arabidopsis TFL1 Gene Affects Inflorescence Meristem Development. Plant Cell **3**: 877–892

Shuai B, Reynaga-Pena CG, Springer PS (2002) The lateral organ boundaries gene defines a novel, plant-specific gene family. Plant Physiol **129**: 747–761

De Smet I, Voß U, Jürgens G, Beeckman T (2009) Receptor-like kinases shape the plant. Nat Cell Biol **11**: 1166–1173

Song XJ, Kuroha T, Ayano M, Furuta T, Nagai K, Komeda N, Suzuki T (2015) Rare allele of a previously unidentified histone H4 acetyltransferase enhances grain weight, yield, and plant biomass in rice. Proc Natl Acad Sci **112**: 76–81

Spielmeyer W, Ellis MH, Chandler PM (2002) Semidwarf (sd-1), “green revolution” rice, contains a defective gibberellin 20-oxidase gene. Proc Natl Acad Sci **99**: 9043–9048

Stamatakis A, Hoover P, Rougemont J (2008) A rapid bootstrap algorithm for the RAxML web servers. Syst Biol **57**: 758–771

Stirnberg P, Zhao S, Williamson L, Ward S, Leyser O (2012) FHY3 promotes shoot branching and stress tolerance in Arabidopsis in an AXR1- dependent manner. Plant J **71**: 907–920

Takada S, Hibara K, Ishida T, Tasaka M (2001) The CUP-SHAPED COTYLEDON1 gene of Arabidopsis regulates shoot apical meristem formation. Development **128**: 1127–1135

Takeda S, Hanano K, Kariya A, Shimizu S, Zhao L, Matsui M, Tasaka M, Aida M (2011) CUP-SHAPED COTYLEDON1 transcription factor activates the expression of LSH4 and LSH3, two members of the ALOG gene family, in shoot organ boundary cells. Plant J **66**: 1066–1077

Takeda T, Suwa Y, Suzuki M, Kitano H, Ueguchi-Tanaka M, Ashikari M, Matsuoka M, Ueguchi C (2003) The OsTB1 gene negatively regulates lateral branching in rice. Plant J **33**: 513–520

Tamura K, Peterson D, Peterson N, Stecher G, Nei M, Kumar S (2011) MEGA5: Molecular evolutionary genetics analysis using maximum likelihood, evolutionary distance, and maximum parsimony methods. Mol Biol Evol **28**: 2731–2739

Tanaka W, Ohmori Y, Ushijima T, Matsusaka H, Matsushita T, Kumamaru T, Kawano S, Hirano H-Y (2015) Axillary Meristem Formation in Rice Requires the *WUSCHEL* Ortholog *TILLERS ABSENT1*. Plant Cell **27**: 1173–1184

Trevaskis B, Tadege M, Hemming MN, Peacock WJ, Dennis ES, Sheldon C (2007) Short Vegetative Phase-Like MADS-Box Genes Inhibit Floral Meristem Identity in Barley. Plant Physiol **143**: 225–235

Vandenbussche M, Horstman A, Zethof J, Koes R, Rijpkema AS, Gerats T (2009) Differential Recruitment of WOX Transcription Factors for Lateral Development and Organ Fusion in Petunia and Arabidopsis. Plant Cell **21**: 2269–2283

Vierstra RD (2009) The ubiquitin-26S proteasome system at the nexus of plant biology. Nat Rev Mol Cell Biol **10**: 385–397

Vroemen CW, Mordhorst AP, Albrecht C, Kwaaitaal MA, de Vries SC (2003) The CUP-SHAPED COTYLEDON3 Gene Is Required for Boundary and Shoot Meristem Formation in Arabidopsis. Plant Cell **15**: 1563–1577

Waddington SR, Cartwright PM, Wall PC (1983) A Quantitative Scale of Spike Initial and Pistil Development in Barley and Wheat. Ann Bot **51**: 119–130

Wang H, Wang H (2015) Multifaceted roles of FHY3 and FAR1 in light signaling and beyond. Trends Plant Sci **20**: 453–461

Wang L, Yin H, Qian Q, Yang J, Huang C, Hu X, Luo D (2009) NECK LEAF 1, a GATA type transcription factor, modulates organogenesis by regulating the expression of multiple regulatory genes during reproductive development in rice. Cell Res **19**: 598–611

Weigel D, Alvarez J, Smyth DR, Yanofsky MF, Meyerowitz EM (1992) *LEAFY* controls floral meristem identity in *Arabidopsis*. Cell **69**: 843–859

Wenzel CL, Chandler PM, Cunningham RB, Passioura JB (1997) Characterization of the leaf epidermis of barley (Hordeum vulgare L. 'Himalaya'). Ann Bot **79**: 41–46

Whipple CJ (2017) Grass inflorescence architecture and evolution: the origin of novel signaling centers. New Phytol **216**: 367–372

Whipple CJ, Hall DH, DeBlasio S, Taguchi-Shiobara F, Schmidt RJ, Jackson DP (2010) A Conserved Mechanism of Bract Suppression in the Grass Family. Plant Cell **22**: 565–578

Wu F, Shi X, Lin X, Liu Y, Chong K, Theißen G, Meng Z (2017) The ABCs of flower development: mutational analysis of AP1/FUL-like genes in rice provides evidence for a homeotic (A)-function in grasses. Plant J **89**: 310–324

Wu X, Chory J, Weigel D (2007) Combinations of WOX activities regulate tissue proliferation during Arabidopsis embryonic development. Dev Biol **309**: 306–316

Xiong GS, Hu XM, Jiao YQ, Yu YC, Chu CC, Li JY, Qian Q, Wang YH (2006) LEAFY HEAD2, which encodes a putative RNA-binding protein, regulates shoot development of rice. Cell Res **16**: 267–276

Xu C, Wang Y, Yu Y, Duan J, Liao Z, Xiong G, Meng X, Liu G, Qian Q, Li J (2012) Degradation of MONOCULM 1 by APC/C TAD1 regulates rice tillering. Nat Commun **3**: 750–759

Zhang X, Clarenz O, Cokus S, Bernatavichute Y V, Pellegrini M, Goodrich J (2007) Whole-Genome Analysis of Histone H3 Lysine 27 Trimethylation in Arabidopsis. PLoS Biol **5**: e129

Zhao Y, Medrano L, Ohashi K, Fletcher JC, Yu H, Sakai H, Meyerowitz EM (2004) HANABA TARANU Is a GATA Transcription Factor That Regulates Shoot Apical Meristem and Flower Development in Arabidopsis. Plant Cell **16**: 2586–2600

Acknowledgements

A barley inflorescence is supported by its stem which is composed of several phytomers. Likewise, this work is based on numerous contributions and the support of a hand full of people who have made this work possible. I would like to take this opportunity and express my gratitude to everyone involved in the completion of this thesis.

I am most grateful to my supervisor Maria von Korff. You gave me the chance to work on this tremendously interesting topic, supported me throughout my PhD and gave me freedom to develop my own way of scientific thinking.

I would like to express a lot of gratitude to my second supervisor Rüdiger Simon for co-supervising this thesis. Your ideas and particularly your advice to perform SEM analysis provided valuable results to this work.

Special thanks go to Wilma van Esse for the contributions to this work. I am thankful for your guidance in the beginning of my PhD and that you are still there for me, scientifically and personally. I hope that we can continue this great team in the future.

Thanks to the whole von Korff group, current and former members, for creating a great work atmosphere and for critically discussing my project. Thanks also go to the Acosta group and the Coupland department for sharing their excellent expertise.

Thanks to Gwendolyn Kirschner for your fruitful work on the MND1 manuscript and for being such a great same-supervisor-sister.

Thanks to the super-power technicians Kerstin, Thea, Andrea, Rainer, Siggi and Marianne. I would also like to thank Caren for being such an excellent gardener and not complaining about my bushy plants.

Thanks to all the CEPLAS members, especially the young researchers, for making CEPLAS such an excellent fun time.

I would like to thank all of my friends. Whenever we met, my carbohydrate storage was more than refilled. I guess that kept me going. Special thanks to Isabel and Miriam for the scientific discussions although our topics are so different.

Since I am a crazy cat lady, I would like to thank my insane cat Mila for keeping me sane.

Special thanks go to Moritz. Thank you for your support, your interest in my work, the work-life-balance and preparing my salads for lunch. You are an enrichment to my life.

Besonderer Dank geht an meine Eltern, Aleksandra und Darius. Eure Unterstützung und Zuversicht haben mich erst dazu gebracht über meinen Horizont hinaus zu denken und mich zu der gemacht, die ich jetzt bin. Ihr seid meine Vorbilder und meine besten Freunde. „*Gdzie serce tam i szczęście*”